Molecular Mechanisms of Immune-Mediated Axon Regeneration in the Injured Central Nervous System

by

Katherine Therese Baldwin

A dissertation submitted in partial fulfillment
of the requirements for the degree of
Doctor of Philosophy
(Cellular and Molecular Biology)
in the University of Michigan
2015

Dissertation Committee:

Professor Roman J. Giger, Chair
Associate Professor Catherine A. Collins
Associate Professor Diane C. Fingar
Associate Professor Geoffrey G. Murphy
Assistant Professor Brian A. Pierchala
Associate Professor Michael M. A. Sutton

On science:

“Somewhere, something incredible is waiting to be known.”
-Carl Sagan

On graduate school:

“The value of a college education is not the learning of many facts, but the training of the mind to think.”
-Albert Einstein

On benchwork:

“If you don't have time to do it right, when will you have time to do it over?”
-John Wooden

On perseverance:

"Just keep swimming, just keep swimming, just keep swimming, swimming, swimming!"
-Dory, Finding Nemo

ACKNOWLEDGMENTS

This work was only possible with the help, support, and encouragement of many individuals. I am sincerely grateful to all of those in my professional and personal life that have helped me reach this point in my scientific career.

I would first like to thank the members of my thesis committee: Cathy Collins, Diane Fingar, Geoff Murphy, Brian Pierchala, and Mike Sutton. Thank you for taking the time out of your busy schedules to lend your scientific expertise to my committee, and for providing valuable feedback and guidance for my scientific training. Many of you have also provided reference letters for various funding applications, and I am truly grateful for your support. The Cellular and Molecular Biology Graduate Program has been an excellent environment for my PhD training. Thank you to Bob Fuller, Jessica Schwartz, Cathy Mitchell, Margarita Bekiares, and Jim Musgrave for all that you have done and continue to do for CMB students. I have also thoroughly enjoyed being a part of the Department of Cell and Developmental Biology. Thank you to all of the faculty, students, postdocs, administrators, and staff members that make this department such a fun and collaborative environment day in and day out. A special thank you to Melissa Karby, who has gone above and beyond helping out our lab with various financial and administrative tasks.

Thank you to all of our collaborators who have provided tools, equipment, advice, and helpful discussion: The Fingar lab, particularly Brian Magnuson, for helping me with biochemistry experiments; The Pierchala lab for providing many antibody aliquots and advice for biochemical experiments; The Sutton lab, particularly Christian Althaus and Amber McCartney, for help with cell culture and electrophysiology experiments; The Allen lab for always letting me borrow your teaching scope, and for all of the other various reagents that you've helped out with when we've needed them. Alex, Brandon, and Justine – thank you for making the lab environment so much fun. To the Segal lab, thank you for all of your help on collaborative projects, particularly Kevin, Julie, Josh, and Heather for helping with all of the bone marrow chimera experiments. Thank you also to the members of our monthly Axon Club meetings, for providing helpful feedback and discussion on projects, and for being so willing to share reagents. I also want to thank Larry Benowitz at Boston Children's Hospital, and Yuqin Yin and Hui-Ya Gilbert in his lab, for their help in training me in surgical techniques. Thank you to the U of M vector core for producing dozens of lentiviral stocks for me over the past few years. Laboratory animal work has been an important part of my scientific training. This would not be possible without all of the wonderful faculty and staff members of ULAM and UCUCA. In particular, I'd like to thank Helen, who has been our primary veterinary technician. Thank you for taking such great care of my mice, especially following the optic nerve crush procedure. To all of the room technicians and ULAM staff members that keep the animals facilities up and running, thank you for all that you do, day in and day out.

One of the most important decisions that I made during graduate school was the selection of my mentor. Roman, you have been a truly outstanding graduate mentor. You always lead by example; your work ethic and enthusiasm for science are contagious, and you inspire us all to keep asking questions and seeking answers. Thank you for supporting me through all of the ups and downs of graduate school, and for teaching me how to think both critically and creatively. You always put your students first – from helping us with practice talk before conferences,

providing feedback on our writing at lightning speed, and joining us at the bench to demonstrate techniques – we are greatly appreciative of all that you do. To all members of the Giger Lab (aka Roman Legion), thank you for creating such a fun and collaborative work environment. Steve, thank you for showing me the ropes during my rotation and when I first joined the lab. Yuntao, thank you for all of your help with experimental techniques and advice over the years. To our undergrads past and present, Derek, Sandy, Sophia, Dava, and Riley – thank you all for your help on various projects and for keeping the lab running smoothly. Jing-Ping, thank you for brining your fun and creative mind to our lab. You have the best hands of anyone I've ever worked with – I think if I ever need surgery done on my brain, I will ask you. Choya, thank you for being our "lab mom," for planning fun lab activities, and for all of the great work you've done testing our optic nerve findings in the spinal cord. Xiaofeng, you have been an excellent addition to the lab. Thank you for being so willing to help out with other people's projects, and for being a calm and friendly presence in the lab. Rafi and Ryan, I'm very excited that you guys have joined the lab, and I know that you both will be excellent scientists. Thank you also for helping continue my projects in the lab – I'm glad to know they are in good hands.

Travis and Yevgeniya – what can I say about the two of you? You are two of the most driven, hard working people that I know. You have both set very high standards in the lab for work ethic and scientific excellence, and I know that you will be very successful in whatever scientific ventures you pursue. Travis, thank you for blazing such a successful trail for me to follow. I benefited greatly from your advice on grant applications, experiments, scientific presentations, and postdoc applications. Yev, thank you for putting up with me on a daily basis, for keeping me sane with your fabulous sense of humor, and for all of the insightful discussions we've had about science, life, and Game of Thrones. Both of you have made graduate school so

much more enjoyable. I feel very fortunate that we got to share so much time together in lab, and I know that the three of us will be lifelong friends.

Thank you to the many friends and family members that have supported me throughout this time. To Meredith and Joe, and Justine and Blu, thank you for playing all kinds of nerdy board games with me and Chris, and providing a nice break from the lab. To my in-laws, Jack and Juani, thank you for your love and support, and for being patient with us during the busier and more stressful times of graduate school. Thank you to my sisters, Emily and Mikaela, and to my brother Jeff. I've enjoyed the times I've been able to spend with you on family vacations and over the holidays. Thank you for your continued love and support. To my parents – I owe so much of my success to you. You are both extremely intelligent, driven individuals, and I feel very fortunate to have you as role models and as parents. Mom, you inspired my interest in science, and helped develop my nerdy sense of humor. Dad, you've taught me mental toughness and shown me how to have a healthy amount of tenacity. Thank you for all of your love, support, and encouragement over the years. One of the biggest things I have to thank you for, specifically related to graduate school, is this: you made a conscious effort to never ask me the two most dreaded questions of any PhD student: 1) when are you going to graduate?, and 2) what are you going to do after you graduate? For that, I am very grateful. Lastly, to my husband Chris: I am so fortunate to have had you at my side throughout this crazy roller coaster called graduate school. When things were stressful, you were there with a smile, a hug, a cheesy joke, or shoulder to cry on. Thank you for your unwavering love and support, for your kindness, your patience, and your understanding. Thank you for all that you do, but most of all, thank you for being you.

TABLE OF CONTENTS

LIST OF FIGURES

LIST OF TABLES

ABSTRACT

In the injured adult mammalian central nervous system (CNS), severed axons fail to undergo spontaneous regeneration, leading to permanent neurological deficits, such as paralysis following spinal cord injury, and cognitive impairment following traumatic brain injury or stroke. A large body of work has established that neuron intrinsic and extrinsic mechanisms pose barriers to efficient CNS repair. Inhibitory molecules, including myelin-associated inhibitors (MAIs) and chondroitin sulfate proteoglycans (CSPGs), are expressed by injured CNS tissue and complex with neuronal surface receptors to prevent regenerative growth of axons. Following retro-orbital crush injury to the mouse optic nerve, injured retinal ganglion cell (RGC) axons do not normally grow beyond the injury site. Deletion of multiple CSPG receptors enables significant, though modest, regeneration of RGC axons. In these mice, RGC axon regeneration can be greatly enhanced by induction of a local immune response. The underlying mechanisms of immune-mediated neurorepair are poorly understood. Here I show that post-injury manipulation of specific immunomodulatory pathways promotes extensive growth of injured RGC axons. Intraocular injection of zymosan, a yeast cell wall extract, leads to a rapid accumulation of blood-derived immune cells in the vitreous, and enables robust RGC axon regeneration by engaging the pattern recognition receptors dectin-1 and Toll-like receptor-2 (TLR2). Dectin-1 is expressed by retina-resident microglia and dendritic cells, but not by RGCs. Dectin-1 is also present on blood-derived myeloid cells that accumulate in the vitreous. Intraocular injection of the dectin-1 ligand curdlan (a particulate form of beta-glucan) elicits

robust regeneration in WT, but not in *dectin-1*$^{-/-}$ mice. Studies with *dectin-1*$^{-/-}$/WT reciprocal bone marrow chimeric mice revealed a requirement for dectin-1 on both retina-resident immune cells and bone-marrow derived cells for beta-glucan-elicited optic nerve regeneration. Collectively, these studies identify a molecular framework for how innate immunity enables repair of injured central nervous system neurons.

CHAPTER I

Introduction:

Regeneration in the adult mammalian central nervous system: inhibitory mechanisms and strategies for repair

1.1 Abstract

In the injured adult mammalian central nervous system (CNS), severed axons fail to undergo spontaneous regeneration. This limited regenerative capacity leads to permanent neurological deficits, such as paralysis following spinal cord injury, and cognitive impairment following traumatic brain injury or stroke. A large body of work has established that neuron intrinsic and extrinsic mechanisms pose barriers to efficient CNS repair. The intrinsic growth potential of injured CNS neurons is extremely poor. In addition, inhibitory molecules expressed by injured CNS tissue complex with neuronal surface receptors to prevent regenerative growth of axons. The majority of the work in the field of CNS regeneration has focused on antagonizing inhibitory mechanisms and stimulating intrinsic growth programs in an effort to identify key molecular targets that may be manipulated therapeutically to promote functional recovery. Recently, a number of studies reported that, under certain conditions, barriers to CNS repair can be surmounted by the induction of a local immune response after injury. A deeper understanding of the cellular and molecular basis of immune-mediated neurorepair may lead to the identification of specific biochemical pathways that can be targeted to promote regeneration following nervous system injury or disease.

1.2 The Limited Regenerative Capacity of the CNS

Spinal cord injury is a devastating form of CNS injury that typically results in lifelong neurological deficits. Recorded incidences of spinal cord injury and attempts at treatment date back thousands of years to Ancient Greece. While advances in modern medicine have extended the life span of spinal cord injury patients, the extent of functional recovery remains extremely limited. In the early 20th century, work by Santiago Ramón Y Cajal provided the first insights into the limited regenerative capacity of the CNS. Cajal observed that injured CNS axons can extend processes into a peripheral nerve graph (Tello, 1907), suggesting that the CNS environment is inhibitory towards regenerative growth. Additional grafting experiments by Albert Aguayo in the 1980s confirmed these findings (Richardson et al., 1980). Subsequent studies in the last several decades have identified molecular mechanisms that contribute to growth inhibition, and revealed additional barriers to repair, such as the poor intrinsic growth potential of injured CNS neurons.

Spontaneous regeneration of severed axons can occur in the peripheral nervous system (PNS). Several differences between the extrinsic environment of the PNS and CNS might help explain their differing regenerative capacities. Axons in both the PNS and CNS are enwrapped with myelin sheaths, allowing for rapid propagation of action potentials and metabolic support of axons. In the PNS, axons are myelinated by Schwann cells. Following injury, Schwann cells perform many tasks, including secreting factors to promote cell survival, directing axon regeneration, and remyelinating axons (Brosius Lutz and Barres, 2014). Importantly, they also help recruit macrophages to clear away myelin debris, highlighting a beneficial aspect of the immune system in promoting nervous system repair (Gaudet et al., 2011). Oligodendrocytes (OLs) are the myelinating cells of the CNS. In contrast to the PNS, OLs in the CNS do little to promote axon regeneration. Myelin debris from damaged OLs in the CNS is not well cleared (George and Griffin, 1994). Damaged OLs express multiple growth inhibitory ligands which complex with axonal surface receptors to inhibit sprouting and regenerative growth (Giger et al., 2008). Rather than helping to clear myelin debris, macrophages exacerbate cell death and damage (Gaudet et al., 2011). In addition to OLs, astrocytes in the CNS become reactive following injury, secreting growth inhibitory ligands such as chondroitin sulfate proteoglycans (CSPGs) (Morgenstern et al., 2002). Furthermore, reactive astrocytes form a glial scar at the site of injury which poses a physical barrier towards regenerative growth.

The intrinsic growth potential of adult CNS neurons is very poor. Neonatal rat retinal ganglion cells (RGCs) undergo a profound loss of intrinsic axon growth ability (Goldberg et al., 2002), and injured RGC axons in adult rodents do not normally regenerate. However, manipulating growth promoting pathways in RGCs has proven a successful method for stimulating regenerative growth (Leibinger et al., 2009, Belin et al., 2015). For example, genetic deletion of phosphatase and tensin homolog (PTEN) in RGCs prior to optic nerve crush injury results in robust regeneration distal to the injury site (Park et al., 2008). PTEN is an upstream inhibitor of several growth promoting signaling molecules, such as mTOR complex 1 (mTORC1), a serine-threonine protein kinase that regulates protein translation and promotes cell growth (Maehama and Dixon, 1998, Gingras et al., 2001). The enhanced regeneration observed with PTEN deletion is abolished by treatment with the mTORC1 inhibitor rapamycin (Park et al., 2008). Manipulation of members of the Krüppel-like factor (KLF) family of transcription factors in RGCs also enables axon regeneration. KLF4 and KLF9 suppress, and KLF6 and KLF7 enhance RGC axon growth (Moore et al., 2009). Extensive work by Mark Tuszynski's laboratory has shown that increasing levels of neurtrophic factors following CNS injury, through infusion or gene therapy, is another viable strategy for stimulating regenerative growth (Hollis and Tuszynski, 2011, Blesch et al., 2012) Collectively, the poor intrinsic growth capability of injured CNS axons, combined with the growth inhibitory environment of CNS tissue results in a severely limited regenerative capacity in the injured adult mammalian CNS.

1.3 CNS Regeneration Inhibitors and Their Receptors

The growth inhibitory environment of injured adult mammalian CNS tissue constitutes a major barrier to robust axonal outgrowth and functional recovery following trauma or disease. CNS tissue is resident to a large and diverse array of inhibitory molecules, including the prototypic myelin-associated inhibitors (MAIs) NogoA, oligodendrocyte myelin glycoprotein (OMgp), and myelin-associated glycoprotein (MAG), and the astrocyte-secreted CSPGs. These structurally diverse molecules strongly inhibit neurite outgrowth *in vitro*, and have been most extensively studied in the context of injured brain and spinal cord *in vivo*.

NogoA

NogoA is a membrane-associated protein that belongs to the reticulon family (GrandPre et al., 2000). Originally identified as a neurite growth inhibitory "activity" enriched in a spinal cord white matter fraction (Caroni et al., 1988, Caroni and Schwab, 1988), three laboratories described the molecular identity of Nogo-A more than 15 years ago (Chen et al., 2000, GrandPre et al., 2000, Prinjha et al., 2000). NogoA is expressed by many cell types, though its expression is highest in OLs and principal neurons in brain regions with a heightened degree of network plasticity, including the hippocampus and neocortex (Huber et al., 2002, Zhang et al., 2014). NogoA harbors at least two distinct growth inhibitory motifs, Nogo-66 (Fournier et al., 2001) and NogoΔ20 (Oertle et al., 2003). In the injured spinal cord, acute antibody blockade of NogoA promotes axonal sprouting and is associated with improved behavioral outcomes (Merkler et al., 2001, Liebscher et al., 2005). Nogo66 receptors include the Nogo receptor (NgR) family member NgR1 (Fournier et al., 2001), and paired Ig-like receptor B (PirB) (Atwal et al., 2008). *In vitro* studies showed that blockade of NgR1 and PirB attenuates Nogo-66 or myelin-mediated inhibition of neurite outgrowth (Atwal et al., 2008). Loss of NgR1 *in vivo* does not result in enhanced regenerative growth of the mouse optic nerve (Dickendesher et al., 2012) or spinal cord (Zheng et al., 2005), though this finding is contested by another study that reported enhanced optic nerve regeneration in a different *NgR1* mutant mouse (Wang et al., 2011). Further studies are needed to assess the contribution of PirB to growth inhibition *in vivo*. The NogoΔ20 domain of NogoA does not interact with PirB or members of the Nogo receptor family. A recent study identified sphingosine 1 phosphate receptor 2 (S1PR2) as a novel receptor for NogoΔ20 that participates in neurite outgrowth inhibition *in vtiro* (Kempf et al., 2014).

OMgp

OMgp is a 110-kDa leucine-rich repeat protein linked to the cell membrane by a glycosylphosphatidylinositol (GPI)-anchor. OMgp is expressed by OLs and neurons in the CNS (Vourc'h et al., 2003) and also found in astrocytes (Zhang et al., 2014). Two independent studies identified OMgp as a potent growth inhibitory molecule enriched in CNS myelin (Kottis et al., 2002, Wang et al., 2002). Similar to Nogo66, OMgp interacts with both NgR1 and PirB (Fournier et al., 2001, Wang et al., 2002, Atwal et al., 2008, Filbin, 2008). Despite the inhibitory activity of OMgp towards neurite outgrowth *in vitro*, studies with two different OMgp knockout mice did not show any significant regeneration in the corticospinal tract following spinal cord injury (Ji et al., 2008, Lee et al., 2010), though one of these studies did observe enhanced growth of serotonergic and dorsal column sensory axons (Ji et al., 2008).

MAG

The neurite outgrowth inhibitory properties of MAG were discovered independently by the laboratories of Marie Filbin (Mukhopadhyay et al., 1994) and Peter Braun (McKerracher et al., 1994) more than 20 years ago. MAG is a type-1 transmembrane protein and a prominent member of the family of sialic acid-binding Ig superfamily (siglec) proteins. MAG is expressed by myelinating glia, Schwann cells in the periphery and OLs in the CNS. MAG is abundant in the CNS and is enriched in Schmidt-Lanterman incisures and the periaxonal membrane of myelin sheath, allowing for complexes with receptors to form on the axonal surface (Trapp et al., 1989). Several receptors for MAG have been identified including the gangliosides GD1a and GT1b (Yang et al., 1996), NgR1 (Domeniconi et al., 2002, Liu et al., 2002), NgR2 (Venkatesh et al., 2005), paired Ig-like receptor B (PirB) (Atwal et al., 2008), β1-integrin (Goh et al., 2008), and low density lipoprotein receptor-related protein 1 (LRP1). Except for the interaction with LRP1, MAG binds to its neuronal receptors in a sialic acid-dependent manner (Robak et al., 2009, Stiles et al., 2013). *In vivo*, loss of MAG enhances compensatory sprouting of corticospinal and raphespinal serotonergic axons, but does not lead to enhanced regenerative growth following spinal cord injury (Cafferty et al., 2010, Lee et al., 2010). Surprisingly, the combined loss of MAG, NogoA, and OMgp is not sufficient to promote regenerative growth of injured axons following spinal cord injury, as mice lacking *NogoA*, *MAG*, and *OMgp* (*NMO*-mice) showed no significant regeneration of injured corticospinal or raphespinal serotonergic axons (Lee et al., 2010). However, this finding remains somewhat controversial, as another study reported significant regeneration of injured spinal cord axons in *NMO*- mice (Cafferty et al., 2010). Overall, these *in vivo* findings suggest that manipulation of MAI inhibition by itself is not sufficient to promote robust functional repair following CNS injury.

CSPGs

Another prominent group of CNS regeneration inhibitors, chondroitin sulfate proteoglycans (CSPGs), are extracellular matrix (ECM) proteoglycans consisting of a protein core with covalently attached glycosaminoglycan (GAG) side chains (Properzi et al., 2003). CSPGs are secreted by astrocytes, neurons, and OLs (Ogawa et al., 2001), and they are strongly enriched at the glial scar after CNS injury where they inhibit regenerative growth and restrict plasticity (Bradbury et al., 2002, Morgenstern et al., 2002, Silver and Miller, 2004). Degradation of CSPGs using the enzyme chondroitinase ABC (ChABC) promotes compensatory sprouting and functional recovery in the injured rodent spinal cord (Bradbury et al., 2002). A number of neuronal surface receptors bind CSPGs and inhibit neurite outgrowth *in vitro*, including NgR1, NgR3, leukocyte common antigen-related protein (LAR), and its homolog receptor protein tyrosine phosphatase sigma (RPTPσ) (Shen et al., 2009, Fisher et al., 2011, Dickendesher et al., 2012). Studies with *LAR* mutant mice and *RPTPσ* mutant mice revealed enhanced regenerative growth of injured spinal cord axons (Fry et al., 2010, Xu et al., 2015). The Nogo receptor family members provide a molecular link between the two major groups of CNS inhibitors, MAIs and CSPGs, and therefore may be promising therapeutic targets to promote CNS repair. *In vivo* regeneration studies with mice lacking multiple CSPG receptors are the focus of the second chapter of this dissertation.

1.4 Immune-Mediated Neurorepair

Despite the inhibitory nature of adult CNS tissue, a number of investigators have observed that, under certain conditions, barriers of CNS regeneration are surmounted by the induction of a local immune response (David et al., 1990, Richardson and Lu, 1994, Donnelly and Popovich, 2008, Benowitz and Popovich, 2011). Hence, inflammation induced near the cell body of injured dorsal root ganglion (DRG) neurons (Lu and Richardson, 1991) or retinal ganglion cells (RGCs) (Leon et al., 2000, Fischer et al., 2001) can activate endogenous repair mechanisms, enhance neuroprotection, and promote axonal regeneration. The therapeutic potential of immune-mediated neurorepair is underscored by the observation that axonal growth is even more effective when inflammation is initiated several days after the insult (Yin et al., 2003). While the ability of the immune system to promote regeneration was discovered over 15 years ago, the underlying molecular and cellular mechanisms are poorly understood. A deeper understanding of these mechanisms may lead to the identification of specific biochemical pathways that can be targeted to promote regeneration following nervous system injury or disease.

Overview of the Innate Immune System

The innate immune system provides a rapid and generic immune response to defend the body against invading pathogens. This is unlike the adaptive immune system, which provides highly specialized responses to specific pathogens and generates a long-term immunological memory. The innate immune system consists of several different types of white blood cells, or leukocytes. These include: 1) phagocytic cells such as monocytes, macrophages, neutrophils, and dendritic cells (DCs), 2) Natural killer cells, 3) mast cells and 4) basophil and eosinophil granulocytes. Cells of the innate immune system are found circulating in the blood, and, in the case of macrophages and DCs, in various tissue-resident populations (Lech et al., 2012). In the CNS, microglia are the primary tissue-resident immune cell. While micrgolia share several properties with cells of the monocyte/macrophage lineage, they are a distinct cell type, originating from the primitive yolk sac, and not from the hematopoietic stem cell lineage (Salter and Beggs, 2014). In addition to their immunological function, microglia have recently been shown to play important roles in the development and refinement of synaptic connections of neuronal networks (Bilimoria and Stevens, 2014).

The cells of the innate immune system express surface pattern-recognition receptors (PRRs) which recognize and respond to common molecular patterns on invading pathogens, so-called pathogen-associated molecular patterns (PAMPs). PRRs also recognize host-derived danger-associated molecular patterns (DAMPs) which are released near sites of tissue damage or injury (Tang et al., 2012). Binding of PAMPs or DAMPs to PRRs on tissue-resident macrophages stimulates the release of cytokines and chemokines, generating an inflammatory response in the tissue and attracting additional blood-derived immune cells, such as neutrophils and monocytes, to the site of inflammation (Newton and Dixit, 2012). Additionally, binding of PAMPs to PRRs on phagocytic cells results in phagocytosis and destruction of invading pathogens (Kapetanovic and Cavaillon, 2007). The influx of blood-derived immune cells into inflamed tissue helps the resident-immune cells to destroy invading pathogens, or delay them long enough for the adaptive immune system to mount a response. Additionally, activation of the innate immune system can help to repair damage associated with injury or infection, as discussed below.

Positive and Negative Consequences of Inflammation in the CNS

The immune system and the nervous system are in constant dialogue, but details of how they are integrated and functionally cooperate in health and disease are only now being revealed. Activation of the innate immune system in the brain or spinal cord occurs not only in response to invading pathogens, but also in response to injury or chronic disease. Depending on the extent and nature of the inflammation that ensues, the innate immune response can have either negative (neurodestructive) or beneficial (neuroprotective) consequences (Gensel et al., 2009, Rivest, 2009, Lang et al., 2014). At sites of CNS injury, activated macrophages and microglia promote regeneration with concurrent neurotoxicity (Gensel et al., 2009). In some instances, innate immunity protects the CNS from further damage (Bsibsi et al., 2006, Glezer et al., 2006), while in others, excessive inflammation exacerbates damage and contributes to neurological dysfunction (Gonzalez-Scarano and Baltuch, 1999, Lehnardt et al., 2003). A great deal is known about the types of immune cells and factors that have detrimental effects in the brain (King et al., 2009, Ashhurst et al., 2014). Less is known about the immune pathways that promote the survival and regeneration of injured nerve cells (Yin et al., 2006, Muller et al., 2009, Vidal et al., 2013). A key question is whether the neurotoxic effects and the pro-regenerative effects of neuroinflammation can be dissociated at the molecular level. This is an important pre-requisite for any strategies aimed at targeting and harnessing immune-based repair mechanisms.

Immune-mediated regeneration in the rodent optic nerve

A well-established animal model to study neuronal responses to CNS injury is retro-orbital crush injury to the optic nerve in adult mice or rats (Berry et al., 2008). Following axonal injury, the majority of RGCs die within a week (Levin, 1999, Lukas et al., 2009), and only a few subtypes survive (Duan et al., 2015). RGCs that survive the optic nerve crush are unable to extend their axons beyond the lesion site, resulting in permanent vision loss on the operated side (Berry et al., 2008). Intra-ocular (i.o.) injection of compounds or viral vectors into the vitreous of the eye allows direct access to RGC cell bodies, and has been used extensively to manipulate the growth behavior of injured RGC axons. Regenerative growth of severed RGC axons is greatly enhanced following induction of intraocular inflammation via lens trauma (Leon et al., 2000, Lorber et al., 2005), i.o. administration of crystallins (Fischer et al., 2008), oxidized galectin-1 (Okada et al., 2005), zymosan (a yeast cell wall extract) (Yin et al., 2003) or Pam3Cys (Hauk et al., 2010). Similar to the visual system, zymosan-elicited inflammation promotes axonal growth of DRG neurons transplanted into the adult rat spinal cord (Gensel et al., 2009). Moreover, injection of zymosan into DRGs combined with chondroitinaseABC treatment drives growth of injured sensory afferents into the spinal cord to a greater extent than either treatment alone (Steinmetz et al., 2005). In spite of numerous reports on the beneficial effects of inflammation on neural repair, relatively little is known about molecular mechanism of immune-mediated axonal regeneration.

Many Unanswered Questions for Immune-Mediated CNS Repair

Understanding the molecular mechanism of immune-mediated neurorepair is vital to understanding whether the pro-regenerative and neurotoxic aspects of neuroinflammation can be dissociated and, furthermore, manipulated therapeutically to promote functional recovery with minimal side effects. Since zymosan promotes robust CNS regeneration with simultaneous neurotoxicity, it is well suited as a tool for studying the mechanisms underlying immune-mediated neurorepair. Zymosan is a yeast cell wall extract composed of carbohydrates, proteins, and lipids (Di Carlo and Fiore, 1958). Zymosan contains highly conserved molecular structures that are associated with fungal pathogens not found in mammalian cells, and generates an experimental, sterile inflammation. PAMPs in zymosan engage several different PRRs, including toll-like receptor (TLR)2, complement receptor 3 (CR3), and the C-type lectin family members CLEC7A (dectin-1) and CLEC6A (dectin-2) (Frasnelli et al., 2005, Tsoni and Brown, 2008). Several different PAMP/PRR interactions have been implicated in zymosan-mediated immune activation. It will be important to identify which PPRs and signaling pathways are activated by zymosan to elicit axon regeneration following nervous system injury, and to determine whether these same biochemical pathways do or do not lead to concurrent neurotoxicity in the CNS.

Intraocular injection of zymosan causes a large and diverse population of immune cells to infiltrate the eye. The identification of the immune cells responsible for neural repair is complicated by the dynamic heterogeneity of the myeloid cell population. Evidence suggests involvement of blood-derived immune cells e.g. macrophages (Yin et al., 2003, Kigerl et al., 2009, Hawthorne and Popovich, 2011) and neutrophils (Kurimoto et al., 2013). In addition, retina-resident cells (Muller et al., 2007) have been shown to participate in inflammation-mediated neurorepair. At present, the use of cell surface typing to identify functionally distinct myeloid subsets *in situ* is at an early stage of development, and there has been no consensus in the field on how to classify myeloid cells *in vivo* (Leon et al., 2000, Lawrence and Natoli, 2011). *In vitro*, macrophages can be polarized to assume different functional roles. Subtypes of polarized macrophages include classically-activated macrophages (M1), which release pro-inflammatory cytokines and have neurotoxic properties (Gordon, 2003), and alternatively-activated macrophages (M2a, M2b, and M2c), that are associated with wound healing, tissue repair, and suppression of destructive immunity (Novak and Koh, 2013). Growing evidence suggests that, similar to macrophages, microglia can be differently activated and may exist in a dynamic continuum (Town et al., 2005, Zhou et al., 2012). It is currently unknown if analogous subtypes of myeloid cells exist *in vivo* and participate in inflammatory responses that elicit neurorepair pathways.

How activation of the innate immune system enables growth of injured RGC axons remains a mystery. PAMPs and DAMPs may engage PRRs expressed on retina-resident and blood-derived immune cells, activating them to produce pro-regenerative cytokines and growth factors, or to recruit a specific subtype of inflammatory cells with growth promoting properties. Immune cells may interact directly with RGCs and promote growth through a contact-mediated mechanism, or they may secret pro-regenerative cytokines and other growth factors which bind to receptors on RGCs to activate growth programs. Alternatively, neurons themselves may express PRRs that engage PAMPs and DAMPs, and thus, regenerate through a cell-autonomous mechanism, with inflammation playing a secondary role. Several growth factors and signaling pathways have been implicated in CNS axon regeneration (Muller et al., 2009, Belin et al., 2015, Duan et al., 2015). Whether any of these molecules are involved in immune-mediated neurorepair remains to be explored. Chapter three of this dissertation provides novel insights into the mechanisms of immune-mediated CNS repair.

1.5 Concluding Remarks

Many barriers oppose the regenerative growth and repair of injured CNS axons. MAIs and CSPGs potently inhibit neurite outgrowth *in vitro* through multiple overlapping receptor mechanisms. Based on studies with single and compound mutant mice, the contribution of these ligands and their receptors towards inhibiting regenerative growth *in vivo* has been underwhelming (Lee et al., 2010). However, the high degree of functional redundancy among growth inhibitory mechanisms could lead to genetic compensation in germline knockout mice, making it difficult to assess the contribution of individual ligands and receptors towards growth inhibition. For the development of therapeutic strategies, it will be necessary to determine whether acute manipulation of these molecules can be accomplished after injury without major adverse consequences. Since many CNS regeneration inhibitors play important physiological roles in the development, refinement, and maintenance of synaptic connections in the healthy brain (Mironova and Giger, 2013), manipulating these molecules to promote neurorepair could affect the integrity and function of intact neural networks.

Manipulation of the innate immune system is an attractive strategy to promote neurorepair in the injured CNS. Injection of zymosan into the eye following injury to the mouse optic nerve elicits a robust regenerative response, much greater than what is achieved by deletion of inhibitory ligands or their receptors. Importantly, zymosan has a large therapeutic window, as enhanced regeneration is observed when zymosan is injected up to three days after injury (Yin et al., 2003). Since zymosan promotes regeneration with concurrent toxicity, further studies are necessary to determine whether the beneficial and detrimental aspects of neuroinflammation can be uncoupled at the molecular level. My thesis provides novel insights into the molecular and cellular mechanisms that govern immune-mediated neuroprepair. The work described in the following chapters provides a strong platform for future studies aimed at understanding the cross talk between the immune system and the nervous system, and how this may be exploited to promote repair following injury or disease.

1.6 Acknowledgements

Portions of this Chapter have been published and are used here with permission:

Baldwin KT and Giger RJ (2015) Insights into the Physiological Role of CNS Regeneration Inhibitors. *Front. Mol. Neurosci. doi:* 10.3389/fnmol.2015.00023.

1.7 References

Ashhurst TM, Vreden CV, Niewold P, King NJ (2014) The plasticity of inflammatory monocyte responses to the inflamed central nervous system. Cellular immunology.

Atwal JK, Pinkston-Gosse J, Syken J, Stawicki S, Wu Y, Shatz C, Tessier-Lavigne M (2008) PirB is a functional receptor for myelin inhibitors of axonal regeneration. Science 322:967-970.

Belin S, Nawabi H, Wang C, Tang S, Latremoliere A, Warren P, Schorle H, Uncu C, Woolf CJ, He Z, Steen JA (2015) Injury-Induced Decline of Intrinsic Regenerative Ability Revealed by Quantitative Proteomics. Neuron.

Benowitz LI, Popovich PG (2011) Inflammation and axon regeneration. Curr Opin Neurol 24:577-583.

Berry M, Ahmed Z, Lorber B, Douglas M, Logan A (2008) Regeneration of axons in the visual system. Restor Neurol Neurosci 26:147-174.

Bilimoria PM, Stevens B (2014) Microglia function during brain development: New insights from animal models. Brain Res.

Blesch A, Fischer I, Tuszynski MH (2012) Gene therapy, neurotrophic factors and spinal cord regeneration. Handb Clin Neurol 109:563-574.

Bradbury EJ, Moon LD, Popat RJ, King VR, Bennett GS, Patel PN, Fawcett JW, McMahon SB (2002) Chondroitinase ABC promotes functional recovery after spinal cord injury. Nature 416:636-640.

Brosius Lutz A, Barres BA (2014) Contrasting the glial response to axon injury in the central and peripheral nervous systems. Dev Cell 28:7-17.

Bsibsi M, Persoon-Deen C, Verwer RW, Meeuwsen S, Ravid R, Van Noort JM (2006) Toll-like receptor 3 on adult human astrocytes triggers production of neuroprotective mediators. Glia 53:688-695.

Cafferty WB, Duffy P, Huebner E, Strittmatter SM (2010) MAG and OMgp synergize with Nogo-A to restrict axonal growth and neurological recovery after spinal cord trauma. J Neurosci 30:6825-6837.

Caroni P, Savio T, Schwab ME (1988) Central nervous system regeneration: oligodendrocytes and myelin as non-permissive substrates for neurite growth. Prog Brain Res 78:363-370.

Caroni P, Schwab ME (1988) Antibody against myelin-associated inhibitor of neurite growth neutralizes nonpermissive substrate properties of CNS white matter. Neuron 1:85-96.

Chen MS, Huber AB, van der Haar ME, Frank M, Schnell L, Spillmann AA, Christ F, Schwab ME (2000) Nogo-A is a myelin-associated neurite outgrowth inhibitor and an antigen for monoclonal antibody IN-1. Nature 403:434-439.

David S, Bouchard C, Tsatas O, Giftochristos N (1990) Macrophages can modify the nonpermissive nature of the adult mammalian central nervous system. Neuron 5:463-469.

Di Carlo FJ, Fiore JV (1958) On the composition of zymosan. Science 127:756-757.

Dickendesher TL, Baldwin KT, Mironova YA, Koriyama Y, Raiker SJ, Askew KL, Wood A, Geoffroy CG, Zheng B, Liepmann CD, Katagiri Y, Benowitz LI, Geller HM, Giger RJ (2012) NgR1 and NgR3 are receptors for chondroitin sulfate proteoglycans. Nat Neurosci.

Domeniconi M, Cao Z, Spencer T, Sivasankaran R, Wang K, Nikulina E, Kimura N, Cai H, Deng K, Gao Y, He Z, Filbin M (2002) Myelin-associated glycoprotein interacts with the Nogo66 receptor to inhibit neurite outgrowth. Neuron 35:283-290.

Donnelly DJ, Popovich PG (2008) Inflammation and its role in neuroprotection, axonal regeneration and functional recovery after spinal cord injury. Exp Neurol 209:378-388.

Duan X, Qiao M, Bei F, Kim IJ, He Z, Sanes JR (2015) Subtype-Specific Regeneration of Retinal Ganglion Cells following Axotomy: Effects of Osteopontin and mTOR Signaling. Neuron 85:1244-1256.

Filbin MT (2008) PirB, a second receptor for the myelin inhibitors of axonal regeneration Nogo66, MAG, and OMgp: implications for regeneration in vivo. Neuron 60:740-742.

Fischer D, Hauk TG, Muller A, Thanos S (2008) Crystallins of the beta/gamma-superfamily mimic the effects of lens injury and promote axon regeneration. Mol Cell Neurosci 37:471-479.

Fischer D, Heiduschka P, Thanos S (2001) Lens-injury-stimulated axonal regeneration throughout the optic pathway of adult rats. Exp Neurol 172:257-272.

Fisher D, Xing B, Dill J, Li H, Hoang HH, Zhao Z, Yang XL, Bachoo R, Cannon S, Longo FM, Sheng M, Silver J, Li S (2011) Leukocyte common antigen-related phosphatase is a functional receptor for chondroitin sulfate proteoglycan axon growth inhibitors. J Neurosci 31:14051-14066.

Fournier AE, GrandPre T, Strittmatter SM (2001) Identification of a receptor mediating Nogo-66 inhibition of axonal regeneration. Nature 409:341-346.

Frasnelli ME, Tarussio D, Chobaz-Peclat V, Busso N, So A (2005) TLR2 modulates inflammation in zymosan-induced arthritis in mice. Arthritis research & therapy 7:R370-379.

Fry EJ, Chagnon MJ, Lopez-Vales R, Tremblay ML, David S (2010) Corticospinal tract regeneration after spinal cord injury in receptor protein tyrosine phosphatase sigma deficient mice. Glia 58:423-433.

Gaudet AD, Popovich PG, Ramer MS (2011) Wallerian degeneration: gaining perspective on inflammatory events after peripheral nerve injury. J Neuroinflammation 8:110.

Gensel JC, Nakamura S, Guan Z, van Rooijen N, Ankeny DP, Popovich PG (2009) Macrophages promote axon regeneration with concurrent neurotoxicity. The Journal of neuroscience : the official journal of the Society for Neuroscience 29:3956-3968.

George R, Griffin JW (1994) Delayed macrophage responses and myelin clearance during Wallerian degeneration in the central nervous system: the dorsal radiculotomy model. Exp Neurol 129:225-236.
Giger RJ, Venkatesh K, Chivatakarn O, Raiker SJ, Robak L, Hofer T, Lee H, Rader C (2008) Mechanisms of CNS myelin inhibition: evidence for distinct and neuronal cell type specific receptor systems. Restorative neurology and neuroscience 26:97-115.
Gingras AC, Raught B, Sonenberg N (2001) Control of translation by the target of rapamycin proteins. Prog Mol Subcell Biol 27:143-174.
Glezer I, Lapointe A, Rivest S (2006) Innate immunity triggers oligodendrocyte progenitor reactivity and confines damages to brain injuries. FASEB J 20:750-752.
Goh EL, Young JK, Kuwako K, Tessier-Lavigne M, He Z, Griffin JW, Ming GL (2008) beta1-integrin mediates myelin-associated glycoprotein signaling in neuronal growth cones. Mol Brain 1:10.
Goldberg JL, Klassen MP, Hua Y, Barres BA (2002) Amacrine-signaled loss of intrinsic axon growth ability by retinal ganglion cells. Science 296:1860-1864.
Gonzalez-Scarano F, Baltuch G (1999) Microglia as mediators of inflammatory and degenerative diseases. Annu Rev Neurosci 22:219-240.
Gordon S (2003) Alternative activation of macrophages. Nature reviews Immunology 3:23-35.
GrandPre T, Nakamura F, Vartanian T, Strittmatter SM (2000) Identification of the Nogo inhibitor of axon regeneration as a Reticulon protein. Nature 403:439-444.
Hauk TG, Leibinger M, Muller A, Andreadaki A, Knippschild U, Fischer D (2010) Stimulation of axon regeneration in the mature optic nerve by intravitreal application of the toll-like receptor 2 agonist Pam3Cys. Invest Ophthalmol Vis Sci 51:459-464.
Hawthorne AL, Popovich PG (2011) Emerging concepts in myeloid cell biology after spinal cord injury. Neurotherapeutics : the journal of the American Society for Experimental NeuroTherapeutics 8:252-261.
Hollis ER, 2nd, Tuszynski MH (2011) Neurotrophins: potential therapeutic tools for the treatment of spinal cord injury. Neurotherapeutics 8:694-703.
Huber AB, Weinmann O, Brosamle C, Oertle T, Schwab ME (2002) Patterns of Nogo mRNA and protein expression in the developing and adult rat and after CNS lesions. J Neurosci 22:3553-3567.
Ji B, Case LC, Liu K, Shao Z, Lee X, Yang Z, Wang J, Tian T, Shulga-Morskaya S, Scott M, He Z, Relton JK, Mi S (2008) Assessment of functional recovery and axonal sprouting in oligodendrocyte-myelin glycoprotein (OMgp) null mice after spinal cord injury. Molecular and cellular neurosciences 39:258-267.
Kapetanovic R, Cavaillon JM (2007) Early events in innate immunity in the recognition of microbial pathogens. Expert Opin Biol Ther 7:907-918.
Kempf A, Tews B, Arzt ME, Weinmann O, Obermair FJ, Pernet V, Zagrebelsky M, Delekate A, Iobbi C, Zemmar A, Ristic Z, Gullo M, Spies P, Dodd D, Gygax D, Korte M, Schwab ME (2014) The sphingolipid receptor S1PR2 is a receptor for Nogo-a repressing synaptic plasticity. PLoS Biol 12:e1001763.
Kigerl KA, Gensel JC, Ankeny DP, Alexander JK, Donnelly DJ, Popovich PG (2009) Identification of two distinct macrophage subsets with divergent effects causing either neurotoxicity or regeneration in the injured mouse spinal cord. J Neurosci 29:13435-13444.

King IL, Dickendesher TL, Segal BM (2009) Circulating Ly-6C+ myeloid precursors migrate to the CNS and play a pathogenic role during autoimmune demyelinating disease. Blood 113:3190-3197.
Kottis V, Thibault P, Mikol D, Xiao ZC, Zhang R, Dergham P, Braun PE (2002) Oligodendrocyte-myelin glycoprotein (OMgp) is an inhibitor of neurite outgrowth. J Neurochem 82:1566-1569.
Kurimoto T, Yin Y, Habboub G, Gilbert HY, Li Y, Nakao S, Hafezi-Moghadam A, Benowitz LI (2013) Neutrophils express oncomodulin and promote optic nerve regeneration. The Journal of neuroscience : the official journal of the Society for Neuroscience 33:14816-14824.
Lang BT, Wang J, Filous AR, Au NP, Ma CH, Shen Y (2014) Pleiotropic molecules in axon regeneration and neuroinflammation. Exp Neurol 258C:17-23.
Lawrence T, Natoli G (2011) Transcriptional regulation of macrophage polarization: enabling diversity with identity. Nature reviews Immunology 11:750-761.
Lech M, Grobmayr R, Weidenbusch M, Anders HJ (2012) Tissues use resident dendritic cells and macrophages to maintain homeostasis and to regain homeostasis upon tissue injury: the immunoregulatory role of changing tissue environments. Mediators Inflamm 2012:951390.
Lee JK, Geoffroy CG, Chan AF, Tolentino KE, Crawford MJ, Leal MA, Kang B, Zheng B (2010) Assessing spinal axon regeneration and sprouting in Nogo-, MAG-, and OMgp-deficient mice. Neuron 66:663-670.
Lehnardt S, Massillon L, Follett P, Jensen FE, Ratan R, Rosenberg PA, Volpe JJ, Vartanian T (2003) Activation of innate immunity in the CNS triggers neurodegeneration through a Toll-like receptor 4-dependent pathway. Proc Natl Acad Sci U S A 100:8514-8519.
Leibinger M, Muller A, Andreadaki A, Hauk TG, Kirsch M, Fischer D (2009) Neuroprotective and axon growth-promoting effects following inflammatory stimulation on mature retinal ganglion cells in mice depend on ciliary neurotrophic factor and leukemia inhibitory factor. J Neurosci 29:14334-14341.
Leon S, Yin Y, Nguyen J, Irwin N, Benowitz LI (2000) Lens injury stimulates axon regeneration in the mature rat optic nerve. J Neurosci 20:4615-4626.
Levin LA (1999) Intrinsic survival mechanisms for retinal ganglion cells. European journal of ophthalmology 9 Suppl 1:S12-16.
Liebscher T, Schnell L, Schnell D, Scholl J, Schneider R, Gullo M, Fouad K, Mir A, Rausch M, Kindler D, Hamers FP, Schwab ME (2005) Nogo-A antibody improves regeneration and locomotion of spinal cord-injured rats. Ann Neurol 58:706-719.
Liu BP, Fournier A, GrandPre T, Strittmatter SM (2002) Myelin-associated glycoprotein as a functional ligand for the Nogo-66 receptor. Science 297:1190-1193.
Lorber B, Berry M, Logan A (2005) Lens injury stimulates adult mouse retinal ganglion cell axon regeneration via both macrophage- and lens-derived factors. Eur J Neurosci 21:2029-2034.
Lu X, Richardson PM (1991) Inflammation near the nerve cell body enhances axonal regeneration. J Neurosci 11:972-978.
Lukas TJ, Wang AL, Yuan M, Neufeld AH (2009) Early cellular signaling responses to axonal injury. Cell communication and signaling : CCS 7:5.

Maehama T, Dixon JE (1998) The tumor suppressor, PTEN/MMAC1, dephosphorylates the lipid second messenger, phosphatidylinositol 3,4,5-trisphosphate. The Journal of biological chemistry 273:13375-13378.
McKerracher L, David S, Jackson DL, Kottis V, Dunn RJ, Braun PE (1994) Identification of myelin-associated glycoprotein as a major myelin-derived inhibitor of neurite growth. Neuron 13:805-811.
Merkler D, Metz GA, Raineteau O, Dietz V, Schwab ME, Fouad K (2001) Locomotor recovery in spinal cord-injured rats treated with an antibody neutralizing the myelin-associated neurite growth inhibitor Nogo-A. The Journal of neuroscience : the official journal of the Society for Neuroscience 21:3665-3673.
Mironova YA, Giger RJ (2013) Where no synapses go: gatekeepers of circuit remodeling and synaptic strength. Trends Neurosci 36:363-373.
Moore DL, Blackmore MG, Hu Y, Kaestner KH, Bixby JL, Lemmon VP, Goldberg JL (2009) KLF family members regulate intrinsic axon regeneration ability. Science 326:298-301.
Morgenstern DA, Asher RA, Fawcett JW (2002) Chondroitin sulphate proteoglycans in the CNS injury response. Prog Brain Res 137:313-332.
Mukhopadhyay G, Doherty P, Walsh FS, Crocker PR, Filbin MT (1994) A novel role for myelin-associated glycoprotein as an inhibitor of axonal regeneration. Neuron 13:757-767.
Muller A, Hauk TG, Fischer D (2007) Astrocyte-derived CNTF switches mature RGCs to a regenerative state following inflammatory stimulation. Brain : a journal of neurology 130:3308-3320.
Muller A, Hauk TG, Leibinger M, Marienfeld R, Fischer D (2009) Exogenous CNTF stimulates axon regeneration of retinal ganglion cells partially via endogenous CNTF. Molecular and cellular neurosciences 41:233-246.
Newton K, Dixit VM (2012) Signaling in innate immunity and inflammation. Cold Spring Harb Perspect Biol 4.
Novak ML, Koh TJ (2013) Macrophage phenotypes during tissue repair. Journal of leukocyte biology 93:875-881.
Oertle T, van der Haar ME, Bandtlow CE, Robeva A, Burfeind P, Buss A, Huber AB, Simonen M, Schnell L, Brosamle C, Kaupmann K, Vallon R, Schwab ME (2003) Nogo-A inhibits neurite outgrowth and cell spreading with three discrete regions. The Journal of neuroscience : the official journal of the Society for Neuroscience 23:5393-5406.
Ogawa T, Hagihara K, Suzuki M, Yamaguchi Y (2001) Brevican in the developing hippocampal fimbria: differential expression in myelinating oligodendrocytes and adult astrocytes suggests a dual role for brevican in central nervous system fiber tract development. J Comp Neurol 432:285-295.
Okada T, Ichikawa M, Tokita Y, Horie H, Saito K, Yoshida J, Watanabe M (2005) Intravitreal macrophage activation enables cat retinal ganglion cells to regenerate injured axons into the mature optic nerve. Experimental neurology 196:153-163.
Park KK, Liu K, Hu Y, Smith PD, Wang C, Cai B, Xu B, Connolly L, Kramvis I, Sahin M, He Z (2008) Promoting axon regeneration in the adult CNS by modulation of the PTEN/mTOR pathway. Science 322:963-966.
Prinjha R, Moore SE, Vinson M, Blake S, Morrow R, Christie G, Michalovich D, Simmons DL, Walsh FS (2000) Inhibitor of neurite outgrowth in humans. Nature 403:383-384.

Properzi F, Asher RA, Fawcett JW (2003) Chondroitin sulphate proteoglycans in the central nervous system: changes and synthesis after injury. Biochem Soc Trans 31:335-336.
Richardson PM, Lu X (1994) Inflammation and axonal regeneration. Journal of neurology 242:S57-60.
Richardson PM, McGuinness UM, Aguayo AJ (1980) Axons from CNS neurons regenerate into PNS grafts. Nature 284:264-265.
Rivest S (2009) Regulation of innate immune responses in the brain. Nature reviews Immunology 9:429-439.
Robak LA, Venkatesh K, Lee H, Raiker SJ, Duan Y, Lee-Osbourne J, Hofer T, Mage RG, Rader C, Giger RJ (2009) Molecular basis of the interactions of the Nogo-66 receptor and its homolog NgR2 with myelin-associated glycoprotein: development of NgROMNI-Fc, a novel antagonist of CNS myelin inhibition. The Journal of neuroscience : the official journal of the Society for Neuroscience 29:5768-5783.
Salter MW, Beggs S (2014) Sublime microglia: expanding roles for the guardians of the CNS. Cell 158:15-24.
Shen Y, Tenney AP, Busch SA, Horn KP, Cuascut FX, Liu K, He Z, Silver J, Flanagan JG (2009) PTPsigma is a receptor for chondroitin sulfate proteoglycan, an inhibitor of neural regeneration. Science 326:592-596.
Silver J, Miller JH (2004) Regeneration beyond the glial scar. Nat Rev Neurosci 5:146-156.
Steinmetz MP, Horn KP, Tom VJ, Miller JH, Busch SA, Nair D, Silver DJ, Silver J (2005) Chronic enhancement of the intrinsic growth capacity of sensory neurons combined with the degradation of inhibitory proteoglycans allows functional regeneration of sensory axons through the dorsal root entry zone in the mammalian spinal cord. The Journal of neuroscience : the official journal of the Society for Neuroscience 25:8066-8076.
Stiles TL, Dickendesher TL, Gaultier A, Fernandez-Castaneda A, Mantuano E, Giger RJ, Gonias SL (2013) LDL receptor-related protein-1 is a sialic-acid-independent receptor for myelin-associated glycoprotein that functions in neurite outgrowth inhibition by MAG and CNS myelin. J Cell Sci 126:209-220.
Tang D, Kang R, Coyne CB, Zeh HJ, Lotze MT (2012) PAMPs and DAMPs: signal 0s that spur autophagy and immunity. Immunol Rev 249:158-175.
Tello F (1907) La regeneration dans les voies optiques. Trab Lab Invest Biol Univ Madr 5:237-248.
Town T, Nikolic V, Tan J (2005) The microglial "activation" continuum: from innate to adaptive responses. Journal of neuroinflammation 2:24.
Trapp BD, Andrews SB, Cootauco C, Quarles R (1989) The myelin-associated glycoprotein is enriched in multivesicular bodies and periaxonal membranes of actively myelinating oligodendrocytes. J Cell Biol 109:2417-2426.
Tsoni SV, Brown GD (2008) beta-Glucans and dectin-1. Ann N Y Acad Sci 1143:45-60.
Venkatesh K, Chivatakarn O, Lee H, Joshi PS, Kantor DB, Newman BA, Mage R, Rader C, Giger RJ (2005) The Nogo-66 receptor homolog NgR2 is a sialic acid-dependent receptor selective for myelin-associated glycoprotein. The Journal of neuroscience : the official journal of the Society for Neuroscience 25:808-822.
Vidal PM, Lemmens E, Dooley D, Hendrix S (2013) The role of "anti-inflammatory" cytokines in axon regeneration. Cytokine Growth Factor Rev 24:1-12.

Vourc'h P, Dessay S, Mbarek O, Marouillat Vedrine S, Muh JP, Andres C (2003) The oligodendrocyte-myelin glycoprotein gene is highly expressed during the late stages of myelination in the rat central nervous system. Brain Res Dev Brain Res 144:159-168.
Wang KC, Koprivica V, Kim JA, Sivasankaran R, Guo Y, Neve RL, He Z (2002) Oligodendrocyte-myelin glycoprotein is a Nogo receptor ligand that inhibits neurite outgrowth. Nature 417:941-944.
Wang X, Duffy P, McGee AW, Hasan O, Gould G, Tu N, Harel NY, Huang Y, Carson RE, Weinzimmer D, Ropchan J, Benowitz LI, Cafferty WB, Strittmatter SM (2011) Recovery from chronic spinal cord contusion after Nogo receptor intervention. Ann Neurol 70:805-821.
Xu B, Park D, Ohtake Y, Li H, Hayat U, Liu J, Selzer ME, Longo FM, Li S (2015) Role of CSPG receptor LAR phosphatase in restricting axon regeneration after CNS injury. Neurobiol Dis 73:36-48.
Yang LJ, Zeller CB, Shaper NL, Kiso M, Hasegawa A, Shapiro RE, Schnaar RL (1996) Gangliosides are neuronal ligands for myelin-associated glycoprotein. Proc Natl Acad Sci U S A 93:814-818.
Yin Y, Cui Q, Li Y, Irwin N, Fischer D, Harvey AR, Benowitz LI (2003) Macrophage-derived factors stimulate optic nerve regeneration. The Journal of neuroscience : the official journal of the Society for Neuroscience 23:2284-2293.
Yin Y, Henzl MT, Lorber B, Nakazawa T, Thomas TT, Jiang F, Langer R, Benowitz LI (2006) Oncomodulin is a macrophage-derived signal for axon regeneration in retinal ganglion cells. Nat Neurosci 9:843-852.
Zhang Y, Chen K, Sloan SA, Bennett ML, Scholze AR, O'Keeffe S, Phatnani HP, Guarnieri P, Caneda C, Ruderisch N, Deng S, Liddelow SA, Zhang C, Daneman R, Maniatis T, Barres BA, Wu JQ (2014) An RNA-sequencing transcriptome and splicing database of glia, neurons, and vascular cells of the cerebral cortex. J Neurosci 34:11929-11947.
Zheng B, Atwal J, Ho C, Case L, He XL, Garcia KC, Steward O, Tessier-Lavigne M (2005) Genetic deletion of the Nogo receptor does not reduce neurite inhibition in vitro or promote corticospinal tract regeneration in vivo. Proc Natl Acad Sci U S A 102:1205-1210.
Zhou X, Spittau B, Krieglstein K (2012) TGFbeta signalling plays an important role in IL4-induced alternative activation of microglia. Journal of neuroinflammation 9:210.

CHAPTER II:

Contribution of CNS Regeneration Inhibitors to Growth Inhibition *in vivo*

2.1 Abstract

In the adult mammalian central nervous system (CNS), chondroitin sulfate proteoglycans (CSPGs) and myelin-associated inhibitors (MAIs) stabilize neuronal structure and restrict compensatory sprouting following injury. The Nogo receptor family members NgR1 and NgR2 bind to MAIs and have been implicated in neuronal inhibition. Recent work from our laboratory revealed that NgR1 and NgR3 bind with high affinity to the sugar moiety of CSPGs and participate in CSPG inhibition in cultured neurons. Here we show that Nogo receptor triple mutants ($NgR123^{-/-}$), but not single mutants, display enhanced axonal regeneration following retro-orbital optic nerve crush injury. The combined loss of NgR1 and NgR3 ($NgR13^{-/-}$), but not NgR1 and NgR2 ($NgR12^{-/-}$), is sufficient to mimic the $NgR123^{-/-}$ regeneration phenotype. Regeneration in $NgR13^{-/-}$ mice is further enhanced by simultaneous ablation of RPTPσ, a known CSPG receptor. In growth-enabled RGCs, loss of multiple CSPG receptors greatly enhances regenerative growth. Collectively, these results identify NgR1 and NgR3 as functional receptors mediating CSPG inhibition *in vivo*, and demonstrate functional redundancy among CSPG and MAI receptors.

2.2 Introduction

In the adult mammalian CNS, structural neuronal plasticity is restricted by a number of extrinsic (environmental) and cell-intrinsic growth-inhibitory mechanisms (Liu et al., 2006; Park et al., 2008). While such mechanisms are believed to be important for stabilization of intricate networks of neuronal connectivity in CNS health, they also limit adaptive neuronal growth and sprouting following brain or spinal cord injury (SCI). Spontaneous repair following severe CNS injury is incomplete and commonly associated with permanent neurological deficits. Thus, a detailed understanding of the mechanisms that block neuronal growth and repair is of great interest, both biologically and clinically.

A large number of CNS inhibitory cues have been identified (Silver and Miller, 2004, Liu et al., 2006, Winzeler et al., 2011). In experimental animal models of SCI, acute blockage of MAIs (Bregman et al., 1995, Li et al., 2004) or enzymatic degradation of CSPGs with chondroitinase ABC (Ch'aseABC) (Bradbury et al., 2002, Massey et al., 2006, Garcia-Alias and Fawcett, 2012) promotes neuronal sprouting and correlates with improved behavioral outcomes. The best characterized MAIs are the reticulon family member Nogo, myelin-associated glycoprotein (MAG), and oligodendrocyte myelin glycoprotein (OMgp) (Liu et al., 2006). Three isoforms of Nogo have been identified, all of which contain a 66 amino acid loop (Nogo66) that signals neuronal inhibition. Mechanistic studies identified the Nogo66 receptor-1 (NgR1) and paired immunoglobulin (Ig)-like receptor B (PirB) as functional receptors for MAIs (Fournier et al., 2001, Atwal et al., 2008). NgR1 and its close relative NgR2 show overlapping, yet distinct binding preferences toward MAIs. Nogo66 and OMgp bind selectively to NgR1 (Liu et al., 2006), while MAG associates with NgR1 and NgR2 (Venkatesh et al., 2005). NgR3 does not interact with Nogo, MAG, or OMgp. *In vitro*, loss of NgR1 renders neurons more resistant to

Nogo66-, MAG-, and OMgp-induced growth cone collapse, but not to longitudinal neurite outgrowth inhibition on substrate-bound inhibitors (Kim et al., 2004, Zheng et al., 2005, Chivatakarn et al., 2007). MAIs activate RhoA, RockII, and conventional isoforms of protein kinase C (PKC) to destabilize the neuronal cytoskeleton (Schweigreiter et al., 2004, Sivasankaran et al., 2004). Similar to NgR1, PirB supports binding of Nogo66, MAG, and OMgp. In culture, functional ablation of PirB promotes neurite outgrowth on substrate-bound MAIs and crude CNS myelin. Interestingly, the combined perturbation of PirB and NgR1 signaling leads to a further release of neurite outgrowth inhibition on crude CNS myelin, but not on recombinant Nogo66 or MAG (Atwal et al., 2008).

CSPGs are a diverse class of extracellular matrix molecules that influence axonal growth and guidance of developing neurons (Kantor et al., 2004). Following injury to the adult CNS, CSPG expression is upregulated and abundant in reactive astrocytes associated with glial scar tissue (Silver and Miller, 2004). CSPGs are comprised of a protein core with covalently attached glycosaminoglycan (GAG) side chains. CSPG inhibition is largely abrogated by bacterial Ch'aseABC, indicating that CS-GAGs are important for neuronal growth inhibition (Bradbury et al., 2002, Pizzorusso et al., 2002, Garcia-Alias and Fawcett, 2012). Similar to MAIs, CSPG-mediated inhibition depends on activation of RhoA and conventional PKCs (Powell et al., 2001, Schweigreiter et al., 2004, Sivasankaran et al., 2004). Mechanistic studies recently identified the receptor protein tyrosine phosphatase sigma (RPTPσ) as a high-affinity receptor for CSPGs (Shen et al., 2009). RPTPσ is a member of the leukocyte common antigen-related protein (LAR) family that also includes LAR and RPTPδ. RPTPσ binds to CS-GAG chains and the structurally related heparan sulfate (HS)-GAG chains via its first Ig-like domain (Aricescu et al., 2002, Shen et al., 2009). The association of RPTPσ with CS- and HS-GAGs critically depends on the presence of an evolutionarily conserved cluster of basic amino acid residues. Functional ablation of RPTPσ enhances neurite outgrowth in the presence of CSPGs *in vitro,* and, following CNS injury, promotes growth of sensory afferents (Shen et al., 2009), corticospinal tract axons (Fry et al., 2010), and retinal ganglion cell axons (Sapieha et al., 2005). The incomplete release of CSPG inhibition in RPTPσ-deficient neurons suggests the existence of additional mechanisms of CSPG inhibition.

Recent work from our laboratory revealed that NgR1 and NgR3 are receptors for CSPGs (Dickendesher et al., 2012). NgR1 and NgR3 bind directly and with high affinity to select types of CS-GAGs and operate as functionally redundant CSPG receptors. Loss of individual NgR family members is not sufficient to overcome CSPG inhibition *in vitro*; however, the combined loss of NgR1 and NgR3 leads to a significant release of CSPG inhibition. Here I describe the *in vivo* studies performed in mutant mice lacking various CSPG receptors individually or in combination.

2.3 Results

Regeneration is enhanced in *NgR123*$^{-/-}$ and *NgR13*$^{-/-}$ mice

In the adult mouse retina, NgR1, NgR2, and NgR3 are all strongly expressed in RGCs (**Figure 2.1a**). Retinal stratification (**Figure 2.1b**) and optic nerve myelination (**Figure 2.1c**) in *NgR123*$^{-/-}$ mice appear normal. To assess RGC axon targeting to the superior colliculus, the suprachiasmatic nucleus, and the lateral geniculate nucleus, the right eye of adult WT and *NgR123*$^{-/-}$ mice was injected with Alexa 594-conjugated Cholera Toxin β (CTB-red) tracer, and the left eye with Alexa 488-conjugated Cholera Toxin β (CTB-green) tracer. No defects in RGC axon central projections or target innervation were observed (**Figure 2.1d-f**). Thus, germline ablation of all three NgRs does not appear to compromise retinal stratification, optic nerve myelination, or RGC axonal pathfinding.

To assess whether NgRs contribute to the regenerative failure of injured CNS axons, we performed retro-orbital optic nerve crush injury in Nogo receptor single and compound mutant mice. Compared to injured wild-type controls, *NgR123*$^{-/-}$ mice show a modest but significant (*P*< 0.001, one-way ANOVA, Tukey's *post hoc*) increase in RGC axon regeneration (**Figure 2.2**). At two weeks post-injury, more GAP-43-positive fibers are observed at 0.2-1.0mm distal to the injury site in *NgR123*$^{-/-}$ mice compared to WT mice. Because NgR1 and NgR2 are known to associate with MAIs, the *NgR123*$^{-/-}$ regeneration phenotype may be a reflection of (i) decreased Nogo, MAG and OMgp inhibition, (ii) decreased CSPG inhibition, or (iii) a combination thereof. To address this issue, we directly compared regeneration of *NgR1*$^{-/-}$, *NgR2*$^{-/-}$, and *NgR3*$^{-/-}$ single mutants, as well as *NgR12*$^{-/-}$ and *NgR13*$^{-/-}$ double mutants, to *NgR123*$^{-/-}$ triple mutants. Loss of NgR1, NgR2, or NgR3 alone, or the combined loss of NgR1 and NgR2 (*NgR12*$^{-/-}$), does not result in substantially enhanced RGC axon regeneration compared to WT mice (**Figures 2.2, 2.3; Table 2.1**). However, *NgR13*$^{-/-}$ mice show a similar degree of axon regeneration as *NgR123*$^{-/-}$ mice. This suggests a novel role for NgR3 in signaling neuronal growth inhibition. When coupled with our neurite outgrowth studies *in vitro*, showing that NgR1 and NgR3 operate as functionally redundant CSPG receptors, this suggests that the optic nerve regeneration in *NgR13*$^{-/-}$ and *NgR123*$^{-/-}$ mice is at least in part a reflection of decreased CSPG inhibition.

As RPTPσ is expressed in adult RGCs (Sapieha et al., 2005), we examined whether the combined loss of NgR1 and NgR3 on an *RPTPσ*$^{-/-}$ background (*NgR13/RPTPσ*$^{-/-}$) results in a further increase of regenerating axons. Few regenerating axons were observed in *RPTPσ*$^{-/-}$ single mutants, with no significant difference compared to WT controls ($P > 0.05$). Compared to *NgR13*$^{-/-}$ double mutants, *NgR13/RPTPσ*$^{-/-}$ triple mutants show a further increase in the number of regenerating axons ($P < 0.001$, one-way ANOVA, Tukey's *post hoc*), suggesting a genetic interaction among these receptors (**Figures 2.2, 2.3; Table 2.1**).

In growth-enabled RGCs, loss of all NgRs greatly enhances optic nerve axon regeneration

An advantage of optic nerve regeneration studies is that the growth potential of RGCs can be sensitized by intraocular (i.o.) injection of the yeast cell wall extract zymosan, resulting in the release of RGC survival and growth-promoting factors, including oncomodulin (Yin et al., 2009), ciliary neurotrophic factor (CNTF), and leukemia inhibitory factor (LIF) (Leibinger et al., 2009). WT mice that receive i.o. zymosan show greatly enhanced regeneration of RGC axons, exceeding the regeneration observed in non-zymosan-treated *NgR123*$^{-/-}$ and *NgR13/RPTPσ*$^{-/-}$ mice (**Figure 2.2**). Importantly, *NgR123*$^{-/-}$ mice that receive i.o. zymosan show significantly more ($P < 0.05$, one-way ANOVA, Tukey's *post hoc*) regenerating axons than WT, *NgR1*$^{-/-}$, *NgR2*$^{-/-}$, *NgR3*$^{-/-}$, or *RPTPσ*$^{-/-}$ single mutants, as well as *NgR12*$^{-/-}$ double mutants, subjected to i.o. zymosan. *NgR13*$^{-/-}$ and *NgR123*$^{-/-}$ mice with i.o. zymosan show a similar regeneration phenotype. At several distances from the injury site, *NgR13/RPTPσ*$^{-/-}$ triple mutants with i.o. zymosan show a further increase in the number of regenerating axons compared to *NgR123*$^{-/-}$ mice with i.o. zymosan ($P < 0.05$, one-way ANOVA, Tukey's *post hoc*) (**Figures 2.2, 2.3; Table 2.1**).

In mice, optic nerve injury leads to the death of ~ 70% of RGCs by two weeks post-injury (**Figure 2.4**). The enhanced regeneration observed in *NgR123*$^{-/-}$ mice is not a result of increased RGC survival, as similar numbers of injury-induced RGC death were observed in WT and

NgR123$^{-/-}$ triple mutants. Intraocular zymosan administration partially protects RGCs from axotomy-induced cell death; however, the protective effect of zymosan is similar in WT and *NgR123*$^{-/-}$ mice (**Figure 2.4**). Consistent with the view that a decrease in RGC death is not sufficient to promote axonal regeneration, p53-deficient RGCs are more resistant to injury-induced cell death but fail to show enhanced regeneration (Park et al., 2008).

Combined Loss of MAI receptors does not enhance regenerative growth, even in growth-enabled RGCs

As discussed above, CNS regeneration inhibitors elicit growth inhibition through several overlapping receptor mechanisms. While the combined loss of *NgR1* and *NgR2* does not lead to enhanced regeneration **(Figure 2.3)**, the contribution of additional MAI receptors to growth inhibition *in vivo* is not known. PirB is a functional receptor for Nogo, MAG, and OMgp (Atwal et al., 2008). To determine whether PirB contributes to inhibition of regeneration *in vivo*, we performed optic nerve crush on *PirB*$^{-/-}$ mice (**Figure 2.5**). Loss of PirB alone did not enhance regeneration. Furthermore, the combined loss of *NgR1*, *NgR2*, and *PirB* (*NgR12/PirB*$^{-/-}$) did not improve regenerative growth, even with intraocular administration of zymosan (**Figure 2.5**). Another recently identified receptor for MAG is LDL receptor-related protein 1 (LRP1) (Stiles et al., 2013). Germline knockout of LRP1 is embryonic lethal, therefore to assess the contribution of LRP1 to growth inhibition *in vivo*, we depleted LRP1 from the retinas of *LRP1*$^{f/f}$ mice by injecting AAV2-GFP-Cre two weeks before optic nerve crush injury. Loss of LRP1 did not significantly enhance optic nerve regeneration (**Figure 2.5**).

2.4 Discussion

One of the main findings of this work is that NgR1 and NgR3 contribute to inhibition of regenerative growth *in vivo*. However, the relatively modest regenerative growth that results from loss of multiple CSPG receptors (NgR1, NgR3, and RPTPs) is unlikely to have functionally significant outcomes. Furthermore, loss of multiple MAI receptors (NgR1, NgR2, PirB) does not enhance regeneration *in vivo*. Collectively, these results show that, by itself, genetic deletion of multiple inhibitory mechanisms is insufficient to surmount the limited regenerative capacity of the CNS, and may not be a viable therapeutic option. However, the greatly enhanced regeneration that occurs by combining intraocular zymosan injection with loss of CSPG receptors suggests that manipulating extrinsic and intrinsic inhibitory mechanism concurrently may be an effective strategy for neurorepair.

Additive effects of manipulating extrinsic and intrinsic pathways

The mild regenerative growth observed in *NgR123*$^{-/-}$ and *NgR13/RPTPσ*$^{-/-}$ mice at two weeks post-injury, could be explained by compensatory mechanisms that arise in germline knockout mice. Perhaps acute blockade of multiple inhibitory mechanisms will have a more robust affect. Alternatively, the contribution of the inhibitory CNS environment to growth inhibition may be relatively minor. Our results are consistent with previous studies showing that expression of a dominant negative form of NgR1 in RGCs (Fischer et al., 2004a) or blocking of RhoA with C3 transferase (Fischer et al., 2004c) is not sufficient to promote substantial regeneration of severed optic nerve axons. Similarly, removal of one or several MAIs results in inconsistent and often poor regeneration in spinal cord-injured mice (Cafferty et al., 2010, Lee et al., 2010). Collectively, mouse genetic studies indicate that germline ablation of multiple growth-inhibitory ligands or receptors is not sufficient to promote robust and long-distance regeneration in different fiber tracts of the injured adult CNS.

However, combining genetic manipulations with activation of RGC intrinsic growth programs revealed a significant impact of environmental inhibitory signals on limiting axon regeneration. On an *NgR13*$^{-/-}$, *NgR123*$^{-/-}$, or *NgR13/RPTPσ*$^{-/-}$ background, i.o. zymosan injection results in significantly enhanced axonal growth distal to the injury site compared to WT, *NgR12*$^{-/-}$, *RPTPσ*$^{-/-}$, or *NgR12/PirB*$^{-/-}$ mutant mice with i.o. zymosan. While the additive effects of simultaneous release of growth-inhibitory mechanisms and activation of intrinsic growth programs have been reported (Fischer et al., 2004a, Kadoya et al., 2009) our data show that in growth-enabled RGCs, members of the NgR family and LAR family collaborate to negatively impact the number and length of regenerating axons following CNS injury.

Implications for experience-dependent neural plasticity

While it has been known for some time that MAIs and CSPGs share similar downstream signaling pathways (Schweigreiter et al., 2004, Sivasankaran et al., 2004), the level at which MAI and CSPG signaling cascades converge to regulate neuronal cytoskeletal dynamics has not yet been determined. Here we identify NgR1 and NgR3 as novel and functionally redundant CSPG receptors. We provide evidence that Nogo, MAG, OMgp, and CSPGs share receptor components and perhaps signal through related receptor complexes to block neuronal plasticity, sprouting, and axonal regeneration. In support of this idea, the myelin inhibitor Nogo-A shares structural and sequential similarities with neurocan, an inhibitory CSPG implicated in blocking neuronal regeneration (Shypitsyna et al., 2011), suggesting a common origin for two seemingly unrelated inhibitors of growth. The newly discovered connection between CSPGs and NgRs is not only relevant for neuronal repair, but may also provide a mechanistic explanation for why two seemingly unrelated manipulations, such as Ch'aseABC infusion into the mature visual cortex and germline ablation of NgR1 or Nogo, result in enhanced ocular dominance plasticity following monocular deprivation (Pizzorusso et al., 2002, McGee et al., 2005). Mounting evidence suggests that mechanisms that limit neuronal growth and plasticity following CNS injury and disease resemble those that negatively regulate neuronal growth and synaptic structure under physiological conditions (Lee et al., 2008, Zagrebelsky et al., 2010).

The identification of NgRs as shared receptors for MAIs and CSPGs provides new insights into how a diverse group of inhibitory cues regulates neuronal structure and function under physiological conditions and following injury. We propose that Nogo receptors are part of a multicomponent receptor system that serves as a signaling platform to initiate pathways that limit neuronal growth and increase structural stability of synapses. When combined with recent findings that NgR1and its ligands Nogo and OMgp influence synaptic transmission (Raiker (Raiker et al., 2010), experience-dependent network refinement (McGee et al., 2005), and spatial memory (Karlen et al., 2009), the present findings expand the function of these molecules beyond neural repair, and shed light on a vital part of the neuronal machinery that limits growth and plasticity in CNS health and disease

2.5 Methods

Transgenic mice: All animal handling and surgical procedures were performed in compliance with local and national animal care guidelines and approved by the University of Michigan Committee on Use and Care of Animals (UCUCA). *RPTPσ*$^{-/-}$, *NgR1*$^{-/-}$, *NgR2*$^{-/-}$ *PirB*$^{-/-}$, and *LRP1*$^{f/f}$ mice have been described (Zheng et al., 2005, Syken et al., 2006, Li et al., 2010). *NgR3*$^{-/-}$ germline mutants were generated by Lexicon Genetics and kindly provided by M. Greenberg (Harvard Medical School). NgR1 and NgR2 conditional mutants have been described elsewhere (Williams et al., 2008). NgR3 conditional knockout mice were generated by flanking exon2 with loxP sites. To generate germline deletion mutants, conditional knockouts were crossed with protamine-cre transgenic mice and then intercrossed with each other, or onto an *RPTPσ*$^{-/-}$ background, to generate double and triple mutants.

Optic nerve surgery: Adult mice (6-8 weeks of age) of either sex were anesthetized with an intraperitoneal injection of Ketamine (100mg/kg; Fort Dodge Animal Health) and Xylazine (10mg/kg; Akorn, Inc.). The optic nerve was exposed through an incision in the conjunctiva and compressed for 10 seconds with angle jeweler's forceps (Dumont #5; Fine Science Tools) at approximately 1mm behind the eyeball. Care was taken not to damage or rupture the ophthalmic artery. For intraocular injection of Zymosan, 5µl of a suspension (12.5µg/µl in sterile PBS; Sigma) was injected manually using a Hamilton syringe with a 30 gauge removable needle. Following optic nerve surgery, the operated eye was rinsed with sterile PBS and ophthalmic ointment was applied (Butler AHS). All surgeries were performed under aseptic conditions. Fourteen days after optic nerve injury, mice were given a lethal dose of anesthesia and perfused through the heart with PBS followed by ice-cold 4% paraformaldehyde (with the exception of mice used for electrophysiology studies). For deletion of LRP1 in *LRP1*$^{f/f}$ mouse RGCs, 2µl of AAV2-GFP (Vector Biolabs) was injected into the left eye and 2µl of AAV2-GFP-Cre (Vector Biolabs) was injected into the right eye, 14 days prior to optic nerve injury.

Immunohistochemistry: For immunohistochemical procedures, cryosections of adult retina were stained with anti-calbindin (Swant; 1:2500 dilution) or anti-calretinin (Swant; 1:2500 dilution), and then counterstained with Hoechst 33342 (1:30000 dilution). For retinal whole-mount immunostaining, eyes were post-fixed in 4% paraformaldehyde overnight at 4°C, and retinal "cups" were dissected out and fixed in 4% paraformaldehyde for 30 minutes at 4°C. Retinas were washed with PBS, blocked in 10% goat serum and 0.2% Triton X-100 for 1 hour, incubated with primary antibodies (anti-GFP, Invitrogen; anti-phospho-S6, Cell Signaling) for 1-2 days at 4°C, and washed with PBS. Following incubation with the appropriate Alexa Fluor-conjugated secondary antibodies (Invitrogen) overnight at 4°C and another round of washing with PBS, retinas were mounted onto slides for imaging. To assess axon density and myelination, optic nerves were embedded in epon and stained with Toluidine Blue. To assess retinal ganglion cell death at various time points following optic nerve injury, retinal sections were stained with anti-class III β-tubulin (TuJ1), and in some instances, with anti-active caspase-3 (Promega). For intraocular injections of anterograde tracer, 6-week-old mice received bilateral injections (2ml) of 1mg/ml Alexa 488- and Alexa 594-conjugated Cholera Toxin β (Invitrogen) in the left and right eye, respectively. Five days post-injection, mice were perfused transcardially, and their brains were dissected, post-fixed in 4% paraformaldehyde overnight, and cryoprotected in 30% sucrose overnight. Brain tissue was embedded in OCT Tissue-Tek Medium (Sakura Finetek) and coronal sections (50μm thickness) were imaged.To visualize regenerating axons in the injured optic nerve, eyes with optic nerves attached were dissected, post-fixed, and cryoprotected. Optic nerves were embedded and longitudinal sections (14μm thickness) were stained with anti-GAP-43 and/or anti-GFP. The appropriate Alexa Fluor-conjugated secondary antibodies (Invitrogen) were then used for fluorescent labeling. Images were acquired using an inverted microscope (IX71; Olympus) attached to a digital camera (DP72; Olympus).

Quantification and Statistical Analysis: To assess regenerative axonal growth, the number of GAP-43-positive axons at prespecified distances from the injury site was counted in at least three sections per nerve. These numbers were converted into the number of regenerating axons per nerve at various distances as described previously (Fischer et al., 2004a). All data were analyzed using one-way analysis of variance followed by Tukey's *post hoc* comparisons. All statistics were performed using GraphPad Prism 5.00 (GraphPad Software). Our finding that loss of all three NgRs elicits significant retinal ganglion cell regeneration is based on two independently generated data sets produced by two independent surgeons (K.T.B. and Y. Koriyama). Both data sets were analyzed separately and lead to the same conclusions (**Table 2.1**). In addition, no significant differences ($P > 0.05$) in axon regeneration following injury (with or without intraocular Zymosan injection) were observed between mice on three different genetic backgrounds (129, C57BL/6, BALB/c) (**Figure 2.6**).

2.6 Acknowledgments

Portions of this chapter have been published, and are used here with permission according to journal guidelines:

Dickendesher TL, Baldwin KT, Mironova YA, Koriyama Y, Raiker SJ, Askew KL, Wood A, Geoffroy CG, Zheng B, Liepmann CD, Katagiri Y, Benowitz LI, Geller HM, Giger RJ (2012) NgR1 and NgR3 are receptors for chondroitin sulfate proteoglycans. Nat Neurosci 15:703-712.

This work was supported by the Neuroscience Training Grant T32EY017878, the University of Michigan Rackham Merit Fellowship (Travis L. Dickendesher.), the Cellular and Molecular Biology Training Grant T32GM007315 (Katherine T. Baldwin and Yevgeniya A. Mironova), the National Research Service Award Ruth Kirschstein Fellowship F31NS061589 (Stephen J. Raiker.), the New York State Spinal Cord Injury Research Program, the Dr. Miriam and Sheldon G. Adelson Medical Foundation on Neural Repair and Rehabilitation, the US Department of Veterans Affairs Grant 1I01RX000229-01, the National Institute of Neurological Disorders and Stroke R56NS047333 (Roman J. Giger) and the National Eye Institute (Larry I. Benowitz). We thank Michel Tremblay for *RPTPσ*$^{-/-}$ mice; Michael Greenberg for *NgR3*$^{-/-}$ mice; Brian Bates, David Howland, and Mary L. Mercado for their assistance in the generation and initial analysis of *NgR123*$^{-/-}$ triple mutant mice.

2.7 Author Contributions

Travis L. Dickendesher (T.L.D.), Katherine T. Baldwin (K.T.B.) and Roman J. Giger (R.J.G.) designed the experiments; T.L.D., K.T.B., Yevgeniya A. Mironova (Y.A.M.), and Yoshiki Koriyama (Y.K.), Stephen J. Raiker, Claire D. Liepmann, Yasuhiro Katagiri,; T.L.D., K.T.B., and Y.K. contributed to data analysis and figure preparation; Kim L. Askew, Andrew Wood, Cedric G. Geoffroy, and Binhai Zheng generated and provided mice or reagents for the study; and T.L.D., K.T.B., and R.J.G. wrote the manuscript.

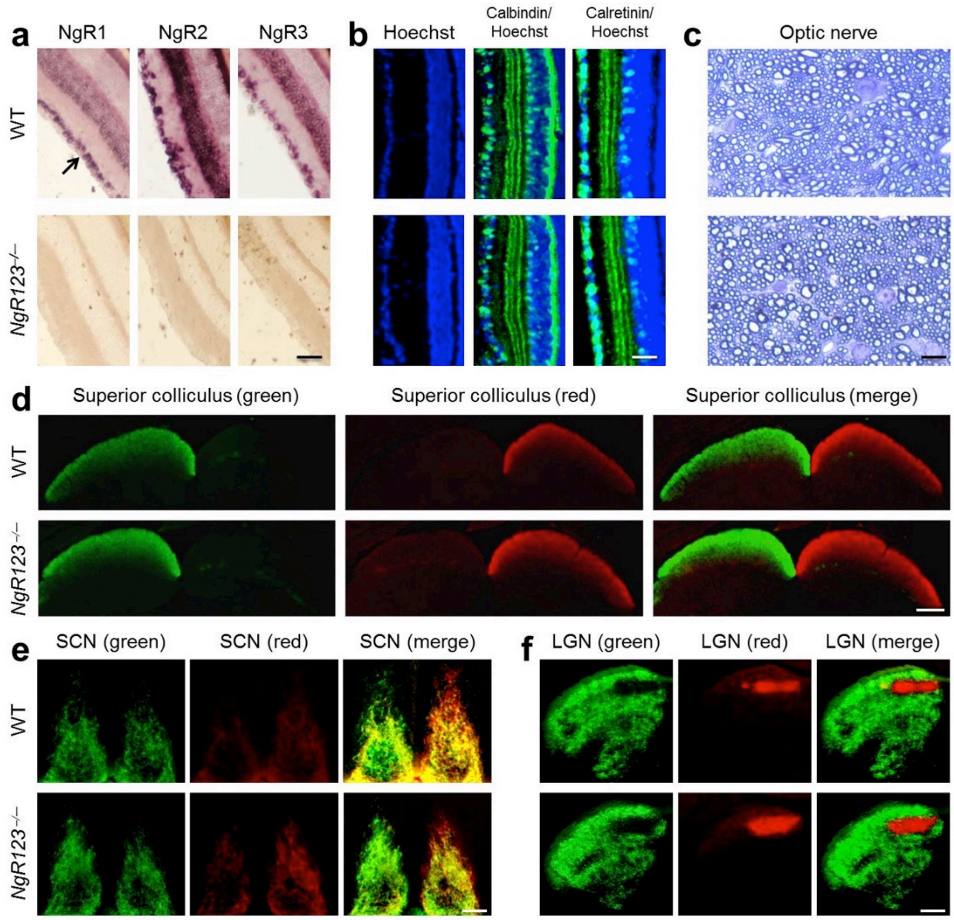

Figure 2.1: Retinal stratification, optic nerve myelination, and RGC central projections appear normal in *NgR123*$^{-/-}$ mice

(**a**) Sections of adult WT and Nogo receptor triple mutant (*NgR123*$^{-/-}$) mouse retina were subjected to *in situ* hybridization with digoxigenin-labeled cRNA probes specific for NgR1, NgR2, and NgR3 transcripts. All three receptors are strongly expressed in the ganglion cell layer (arrow) and the inner nuclear layer, but are absent from the outer nuclear layer of the retina. No signal was detected on parallel-processed sections of *NgR123*$^{-/-}$ retina. (**b**) Hoechst 33342 nuclear staining, as well as anti-calbindin and anti-calretinin immunolabeling, of adult WT and *NgR123*$^{-/-}$ retina did not reveal any noticeable differences in retinal organization among the two genotypes. (**c**) Toluidine Blue labeling of epon-embedded adult WT and *NgR123*$^{-/-}$ optic nerve cross sections reveals a comparable number of axons and degree of myelinated fibers. (**d**-**f**) The fidelity of RGC central projections in six-week-old WT and *NgR123*$^{-/-}$ mice was assessed by anterograde fiber tracing. Five days after injection of Alexa 594-conjugated Cholera Toxin β into the right eye and Alexa 488-conjugated Cholera Toxin β into the left eye, mice were sacrificed, perfused, and brain sections analyzed by fluorescence microscopy. Right eye (red) and left eye (green) RGC projections to the (**d**) superior colliculus, (**e**) suprachiasmatic nucleus and (**f**) lateral geniculate nucleus in *NgR123*$^{-/-}$ mice are indistinguishable from age-matched WT controls. Scale bar: a, b, 80µm; c, 5µm; d, 100µm; e, f, 60µm.

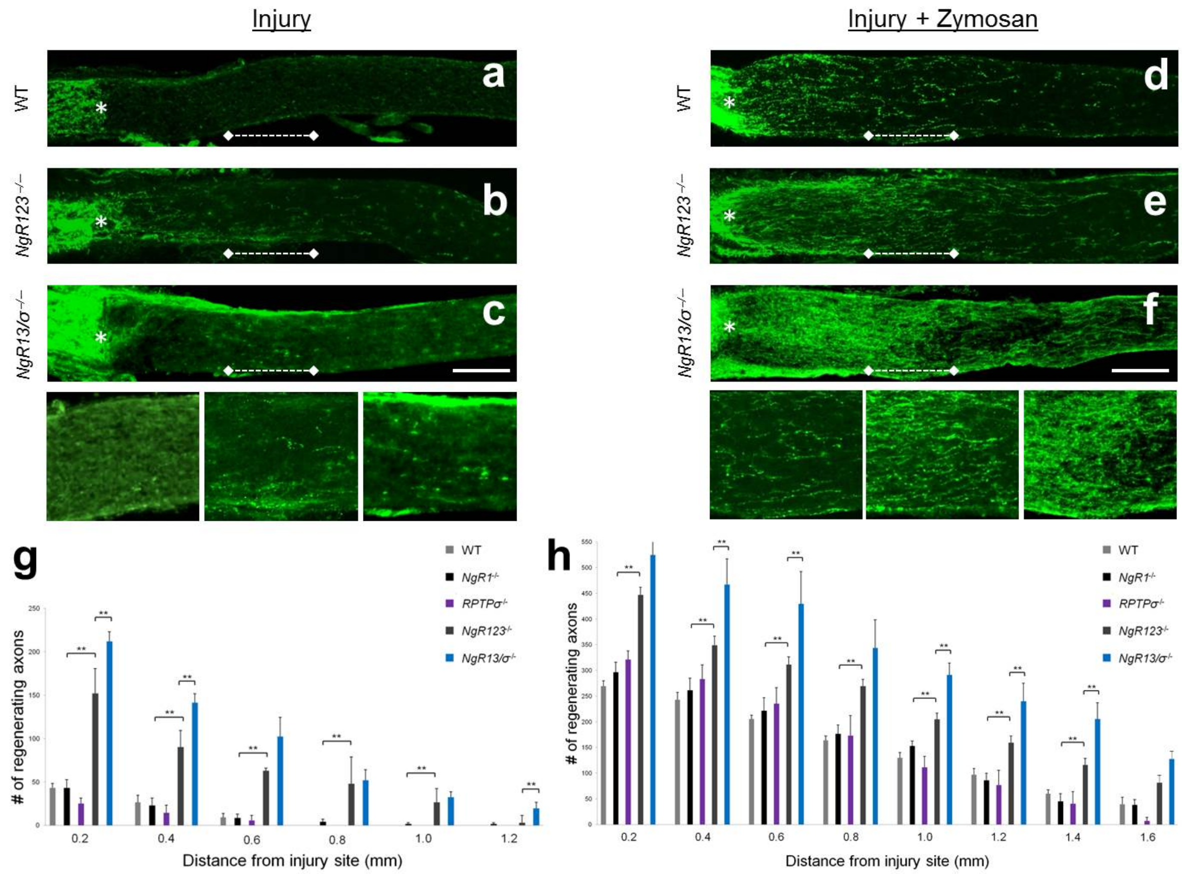

Figure 2.2: *NgR123*$^{-/-}$ and *NgR13/RPTPσ*$^{-/-}$ compound mutants show enhanced fiber regeneration following crush injury to the optic nerve

Two weeks following injury, regenerating axons in optic nerve sections were visualized by anti-GAP-43 immunolabeling. The injury site is marked with an asterisk. (**a**) WT mice show very limited regenerative axonal growth following injury. (**b**) In *NgR123*$^{-/-}$ mice, many GAP-43-positive fibers grow beyond the lesion site. (**c**) In *NgR13/RPTPσ*$^{-/-}$ (*NgR13/σ*$^{-/-}$) mice, a further increase of GAP-43-positive fiber growth is observed. (**g**) Quantification of the number of GAP-43-positive axons at 0.2 to 1.2mm distal to the lesion site. Light gray bars (WT, n=6); black bars (*NgR1*$^{-/-}$, n=7); purple bars (*RPTPσ*$^{-/-}$, n=5); dark gray bars (*NgR123*$^{-/-}$, n=8); blue bars (*NgR13/σ*$^{-/-}$, n=4). (**d**) Intraocular injection of Zymosan enhances regenerative axonal growth in WT mice. A further increase is observed in (**e**) *NgR123*$^{-/-}$ mice, which is further enhanced in (**f**) *NgR13/σ*$^{-/-}$, mice. (**h**) Quantification of the number of GAP-43-positive axons at 0.2 to 1.6mm distal to the lesion site in Zymosan-injected mice. Light gray bars (WT + Zymosan, n=6); black bars (*NgR1*$^{-/-}$ + Zymosan, n=6); purple bars (*RPTPσ*$^{-/-}$ + Zymosan, n=4); dark gray bars (*NgR123*$^{-/-}$ + Zymosan, n=8); blue bars (*NgR13/σ*$^{-/-}$ + Zymosan, n=3). Results are presented as mean ±SEMs. ** $P< 0.05$ (one-way ANOVA, Tukey's *post hoc*). Scale bar, 200µm.

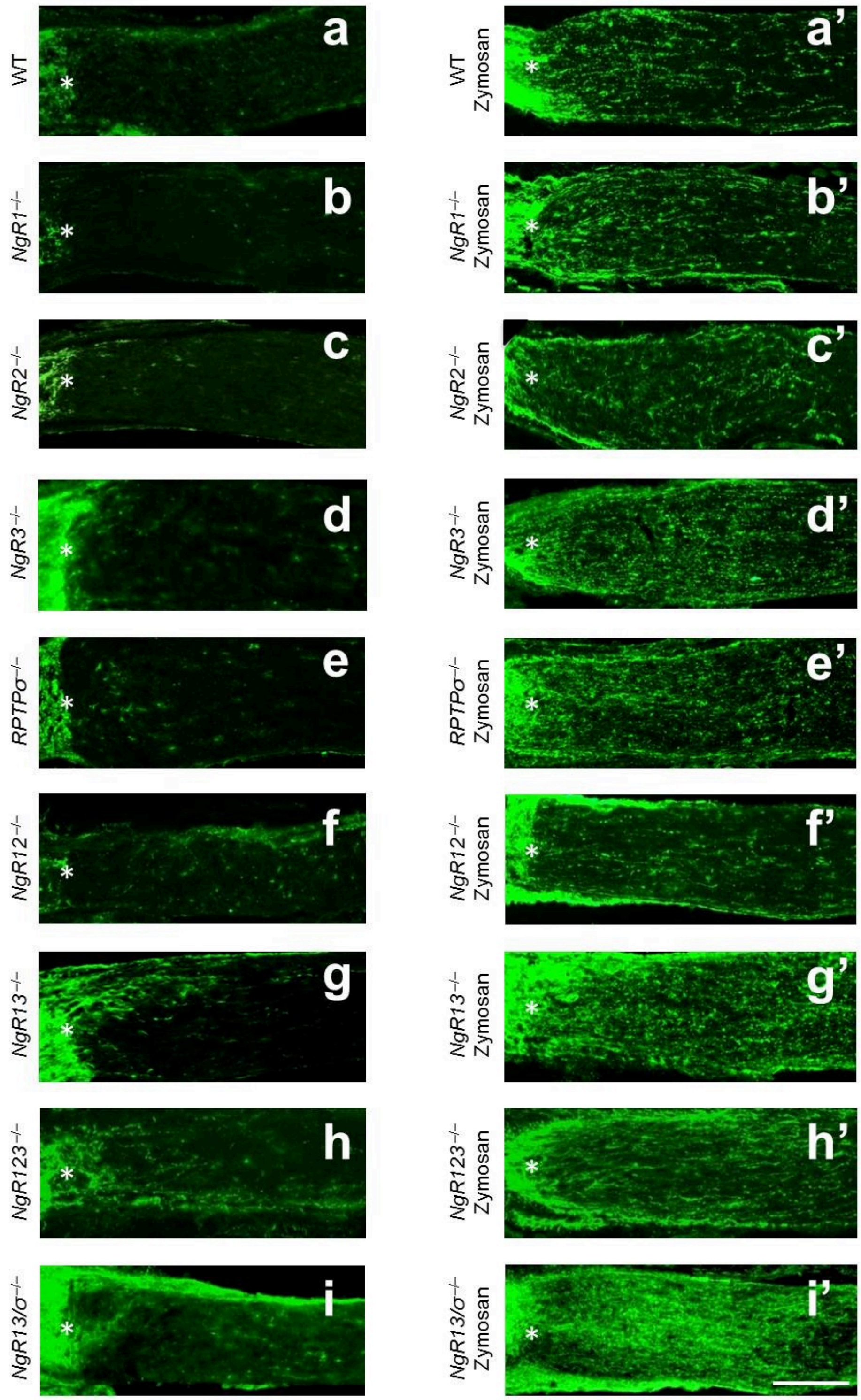

WT
a
NgR1−/−
b
NgR2−/−
c
NgR3−/−
d
RPTPσ−/−
e
NgR12−/−
f
NgR13−/−
g
NgR123−/−
h
NgR13/σ−/−
i
WT Zymosan
a’
NgR1−/− Zymosan
b’
NgR2−/− Zymosan
c’
NgR3−/− Zymosan
d’
RPTPσ−/− Zymosan
e’
NgR12−/− Zymosan
f’
NgR13−/− Zymosan
g’
NgR123−/− Zymosan
h’
NgR13/σ−/− Zymosan
i’

Figure 2.3: In adult mice, the combined loss of NgR1 and NgR3, but not NgR1 and NgR2, is sufficient to significantly enhance axon regeneration following retro-orbital optic nerve crush injury

(**a**-**i**) 2 weeks following optic nerve injury, regenerative axonal growth was assessed by anti-GAP-43 immunolabeling of longitudinal optic nerve sections. (**a'**-**i'**) To assess whether RGCs in a growth-activated state show an additive growth effect when combined with genetic ablation of Nogo receptors, a separate group of animals received an intraocular injection (i.o.) of Zymosan at the time of optic nerve injury. Anti-GAP-43 immunolabeling of injured optic nerve from (**a**) WT, (**b**) *NgR1*$^{-/-}$, (**c**) *NgR2*$^{-/-}$, (**d**) *NgR3*$^{-/-}$, (**e**) *RPTPσ*$^{-/-}$, and (**f**) *NgR12*$^{-/-}$ mice fails to identify significant regenerative growth of axons beyond the lesion site (asterisk). (**g**) *NgR13*$^{-/-}$ and (**h**) *NgR123*$^{-/-}$ mice show increased and comparable axonal regeneration, which is further enhanced in (**i**) *NgR13/RPTPσ*$^{-/-}$ (*NgR13/σ*$^{-/-}$) triple mutant mice. Following i.o. Zymosan injection, (**b'**) *NgR1*$^{-/-}$, (**c'**) *NgR2*$^{-/-}$, (**d'**) *NgR3*$^{-/-}$, (**e'**) *RPTPσ*$^{-/-}$, and (**f'**) *NgR12*$^{-/-}$ mice do not show enhanced regeneration compared to (**a'**) WT mice with i.o. Zymosan. An additive effect of i.o. Zymosan with genetic manipulation was observed for (**g'**) *NgR13*$^{-/-}$ and (**h'**) *NgR123*$^{-/-}$ mice. (**i'**) Loss of NgR1, NgR3 and RPTPσ (*NgR13/σ*$^{-/-}$) combined with i.o. Zymosan resulted in a further increase of fiber growth. Scale bar, 200μm.

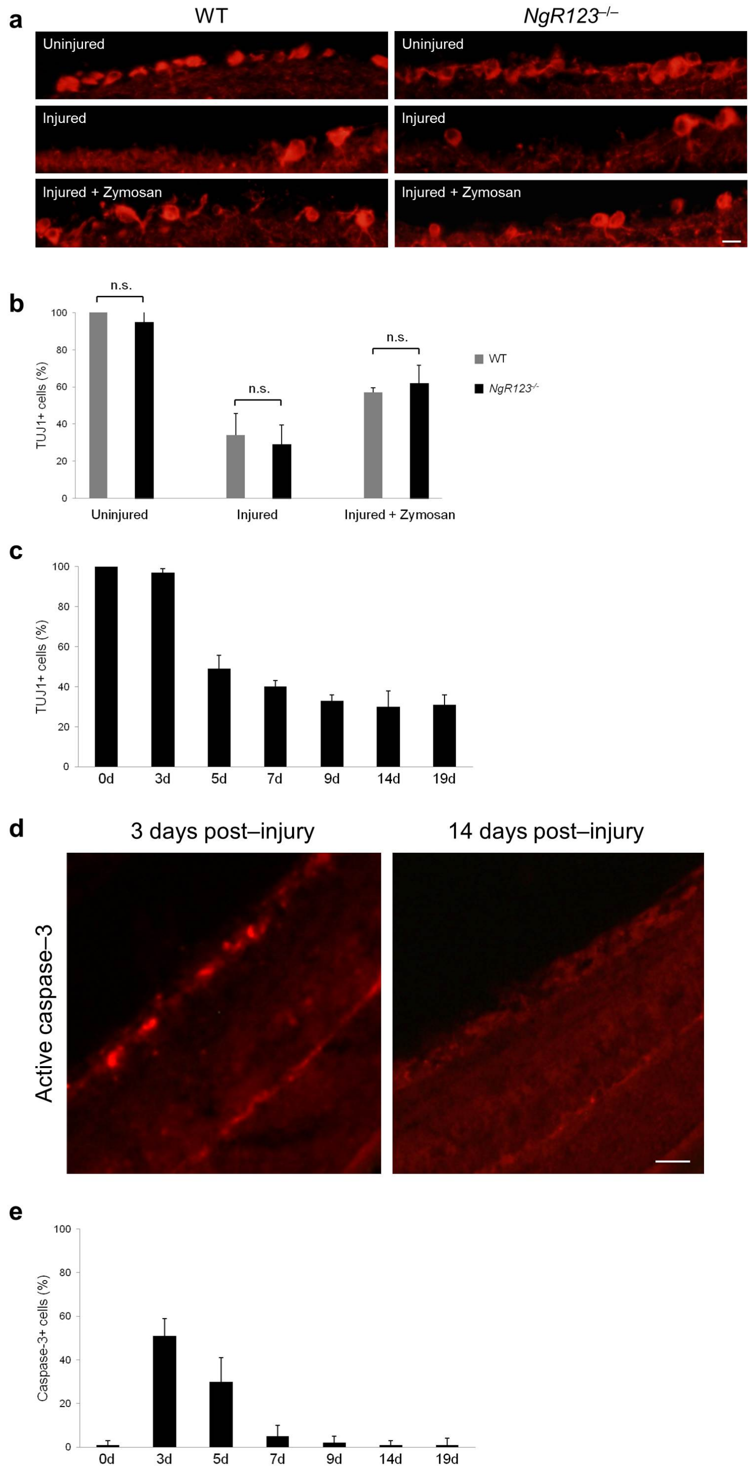

Figure 2.4: Optic nerve injury-induced retinal ganglion cell death is similar in WT and *NgR123*$^{-/-}$ triple mutants

(**a**) To assess cell loss in the RGC layer 14 days after nerve crush injury, coronal sections of WT and *NgR123*$^{-/-}$ retina were immunolabeled with TuJ1 and compared to uninjured retina.

Intraocular injection of Zymosan increased the density of TuJ1-labeled cells in the RGC layer; however, this effect was independent of the Nogo receptor genotype. (**b**) Quantification of the density of $TuJ1^{+}$ cells in the RGC layer per field of view as a percentage of the uninjured WT control. Cell counts were performed on at least 15 sections per condition (n=3 independent experiments). Gray bars (WT); black bars (*NgR123*$^{-/-}$). Results are presented as mean ±SEMs (one-way ANOVA, Tukey's *post hoc*), n.s.=not significant. (**c**) Time course of RGC death following optic nerve injury. Shown is the quantification of the density of $TuJ1^{+}$ cells in the RGC layer per field of view (at 0, 3, 5, 7, 9, 14, and 19 days following injury) as a percentage of the uninjured retina. The majority of cell death occurs by 7 days post-optic nerve injury. Cell counts were performed on at least 10 sections per condition. Results are presented as mean ±SEMs. (**d**-**e**) Time course of caspase-3 activation following optic nerve injury. The number of RGCs labeled for activated caspase-3 is shown as a percentage of the total number of cells (TUJ1-positive) per field of view at each time point (0, 3, 5, 7, 9, 14, and 19 days following injury). The peak of activated caspase-3 labeling is seen between 3 and 5 days post-injury. Cell counts were performed on at least 10 sections per condition. Results are presented as mean ±SEMs. Scale bar: a, 30µm; d, 60µm.

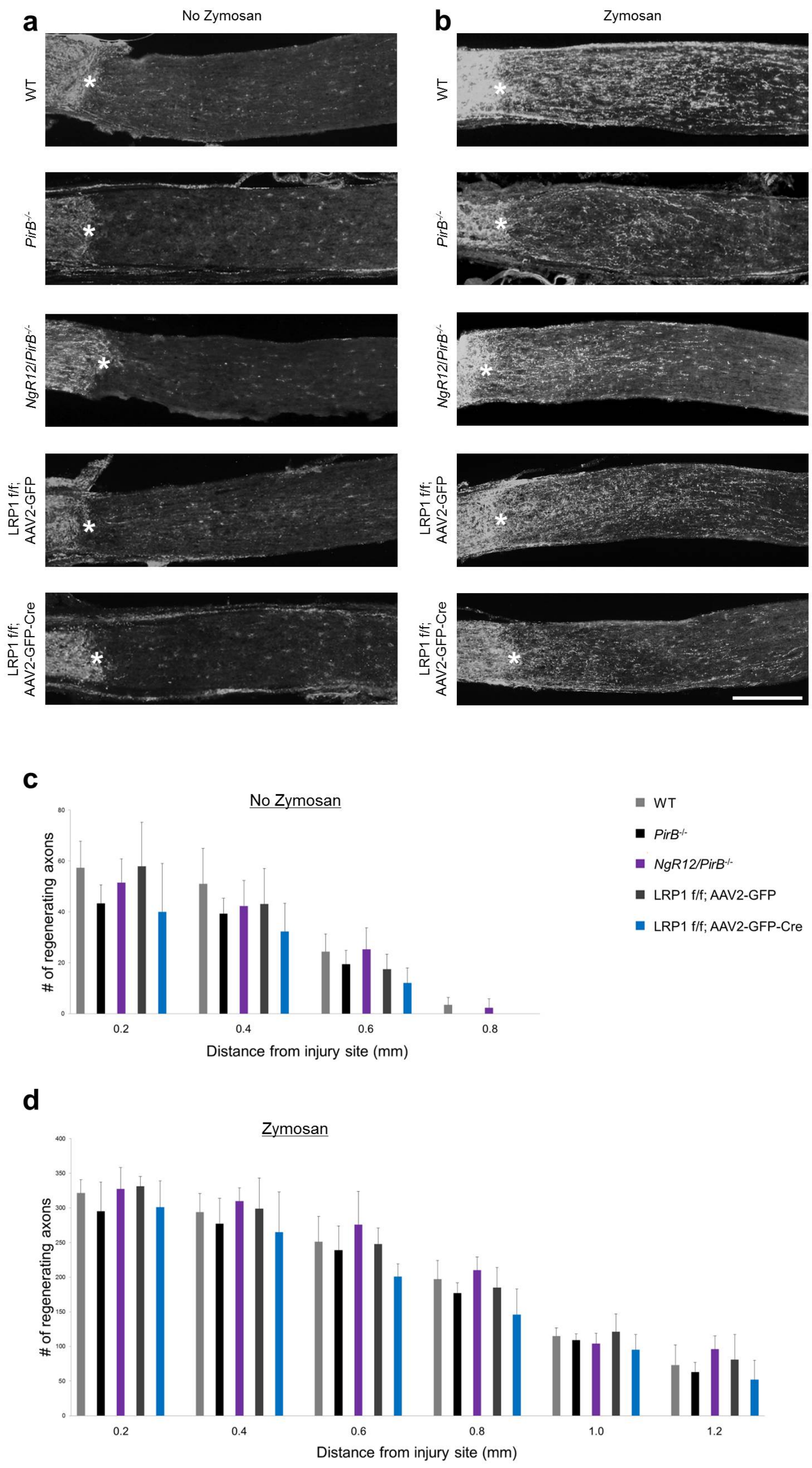

Figure 2.5: Loss of multiple MAI receptors is not sufficient to enhance axon regeneration following retro-orbital optic nerve crush injury

(**a**) 2 weeks following optic nerve injury, regenerative axonal growth was assessed by GAP-43 immunolabeling of longitudinal optic nerve sections. GAP-43 immunolabeling of injured optic nerve from WT, *PirB*$^{-/-}$, and *NgR12/PirB*$^{-/-}$ mice fails to identify regenerative growth of axons beyond the lesion site (asterisk). Similarly, *LRP1*$^{f/f}$ mice with intravitreal injections of AAV2-GFP or AAV2-GFP-Cre show no substantial axon regeneration. (**b**) To test whether growth-activated RGCs show an additive regenerative effect when combined with genetic ablation of MAG receptors, a separate group of animals received an intravitreal injection of Zymosan at the time of optic nerve injury. Following Zymosan injection, *PirB*$^{-/-}$, *NgR12/PirB*$^{-/-}$ *LRP1*$^{f/f}$; AAV2-GFP, and *LRP1*$^{f/f}$; AAV2-GFP-Cre mice do not show enhanced regeneration compared to WT mice with Zymosan. (**c**) Quantification of the number of GAP-43-positive axons at 0.2 to 0.8mm distal to the lesion site. Light gray bars (WT, n=5); black bars (*PirB*$^{-/-}$, n=6); purple bars (*NgR12/PirB*$^{-/-}$, n=5); dark gray bars (*LRP1*$^{f/f}$; AAV2-GFP, n=6); blue bars (*LRP1*$^{f/f}$; AAV2-GFP-Cre, n=6). (**d**) Quantification of the number of GAP-43-positive axons at 0.2 to 1.2mm distal to the lesion site in Zymosan-injected mice. Light gray bars (WT, n=5); black bars (*PirB*$^{-/-}$, n=5); purple bars (*NgR12/PirB*$^{-/-}$, n=5); dark gray bars (*LRP1*$^{f/f}$; AAV2-GFP, n=6); blue bars (*LRP1*$^{f/f}$; AAV2-GFP-Cre, n=5). Results are presented as mean ±SEMs. Scale bar, 200µm.

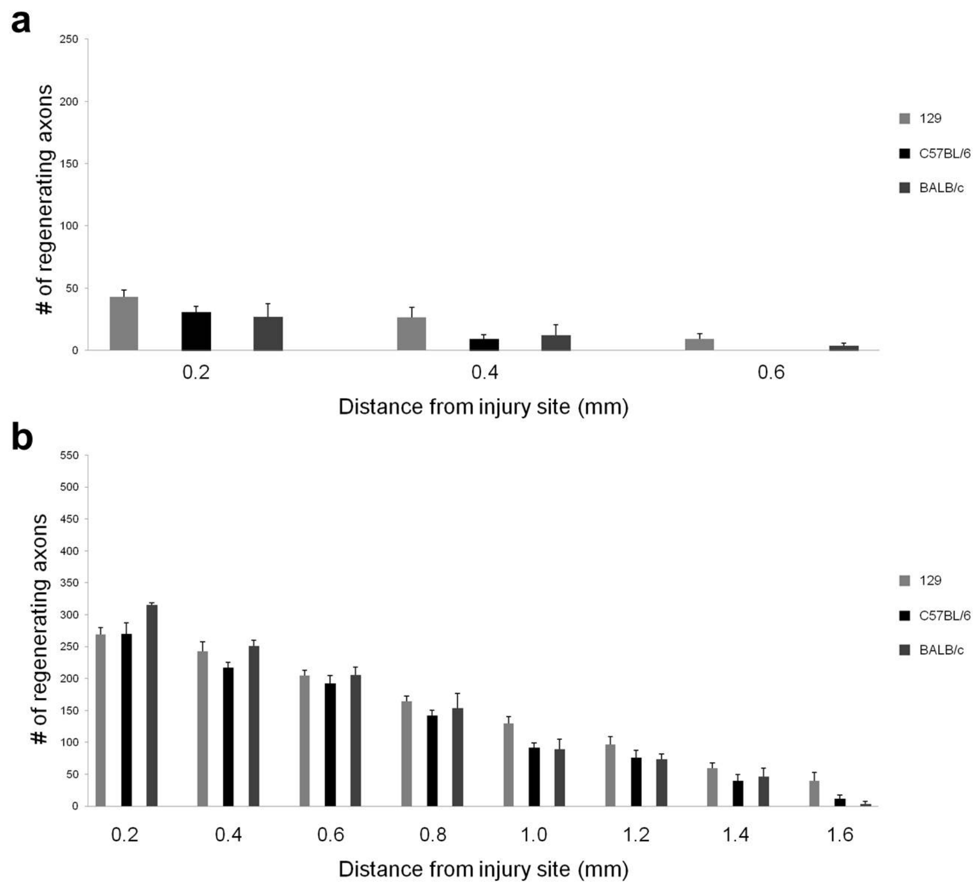

Figure 2.6: The genetic background of wild-type mice does not significantly influence RGC axon regeneration

(**a**) Quantification of the number of GAP-43-positive axons at 0.2 to 0.6mm distal to the lesion site in 129 (light gray bars, n=6), C57BL/6 (black bars, n= 6), and BALB/c (dark gray bars, n= 4) wild-type mice 2 weeks following optic nerve injury revealed no significant differences. (**b**) Quantification of the number of GAP-43-positive axons at 0.2 to 1.6mm distal to the lesion site following intraocular Zymosan injection in 129 (light gray bars, n=6), C57BL/6 (black bars, n=7), and BALB/c (dark gray bars, n=3) wild-type mice, 2 weeks following optic nerve injury. No significant differences at any distance were observed. Results are presented as mean ±SEMs (one-way ANOVA, Tukey's *post hoc*).

a

Injury

Genotype	Number of Nerves	Significance vs. WT 0.2 mm	Significance vs. WT 0.4 mm
NgR123$^{-/-}$	8	***	***
NgR1$^{-/-}$	7	ns	ns
NgR2$^{-/-}$	3	ns	ns
NgR3$^{-/-}$	3	ns	ns
NgR12$^{-/-}$	3	ns	ns
NgR13$^{-/-}$	4	***	***
RPTPσ$^{-/-}$	5	ns	ns
NgR13/RPTPσ$^{-/-}$	4	***	***

b

Injury + Zymosan

Genotype	Number of Nerves	Significance vs. WT 0.2 mm	Significance vs. WT 0.8 mm
NgR123$^{-/-}$	8	***	**
NgR1$^{-/-}$	6	ns	ns
NgR2$^{-/-}$	3	ns	ns
NgR3$^{-/-}$	3	ns	ns
NgR12$^{-/-}$	3	ns	ns
NgR13$^{-/-}$	3	***	**
RPTPσ$^{-/-}$	4	ns	ns
NgR13/RPTPσ$^{-/-}$	3	***	***

c

Injury

Genotype	Number of Nerves	Significance vs. *NgR123*$^{-/-}$ 0.2 mm	Significance vs. *NgR123*$^{-/-}$ 0.4 mm
WT	6	***	***
NgR1$^{-/-}$	7	***	***
NgR2$^{-/-}$	3	***	***
NgR3$^{-/-}$	3	***	***
NgR12$^{-/-}$	3	***	***
NgR13$^{-/-}$	4	ns	ns
RPTPσ$^{-/-}$	5	***	***
NgR13/RPTPσ$^{-/-}$	4	***	**

d

Injury + Zymosan

Genotype	Number of Nerves	Significance vs. *NgR123*$^{-/-}$ 0.2 mm	Significance vs. *NgR123*$^{-/-}$ 0.8 mm
WT	6	***	**
NgR1$^{-/-}$	6	***	**
NgR2$^{-/-}$	3	***	**
NgR3$^{-/-}$	3	***	**
NgR12$^{-/-}$	3	***	*
NgR13$^{-/-}$	3	ns	ns
RPTPσ$^{-/-}$	4	***	*
NgR13/RPTPσ$^{-/-}$	3	ns	ns

e

Genotype	P-value of K.B. vs. Y.K. data (0.4 mm)	P-value of K.B. vs. Y.K. data (1.0 mm)
WT (C57BL/6)	0.9181	n/a
WT (C57BL/6) with Zymosan	0.3643	0.5888
NgR1$^{-/-}$	0.7067	n/a
NgR1$^{-/-}$ with Zymosan	0.3845	0.0818
WT (129)	0.4323	n/a
WT (129) with Zymosan	0.9905	0.6718
NgR123$^{-/-}$	0.8359	0.3945
NgR123$^{-/-}$ with Zymosan	0.7162	0.2738

Table 2.1: Summary of optic nerve regeneration studies. (**a**) 2 weeks following injury, regeneration in *NgR123*$^{-/-}$, *NgR13*$^{-/-}$, and *NgR13/RPTPσ*$^{-/-}$ compound mutant mice is significantly increased compared to WT mice at 0.2 and 0.4mm distal to the injury site. Compared to WT mice, regeneration in *NgR1*$^{-/-}$, *NgR2*$^{-/-}$, *NgR3*$^{-/-}$, *NgR12*$^{-/-}$, or *RPTPσ*$^{-/-}$ at 0.2 and 0.4mm is not significantly enhanced. *** $P< 0.001$ (one-way ANOVA, Tukey's *post hoc*), n.s.= not significant. (**b**) Following intraorbital Zymosan injection, regeneration in *NgR123*$^{-/-}$, *NgR13*$^{-/-}$, and *NgR13/RPTPσ*$^{-/-}$ compound mutant mice is significantly enhanced compared to WT mice at 0.2 and 0.8mm distal to the injury site. There is no significant difference in axon regeneration between WT mice and *NgR1*$^{-/-}$, *NgR2*$^{-/-}$, *NgR3*$^{-/-}$, *NgR12*$^{-/-}$, or *RPTPσ*$^{-/-}$ mutant mice. *** $P< 0.001$, ** $P< 0.01$ (one-way ANOVA, Tukey's *post hoc*), n.s.= not significant. (**c**) 2 weeks following injury, regeneration in *NgR123*$^{-/-}$ mice is significantly increased compared to WT, *NgR1*$^{-/-}$, *NgR2*$^{-/-}$, *NgR3*$^{-/-}$, *NgR12*$^{-/-}$, and *RPTPσ*$^{-/-}$ mice, and decreased compared to *NgR13/RPTPσ*$^{-/-}$ mice, at 0.2 and 0.4mm distal to the injury site. There is no significant difference in the regeneration phenotype of *NgR123*$^{-/-}$ and *NgR13*$^{-/-}$ compound mutants. *** $P< 0.001$, ** $P< 0.01$ (one-way ANOVA, Tukey's *post hoc*), n.s.= not significant. (**d**) Following intraocular Zymosan injection, axon regeneration in *NgR123*$^{-/-}$ mice is significantly increased compared to WT, *NgR1*$^{-/-}$, *NgR2*$^{-/-}$, *NgR3*$^{-/-}$, *NgR12*$^{-/-}$, and *RPTPσ*$^{-/-}$ mice at 0.2 and 0.8mm distal to the injury site. There is no significant difference in axon regeneration between *NgR123*$^{-/-}$ and *NgR13*$^{-/-}$ or *NgR13/RPTPσ*$^{-/-}$ mutant mice (with intraocular Zymosan injection) at these distances. At distances 0.4, 0.6, 1.0, 1.2, and 1.4mm beyond the injury site, axon regeneration in *NgR13/RPTPσ*$^{-/-}$ mice is significantly greater than in *NgR123*$^{-/-}$ mice (with intraocular Zymosan injection). *** $P< 0.001$, ** $P< 0.01$, * $P< 0.05$ (one-way ANOVA, Tukey's *post hoc*), n.s.= not significant. (**e**) For an unbiased assessment of the optic nerve regeneration phenotype in Nogo receptor single and compound mutants, two independent data sets were generated by two independent surgeons: K. Baldwin (University of Michigan) and Y. Koriyama (visiting scientist from Kanazawa University). Both surgeons were originally trained in the laboratory of L. Benowitz. A total of 84 mice (K.B. - 51 mice, Y.K. - 33 mice) were operated on, and each surgeon performed crush injury on the following genotypes: WT, *NgR1*$^{-/-}$, and *NgR123*$^{-/-}$ mice. Only optic nerves from mice that showed no bleeding, infection, degeneration, or other complications of the operated eye were included for quantification of regenerating axons. The two data sets were then compared and analyzed for any significant differences between them, comparing the total number of GAP-43-positive axons for each genotype at two prespecified distances (0.4mm, 1.0mm) beyond the lesion site (unpaired *t* test). While there is some variation in the number of regenerating fibers, the principal findings of the two independently generated data sets are very comparable: WT mice (129 background or C57BL/6 background) show minimal regeneration of GAP-43-positive retinal ganglion cell axons. Regeneration in *NgR1*$^{-/-}$ mice is not enhanced compared to WT mice. Both data sets show a modest but significant increase in regenerating axons in *NgR123*$^{-/-}$ mice ($P< 0.001$, K.B; $P< 0.05$, Y.K.). WT mice that received Zymosan show greatly enhanced axon regeneration compared to WT mice that did not receive Zymosan. Notably, regeneration in Zymosan-treated WT mice is significantly enhanced compared to *NgR123*$^{-/-}$ mice without Zymosan ($P< 0.001$ for both data sets). Importantly, both data sets show significantly enhanced fiber growth at 0.2-1.4mm beyond the injury site in *NgR123*$^{-/-}$ mice with Zymosan compared to WT mice with Zymosan ($P< 0.05$ at 1.0, 1.2, and 1.4mm; $P< 0.01$ at 0.8mm; $P< 0.001$ at 0.2, 0.4, and 0.6mm - K.B.; $P< 0.05$ at 0.4 and 0.6mm; $P< 0.01$ at 0.2, 1.2, and 1.4mm; $P< 0.001$ at 0.8 and 1.0mm - Y.K.).

2.8 References

Aricescu AR, McKinnell IW, Halfter W, Stoker AW (2002) Heparan sulfate proteoglycans are ligands for receptor protein tyrosine phosphatase sigma. Mol Cell Biol 22:1881-1892.

Atwal JK, Pinkston-Gosse J, Syken J, Stawicki S, Wu Y, Shatz C, Tessier-Lavigne M (2008) PirB is a functional receptor for myelin inhibitors of axonal regeneration. Science 322:967-970.

Bradbury EJ, Moon LD, Popat RJ, King VR, Bennett GS, Patel PN, Fawcett JW, McMahon SB (2002) Chondroitinase ABC promotes functional recovery after spinal cord injury. Nature 416:636-640.

Bregman BS, Kunkel-Bagden E, Schnell L, Dai HN, Gao D, Schwab ME (1995) Recovery from spinal cord injury mediated by antibodies to neurite growth inhibitors. Nature 378:498-501.

Cafferty WB, Duffy P, Huebner E, Strittmatter SM (2010) MAG and OMgp synergize with Nogo-A to restrict axonal growth and neurological recovery after spinal cord trauma. J Neurosci 30:6825-6837.

Chivatakarn O, Kaneko S, He Z, Tessier-Lavigne M, Giger RJ (2007) The Nogo-66 receptor NgR1 is required only for the acute growth cone-collapsing but not the chronic growth-inhibitory actions of myelin inhibitors. The Journal of neuroscience : the official journal of the Society for Neuroscience 27:7117-7124.

Dickendesher TL, Baldwin KT, Mironova YA, Koriyama Y, Raiker SJ, Askew KL, Wood A, Geoffroy CG, Zheng B, Liepmann CD, Katagiri Y, Benowitz LI, Geller HM, Giger RJ (2012) NgR1 and NgR3 are receptors for chondroitin sulfate proteoglycans. Nat Neurosci.

Fischer D, He Z, Benowitz LI (2004a) Counteracting the Nogo receptor enhances optic nerve regeneration if retinal ganglion cells are in an active growth state. J Neurosci 24:1646-1651.

Fischer D, Petkova V, Thanos S, Benowitz LI (2004c) Switching mature retinal ganglion cells to a robust growth state in vivo: gene expression and synergy with RhoA inactivation. J Neurosci 24:8726-8740.

Fournier AE, GrandPre T, Strittmatter SM (2001) Identification of a receptor mediating Nogo-66 inhibition of axonal regeneration. Nature 409:341-346.

Fry EJ, Chagnon MJ, Lopez-Vales R, Tremblay ML, David S (2010) Corticospinal tract regeneration after spinal cord injury in receptor protein tyrosine phosphatase sigma deficient mice. Glia 58:423-433.

Garcia-Alias G, Fawcett JW (2012) Training and anti-CSPG combination therapy for spinal cord injury. Exp Neurol 235:26-32.

Kadoya K, Tsukada S, Lu P, Coppola G, Geschwind D, Filbin MT, Blesch A, Tuszynski MH (2009) Combined intrinsic and extrinsic neuronal mechanisms facilitate bridging axonal regeneration one year after spinal cord injury. Neuron 64:165-172.

Kantor DB, Chivatakarn O, Peer KL, Oster SF, Inatani M, Hansen MJ, Flanagan JG, Yamaguchi Y, Sretavan DW, Giger RJ, Kolodkin AL (2004) Semaphorin 5A is a bifunctional axon guidance cue regulated by heparan and chondroitin sulfate proteoglycans. Neuron 44:961-975.

Karlen A, Karlsson TE, Mattsson A, Lundstromer K, Codeluppi S, Pham TM, Backman CM, Ogren SO, Aberg E, Hoffman AF, Sherling MA, Lupica CR, Hoffer BJ, Spenger C, Josephson A, Brene S, Olson L (2009) Nogo receptor 1 regulates formation of lasting memories. Proc Natl Acad Sci U S A 106:20476-20481.

Kim JE, Liu BP, Park JH, Strittmatter SM (2004) Nogo-66 receptor prevents raphespinal and rubrospinal axon regeneration and limits functional recovery from spinal cord injury. Neuron 44:439-451.

Lee H, Raiker SJ, Venkatesh K, Geary R, Robak LA, Zhang Y, Yeh HH, Shrager P, Giger RJ (2008) Synaptic function for the Nogo-66 receptor NgR1: regulation of dendritic spine morphology and activity-dependent synaptic strength. The Journal of neuroscience : the official journal of the Society for Neuroscience 28:2753-2765.

Lee JK, Geoffroy CG, Chan AF, Tolentino KE, Crawford MJ, Leal MA, Kang B, Zheng B (2010) Assessing spinal axon regeneration and sprouting in Nogo-, MAG-, and OMgp-deficient mice. Neuron 66:663-670.

Leibinger M, Muller A, Andreadaki A, Hauk TG, Kirsch M, Fischer D (2009) Neuroprotective and axon growth-promoting effects following inflammatory stimulation on mature retinal ganglion cells in mice depend on ciliary neurotrophic factor and leukemia inhibitory factor. J Neurosci 29:14334-14341.

Li S, Liu BP, Budel S, Li M, Ji B, Walus L, Li W, Jirik A, Rabacchi S, Choi E, Worley D, Sah DW, Pepinsky B, Lee D, Relton J, Strittmatter SM (2004) Blockade of Nogo-66, myelin-associated glycoprotein, and oligodendrocyte myelin glycoprotein by soluble Nogo-66 receptor promotes axonal sprouting and recovery after spinal injury. J Neurosci 24:10511-10520.

Li S, Overman JJ, Katsman D, Kozlov SV, Donnelly CJ, Twiss JL, Giger RJ, Coppola G, Geschwind DH, Carmichael ST (2010) An age-related sprouting transcriptome provides molecular control of axonal sprouting after stroke. Nature neuroscience 13:1496-1504.

Liu BP, Cafferty WB, Budel SO, Strittmatter SM (2006) Extracellular regulators of axonal growth in the adult central nervous system. Philos Trans R Soc Lond B Biol Sci 361:1593-1610.

Massey JM, Hubscher CH, Wagoner MR, Decker JA, Amps J, Silver J, Onifer SM (2006) Chondroitinase ABC digestion of the perineuronal net promotes functional collateral sprouting in the cuneate nucleus after cervical spinal cord injury. J Neurosci 26:4406-4414.

McGee AW, Yang Y, Fischer QS, Daw NW, Strittmatter SM (2005) Experience-driven plasticity of visual cortex limited by myelin and Nogo receptor. Science 309:2222-2226.

Park KK, Liu K, Hu Y, Smith PD, Wang C, Cai B, Xu B, Connolly L, Kramvis I, Sahin M, He Z (2008) Promoting axon regeneration in the adult CNS by modulation of the PTEN/mTOR pathway. Science 322:963-966.

Pizzorusso T, Medini P, Berardi N, Chierzi S, Fawcett JW, Maffei L (2002) Reactivation of ocular dominance plasticity in the adult visual cortex. Science 298:1248-1251.

Powell EM, Mercado ML, Calle-Patino Y, Geller HM (2001) Protein kinase C mediates neurite guidance at an astrocyte boundary. Glia 33:288-297.

Raiker SJ, Lee H, Baldwin KT, Duan Y, Shrager P, Giger RJ (2010) Oligodendrocyte-myelin glycoprotein and Nogo negatively regulate activity-dependent synaptic plasticity. J Neurosci 30:12432-12445.
Sapieha PS, Duplan L, Uetani N, Joly S, Tremblay ML, Kennedy TE, Di Polo A (2005) Receptor protein tyrosine phosphatase sigma inhibits axon regrowth in the adult injured CNS. Mol Cell Neurosci 28:625-635.
Schweigreiter R, Walmsley AR, Niederost B, Zimmermann DR, Oertle T, Casademunt E, Frentzel S, Dechant G, Mir A, Bandtlow CE (2004) Versican V2 and the central inhibitory domain of Nogo-A inhibit neurite growth via p75NTR/NgR-independent pathways that converge at RhoA. Molecular and cellular neurosciences 27:163-174.
Shen Y, Tenney AP, Busch SA, Horn KP, Cuascut FX, Liu K, He Z, Silver J, Flanagan JG (2009) PTPsigma is a receptor for chondroitin sulfate proteoglycan, an inhibitor of neural regeneration. Science 326:592-596.
Shypitsyna A, Malaga-Trillo E, Reuter A, Stuermer CA (2011) Origin of Nogo-A by domain shuffling in an early jawed vertebrate. Mol Biol Evol 28:1363-1370.
Silver J, Miller JH (2004) Regeneration beyond the glial scar. Nat Rev Neurosci 5:146-156.
Sivasankaran R, Pei J, Wang KC, Zhang YP, Shields CB, Xu XM, He Z (2004) PKC mediates inhibitory effects of myelin and chondroitin sulfate proteoglycans on axonal regeneration. Nat Neurosci 7:261-268.
Stiles TL, Dickendesher TL, Gaultier A, Fernandez-Castaneda A, Mantuano E, Giger RJ, Gonias SL (2013) LDL receptor-related protein-1 is a sialic-acid-independent receptor for myelin-associated glycoprotein that functions in neurite outgrowth inhibition by MAG and CNS myelin. J Cell Sci 126:209-220.
Syken J, Grandpre T, Kanold PO, Shatz CJ (2006) PirB restricts ocular-dominance plasticity in visual cortex. Science 313:1795-1800.
Winzeler AM, Mandemakers WJ, Sun MZ, Stafford M, Phillips CT, Barres BA (2011) The lipid sulfatide is a novel myelin-associated inhibitor of CNS axon outgrowth. The Journal of neuroscience : the official journal of the Society for Neuroscience 31:6481-6492.
Yin Y, Cui Q, Gilbert HY, Yang Y, Yang Z, Berlinicke C, Li Z, Zaverucha-do-Valle C, He H, Petkova V, Zack DJ, Benowitz LI (2009) Oncomodulin links inflammation to optic nerve regeneration. Proc Natl Acad Sci U S A 106:19587-19592.
Zagrebelsky M, Schweigreiter R, Bandtlow CE, Schwab ME, Korte M (2010) Nogo-A stabilizes the architecture of hippocampal neurons. The Journal of neuroscience : the official journal of the Society for Neuroscience 30:13220-13234.
Zheng B, Atwal J, Ho C, Case L, He XL, Garcia KC, Steward O, Tessier-Lavigne M (2005) Genetic deletion of the Nogo receptor does not reduce neurite inhibition in vitro or promote corticospinal tract regeneration in vivo. Proc Natl Acad Sci U S A 102:1205-1210.

CHAPTER III:

Neuroinflammation triggered by β-glucan/dectin-1 signaling enables CNS axon regeneration

3.1 Abstract

Innate immunity can facilitate nervous system regeneration, yet the underlying cellular and molecular mechanisms are not well understood. Here we show that intraocular injection of lipopolysaccharide (LPS), a bacterial cell wall component, or the fungal cell wall extract zymosan both lead to rapid and comparable intravitreal accumulation of blood-derived myeloid cells. However, when combined with retro-orbital optic nerve crush injury, lengthy growth of severed retinal ganglion cell (RGC) axons occurs only in zymosan-injected mice, and not in LPS-injected mice. In mice deficient for the pattern recognition receptor *dectin-1*, but not Toll-like receptor-2 (*TLR2*), zymosan-mediated RGC regeneration is greatly reduced. The combined loss of *dectin-1* and *TLR2* completely blocks the proregenerative effects of zymosan. In the retina, dectin-1 is expressed by microglia and dendritic cells, but not by RGCs. Dectin-1 is also present on blood-derived myeloid cells that accumulate in the vitreous. Intraocular injection of the dectin-1 ligand curdlan [a particulate form of β(1,3)-glucan] promotes optic nerve regeneration comparable to zymosan in WT mice, but not in *dectin-1*$^{-/-}$ mice. Particulate β(1, 3)-glucan leads to in- creased Erk1/2 MAP-kinase signaling and cAMP response element- binding protein (CREB) activation in myeloid cells in vivo. Loss of the dectin-1 downstream effector caspase recruitment domain 9 (CARD9) blocks CREB activation and attenuates the

axon-regenerative effects of β(1,3)-glucan. Studies with *dectin-1*$^{-/-}$/WT reciprocal bone marrow chimeric mice revealed a requirement for *dectin-1* in both retina-resident immune cells and bone marrow-derived cells for β(1,3)-glucan–elicited optic nerve regeneration. Collectively, these studies identify a molecular framework of how innate immunity enables repair of injured central nervous system neurons.

3.2 Introduction

Following injury to the adult mammalian central nervous system (CNS), severed axons fail to undergo spontaneous regeneration. The limited and transient growth response of injured CNS neurons is, in part, responsible for poor clinical outcomes following brain or spinal cord trauma. Neuron intrinsic (Sun et al., 2011) and extrinsic mechanisms (Fawcett et al., 2012) pose barriers to efficient CNS repair. However, there is accumulating evidence that, under certain circumstances, endogenous repair mechanisms can be unleashed by the induction of a local innate immune response (Yin et al., 2003, Gensel et al., 2012).

Retro-orbital optic nerve crush (ONC) is widely used as a rodent model to investigate factors that influence axonal growth in the injured CNS (Leon et al., 2000). Normally, retinal ganglion cells (RGC), the neurons that give rise to the optic nerve, do not extend lengthy axons beyond the injury site. However, robust axonal growth occurs following induction of intraocular inflammation via lens trauma (Leon et al., 2000) or intra-ocular (i.o.) injection of zymosan (Yin et al., 2003, Leibinger et al., 2009), Pam3cys (Hauk et al., 2010), or oxidized galectin-1 (Okada et al., 2005). This phenomenon is not restricted to the visual system, since injection of zymosan into dorsal root ganglia or spinal cord parenchyma triggers local inflammation and growth of injured or transplanted sensory neurons (Steinmetz et al., 2005, Gensel et al., 2009).

Macrophages (Yin et al., 2003, Gensel et al., 2009), neutrophils (Kurimoto et al., 2013) and astrocytes (Muller et al., 2007) have been implicated in the pro-regenerative effects of inflammation. The benefits of neuroinflammation on axonal growth can be undermined by concurrent toxicity (Gensel et al., 2009). A deeper understanding of these opposing effects will be important for exploiting immuno-modulatory pathways to promote neural repair while minimizing bystander damage.

In the current paper we investigate the pathways that drive innate immune mediated axon regeneration following ONC. We induced sterile inflammation in the vitreous on the day of injury by i.o. administration of zymosan or constituents of zymosan classified as pathogen associated molecular patterns (PAMPs). PAMPs are highly conserved microbial structures that serve as ligands for pattern recognition receptors (PRRs). PRRs for zymosan are widely expressed on innate immune cells and include toll-like receptors (TLR) 1 and 2, complement receptor 3 (CR3), and the C-type lectin family members CLEC7A (dectin-1) and CLEC6A (dectin-2) (Frasnelli et al., 2005, Tsoni and Brown, 2008). Engagement of PRRs on myeloid cells, such as monocytes, macrophages, neutrophils, and myeloid dendritic cells (DCs), results in their activation and induces phagocytosis and oxidative burst, as well as cytokine and chemokine production. The mechanism by which PRR signaling confers regenerative properties to myeloid cells is poorly understood. Here we elucidate the PAMP-PRR interactions critical for zymosan-mediated axonal regeneration, and thereby introduce a novel panel of signaling molecules that may be targeted to promote post-traumatic neurorepair.

3.3 Results

Zymosan, but not LPS, enables immune-mediated axon regeneration

Intra-ocular (i.o.) injection of the yeast cell wall extract zymosan into the posterior chamber of the mouse eye triggers a local inflammatory response. Flow cytometric analysis of the cellular composition of vitreous infiltrates, at 7 days post- zymosan injection and ONC, revealed accumulation of large numbers of monocytes/macrophages (Yin et al., 2003), neutrophils (Kurimoto et al., 2013), and dendritic cells (DCs). Small numbers of B-cells, $CD4^+$ and $CD8^+$ T-cells, and natural killer cells were also observed (**Fig. 3.1a**). We found that i.o. injection of lipopolysaccharide (LPS), a cell wall component of Gram-negative bacteria and selective ligand for TLR4 (Underhill et al., 1999, McGettrick and O'Neill, 2010), induced vitreous infiltrates with a similar cellular composition to those induced by zymosan. Moreover, no differences in ROS production of macrophages in eyes injected with LPS or zymosan was observed (**Fig. 3.2**). Remarkably, i.o. zymosan induced lengthy regrowth of severed RGC axons (Yin et al., 2003), while i.o. LPS failed to do so (**Fig 3.1b-e**). Because zymosan and LPS are recognized by different PRRs, this suggests that engagement of specific immune receptors is required to generate an inflammatory milieu conducive for CNS axon regeneration.

TLR2 and MyD88 are not necessary for zymosan-elicited axon regeneration

Zymosan has been used to induce sterile inflammation in animal models of peritonitis and arthritis. In these experimental paradigms, zymosan stimulates activation of myeloid cells via the TLR2/MyD88 pathway (Underhill et al., 1999, Frasnelli et al., 2005, Choi et al., 2011). TLR2 signaling has also been implicated in RGC axon regeneration since repeated i.o. injections of Pam3Cys, a synthetic agonist of TLR2, promotes axon growth following ONC (Hauk et al., 2010). However, the importance of the TLR2/MyD88 pathway in zymosan-mediated axonal regeneration has not been explicitly demonstrated. Myeloid cells, but not lymphocytes, that infiltrate the eye 7 days following i.o. zymosan and ONC, express TLR2 (**Fig. 3.3a-b**). Retina-resident DCs and microglia both express TLR2 during homeostasis (**Fig. 3.3c-d**). The number of $TLR2^+$ microglia and DCs increases by 4- and 14-fold, respectively, by day 7 post-ONC without i.o. zymosan (**Fig. 3.3e-f**). This shows that ONC alone, in the absence of i.o. PAMPs, is sufficient to activate retinal immune cells. Surprisingly, i.o. administration of zymosan depleted of all its TLR2-stimulating properties ("depleted zymosan") caused robust regeneration of $GAP43^+$ RGC axons (**Fig. 3.3i**). The majority of TLR family members signal through the downstream adaptor MyD88. However, similar to *TLR2*$^{-/-}$ mice, i.o. zymosan in *MyD88*$^{-/-}$ mice subjected to ONC results in robust axonal regeneration, indistinguishable from WT mice (**Fig. 3.3j-l**). I.o. PBS failed to elicit axonal extension beyond the lesion site in WT, *TLR2*$^{-/-}$ or *MyD88*$^{-/-}$ mice (**Fig. 3.4**). Collectively, these studies demonstrate that *TLR2* and *MyD88* are dispensable for zymosan-elicited RGC axon regeneration.

Zymosan promotes axon regeneration through dectin-1

In addition to TLRs, several other zymosan receptors have been identified including the β-glucan binding transmembrane proteins CR3 (Thornton et al., 1996) and dectin-1 (Tsoni and Brown, 2008). Regrowth of injured RGC axons was significantly attenuated in *dectin-1*$^{-/-}$, but not *CR3*$^{-/-}$, mice compared with WT mice (**Fig. 3.5a-f**). To directly test whether the residual optic nerve regeneration observed in *dectin-1*$^{-/-}$ mice is TLR/MyD88-dependent, we generated *dectin-1*$^{-/-}$;*MyD88*$^{-/-}$ compound mutants. Zymosan-elicited optic nerve regeneration was completely abolished in *dectin-1*$^{-/-}$;*MyD88*$^{-/-}$ mice (**Fig. 3.5d, 3.5f**). To examine whether dectin-

1 collaborates more specifically with TLR2, we generated *dectin-1*$^{-/-}$*;TLR2*$^{-/-}$ compound mutants (**Fig. 3.6a**), and found that zymosan-elicited optic nerve regeneration was also fully abrogated (**Fig. 3.5e-f**). Interestingly, the inflammatory responses triggered by i.o. administration of zymosan into WT, *dectin-1*$^{-/-}$*;MyD88*$^{-/-}$ or *dectin-1*$^{-/-}$*;TLR2*$^{-/-}$ compound mutants at 7 days post-ONC are comparable, both with respect to cell number and composition (**Fig. 3.5g**). Thus, reminiscent of our findings with i.o. LPS, these experiments demonstrate that intra-ocular inflammation does not always result in RGC regenerative growth. Germline ablation of *dectin-1*$^{-/-}$*;TLR2*$^{-/-}$ could, theoretically, adversely affect RGC health and thereby their regenerative capacity. In order to determine whether post-traumatic RGCs in *dectin-1*$^{-/-}$*;TLR2*$^{-/-}$ mice can regenerate their axons, we knocked-down PTEN and found long-distance axon regeneration following ONC (**Fig. 3.6b-d**). Thus, RGCs of compound mutants are capable of regenerative growth in a conducive setting, but fail to do so following i.o. zymosan application.

β **-(1,3)glucan promotes dectin-1-dependent long-distance axon regeneration**

β-glucans are the ingredient of zymosan that complex with dectin-1. They exist as large polymers composed of linear *β*-(1,3) D-glycosidic linkages with occasional side chains bound by *β*-(1,6) D-glycosidic linkages. We found that in WT mice, i.o. administration of curdlan (**Fig. 3.7a, 3.7d**), a particulate form of *β*-(1,3)glucan, is as effective as zymosan (**Fig. 3.1b, 3.1e**) in promoting RGC axon regeneration following ONC. The number and composition of infiltrating immune cells at 7 days after ONC and i.o. curdlan or zymosan is similar (**Fig. 3.8a**). Delayed administration of curdlan at 48 hours after ONC, was equally robust in triggering RGC axon regeneration (**Fig. 3.9**). Curdlan binds directly to dectin-1, but not TLR2, and i.o. administration of curdlan in *dectin-1*$^{-/-}$ mice failed to induce RGC regeneration (**Fig. 3.7b, 3.7d**). This indicates that curdlan, unlike zymosan, exerts its pro-regenerative effects solely through *dectin-1*, and that engagement of dectin-1 is necessary and sufficient for RGC axon regeneration.

Curdlan signals in a dectin-1 and CARD9 dependent manner to activate CREB

Ligation of dectin-1 leads to activation of multiple downstream signaling events implicated in fungal immune defense, including phagocytosis of fungal particles, ROS production and regulation of gene expression (Gross et al., 2006, Gringhuis et al., 2009, Jia et al., 2014). One pathway, comprised of spleen tyrosine kinase (syk) and caspase recruitment domain 9 (CARD9), couples dectin-1 to multiple downstream effectors (Ruland, 2008, Roth and Ruland, 2013). The role of this pathway in PAMP-induced RGC axonal regeneration was assessed in *CARD9*$^{-/-}$ mice. In WT and *CARD9*$^{-/-}$, but not *dectin-1*$^{-/-}$ mice, i.o. curdlan combined with ONC leads to a rapid increase in syk and p-syk, an important dectin-1 adaptor protein (**Fig. 3.7e**). A partial, yet significant reduction in regenerative RGC growth was observed in optic nerve sections of curdlan injected *CARD9*$^{-/-}$ mice when compared to WT mice (**Fig. 3.7c, 3.7d**). This shows that CARD9 functions downstream of dectin-1, but also implies the existence of parallel, *CARD9*-independent signaling mechanism(s). Dectin-1 mediated activation of the MAP kinase pathway in bone marrow derived macrophages leads to activation of cAMP response element-binding protein (CREB) (Elcombe et al., 2013). Biochemical analysis of eye lysates revealed rapid activation of extracellular signal-regulated protein kinase (Erk1/2) and CREB in WT, but not *dectin-1*$^{-/-}$, mice 6 hours following ONC and i.o. curdlan (**Fig. 3.7e, 3.7f**). *CARD9*$^{-/-}$ mice displayed increased activation of Erk1/2, but not of CREB (**Fig. 3.7f**). This places Erk1/2 activation downstream of dectin-1 and upstream or parallel of CARD9. Dectin-1/CARD9 signaling can activate the canonical NF-kB pathway (Gross et al., 2006), however we did not observe an increase in NF-kB activity, as assessed by phosphorylation of p65 at S536 (**Fig. 3.7e, 3.7f**). Together, this suggests dectin-1/CARD9 signaling in myeloid cells participates in inflammation-mediated neuronal regeneration.

Dectin-1 is expressed by retina-resident and blood-derived infiltrating immune cells

We next sought to identify the cell type(s) that curdlan targets to elicit RGC axon regeneration. We used flow cytometric analysis to measure dectin-1 expression on retina-resident cells at baseline and following ONC alone, and on immune cells that infiltrate the eye in response to i.o. curdlan or zymosan in the setting of ONC. These experiments were performed in $CX3CR1^{GFP/+}$ reporter mice in which microglia are GFP^{+}. We found that dectin-1 is constitutively expressed at low levels on $CD11b/CX3CR1^{GFP/+}$ microglia and $CD11b^{+}/CD11c^{+}$ retinal DCs in naïve eyes (**Fig. 3.10a**), and is up-regulated on both cell types 7 days post-ONC (**Fig. 3.10b**). Following i.o. zymosan, dectin-1 is expressed on infiltrating monocytes/macrophages, neutrophils, and myeloid DCs, but not on lymphocytes (**Fig. 3.10c**). Immunohistochemical studies confirmed that dectin-1 is strongly expressed by myeloid cells that accumulate in the vitreous of zymosan-injected WT mice (**Fig. 3.10d**), but no labeling was observed in the RGC layer or on $GFAP^{+}$ retinal astrocytes (**Fig. 3.10e**). Hence, dectin-1 signaling promotes RGC axon regeneration through an indirect, non-cell autonomous mechanism.

Microglia and infiltrating myeloid cells rapidly phagocytose zymosan particles

Dectin-1 ligation induces phagocytosis (Tsoni and Brown, 2008). To identify the cell types that ingest zymosan in our experimental system, we injected Alexa-555 conjugated zymosan into the eyes of CX3CR1$^{GFP/+}$ reporter mice immediately following ONC. At both, 6 and 18 hours post-injection, CX3CR1-expressing microglia (**Fig. 3.11a**) and Ly6G^{+} neutrophils (**Fig. 3.11b**) stained positively for intracellular zymosan. GFP^{+} microglia are highly branched and negative for zymosan particles in retinal sections at 2 hours post-ONC and i.o. zymosan, (**Fig. 3.11c, 3.11d**). By 6 hours post-injection, labeled zymosan particles are observed within GFP^{+} microglia with a more rounded morphology (**Fig. 3.11e-i**), indicating that retina-resident microglia actively phagocytose zymosan.

Dectin-1 is required on both radioresistant retina-resident cells and infiltrating bone marrow-derived cells for curdlan-induced axon regeneration

The broad expression of dectin-1 by infiltrating myeloid cells, retina-resident microglia and DCs raises the question of which of these cells contributes to immune-mediated RGC axon regeneration. To functionally assess the role of dectin-1 in radioresistant retina-resident cells (such as microglia) versus radiosensitive hematopoietic cells (such as infiltrating monocytes/ macrophages and neutrophils), we constructed reciprocal bone marrow (BM) chimeric mice. *Dectin-1*$^{-/-}$ BM was transplanted into irradiated WT hosts [KO → WT] in order to restrict dectin-1 expression in the eye to retina-resident cells. Conversely, we generated [WT→KO] BM chimeras in which dectin-1 expression is restricted to blood-derived immune cells. [WT→ WT] and [KO→KO] chimeric mice served as positive and negative controls respectively. Chimerism for dectin-1 was confirmed by flow cytometry (**Fig. 3.12**). As expected, i.o. curdlan triggered regenerative growth of injured RGC axons in [WT→ WT] mice (**Fig. 3.13a**), but not [KO→KO] mice (**Fig. 3.13d**). A significant reduction in the number of regenerating axons was observed in [KO→WT] as well as in [WT→KO] chimeric mice (**Fig. 3.13b, 3.13c, 3.13e**). These studies show that *dectin-1* function is necessary in both retina-resident and infiltrating immune cells for the full extent of curdlan-elicited RGC axon regeneration.

Analysis of the immune infiltrate in the eye at 7 days post ONC revealed that i.o. curdlan elicits robust vitreous inflammation and accumulation of myeloid cells in [WT→KO] but not in [KO→WT] mice (**Fig. 3.13f**). Yet, the accumulation of dectin-1+ myeloid cells in the vitreous of [WT→KO] mice is not sufficient to promote optimal RGC axon regeneration (**Fig. 3.13c**). Conversely, dectin-1 expression on radioresistant retina-resident cells in [KO→WT] mice is dispensable for curdlan-induced i.o. inflammation, but is not sufficient to support optimal RGC axon regeneration (**Fig. 3.13b,f**).

3.4 Discussion

In the current study we identify particulate β-glucan as the active ingredient in zymosan, capable of eliciting long-distance axon regeneration in a dectin-1 dependent manner. This is a novel finding since previously only TLR2 agonists have been shown to simulate the therapeutic effects of zymosan in the ONC model (Yin et al., 2003, Hauk et al., 2010). Moreover, our studies indicate that, although TLR2 and dectin-1 act in a complementary manner to promote axonal regrowth, dectin-1 is dominant. Particulate β-glucan engages dectin-1 on blood-derived myeloid cells, as well as on retina-resident immune cells to enable RGC axon regeneration in a non cell-autonomous manner. The dectin-1 downstream effector CARD9 is required for β-glucan-induced CREB activation and plays an important role in inflammation-mediated RGC axon regeneration. Of clinical interest, administration of β-glucan at the time of ONC or two days later, promotes equally robust axonal growth, suggesting a large therapeutic window for β-glucan/dectin-1 elicited neurorepair.

It has been widely assumed that the vitreous inflammation induced by i.o. PAMPs is causally linked to enhanced RGC axon growth. Consistent with that contention, we found that β-glucan-mediated RGC axon regeneration is mitigated in [KO→WT] chimeric mice, in which radiosensitive hematopoietic cells are exclusively deficient in dectin-1. However, we also found regeneration to be impaired in [WT→KO] chimeric mice, implicating the participation of a radioresistant retina-resident cell in the repair process. These data suggest that full blown neurorepair is dependent on multiple cell types that act via parallel, non-redundant mechanisms. The specific phenotypes of the retina-resident and infiltrating immune cells that promote regeneration via a dectin-1-dependent pathway remain to be elucidated. Other investigators have reported that activation of retinal astrocytes and Muller cells correlates with axonal regeneration (Muller et al., 2007). However, the only retinal cells that we found to express dectin-1 are microglia and resident DCs. A direct role of retinal microglia in RGC regeneration is further supported by our observation that those cells efficiently phagocytose zymosan particles. In animal models of white matter injury (Miron and Franklin, 2014) or neurodegenerative disease (Magnus et al., 2005), microglia facilitate remyelination and suppress destructive neuroimmune responses. Thus, microglia could promote dectin-1 mediated neurorepair by clearing cellular debris, release of growth factors or by regulating the toxic aspects of inflammation.

While the inflammatory response triggered by i.o. curdlan activates RGC growth promoting programs, we observed concurrent toxicity, reminiscent of experimental autoimmune uveitis (Forrester et al., 2013). Curdlan causes retinal folding and detachment, and similar to zymosan in the spinal cord or DRGs (Gensel et al., 2009) is associated with tissue damage. Hence, β-glucan/dectin-1 signaling is sufficient to mimic the pro-regenerative effects of zymosan, but causes concomitant pathology. In *dectin-1*$^{-/-}$ mice, curdlan-elicited RGC regeneration and retinal toxicity are no longer observed (**Fig. 3.8**), suggesting that the two processes may be coupled. However the intensity of vitreous inflammation did not always correlate with extent of axonal growth. For example, i.o. zymosan induced comparable vitreous infiltrates in WT, *dectin-1;MyD88* and *dectin-1;TLR2* compound mutant mice, yet axonal regeneration was only observed in WT mice. Similarly, i.o. LPS or zymosan both lead to strong vitreous inflammation and comparable ROS production, but LPS fails to promote RGC regeneration. This paradox could reflect the fact that a distinct subset of leukocytes, yet to be identified, possesses the pro-regenerative properties, and that this subset is relatively depleted in infiltrates of the compound mutants or following i.o. LPS administration. Dectin-1$^+$ monocyte/macrophages and neutrophils are universally the most prominent constituents of PRR-induced vitreous infiltrates. Both of these myeloid cells have been touted as candidates for the immune cell that facilitates RGC axon growth (Yin et al., 2003, Kurimoto et al., 2013). However, there is growing recognition of the heterogeneity of myeloid cells (Gordon and Martinez, 2010, Miron and Franklin, 2014, Murray et al., 2014). For example, macrophages, and possibly microglia, can be polarized along a continuum of activation states including the well-known proinflmmatiory (M1-like) and anti-inflammatory (M2-like) phenotypes. Myeloid cell polarization can positively or negatively impact repair following nervous system injury (Kigerl et al., 2009, Shechter et al., 2009, Kroner et al., 2014). Stimulus-specific transcriptional programs downstream of PRRs can modulate the macrophage phenotype (Lawrence and Natoli, 2011). Transcription factors activated in a dectin-1/CARD9 dependent manner include NF-kB (Gross et al., 2006, Gringhuis et al., 2009), IRF5 (del Fresno et al., 2013) and CREB (Kelly et al., 2010, Elcombe et al., 2013, Jia et al., 2014). Dectin-1/CARD9 dependent activation of CREB downstream of curdlan coincides with enhanced regenerative growth of injured RGCs.

Dectin-1 and CREB signaling in macrophages mediates polarization toward an M2-like phenotype, and in non-neural tissue, has been shown to promote repair following injury (Ruffell et al., 2009). The partial loss of RGC axon regeneration in *CARD9*$^{-/-}$ mice suggests the involvement of additional, dectin-1-dependent pathways that function independently of CARD9.

We propose that activation of myeloid cells through β-glucan/dectin-1 leads to the expression and secretion of pro-regenerative factors that ultimately enable injured RGCs to switch to a pro-regenerative state and extend long axons. A growing list of molecules has been identified that directly or indirectly participate in inflammation mediated axonal repair, including chemokines, "anti-inflammatory" cytokines, growth factors and the calcium binding protein oncomodulin (Leibinger et al., 2009, Benowitz and Popovich, 2011, Gensel et al., 2012, Vidal et al., 2013). It therefore appears likely that multiple factors participate in *β*-glucan-elicited RGC axon regeneration. Future studies, including an in-depth analysis of the cellular and molecular milieu under inflammatory conditions that do promote (e.g. *β*-glucan) or fail to promote (e.g. LPS) RGC axon regeneration, will be needed to identify the myeloid cell type(s), their activation state, and growth factors underling inflammation-mediated neuronal repair. The molecular framework described here provides a strong platform for future studies aimed at understanding the cross talk between the immune system and the nervous system and how this may be exploited to promote repair following injury or disease.

3.5 Future Directions

The findings from this work provide several avenues for future study. We have established the ligands and receptors necessary for immune-mediated regeneration, as well as demonstrated a requirement for dectin-1 expression on both retina-resident and blood-derived immune cells. However, we do not yet know what specific types of immune cell populations are important for immune-mediated regeneration. Furthermore, downstream of dectin-1, the signaling pathways necessary for immune-mediated regeneration are yet to be elucidated. Here I discuss ongoing follow-up work, and propose areas for future study.

Conditional ablation of dectin-1 signaling

Bone marrow chimeric studies revealed a requirement for dectin-1 expression on both retina-resident and blood-derived immune cells. Dectin-1 signals through spleen tyrosine kinase (syk) to activate several pathways, including MAPK/ERK and CARD9, as discussed above. To convincingly demonstrate that dectin-1 signaling, and not just dectin-1 expression, in these immune cells is necessary for curdlan-induced regeneration we bred $syk^{flox/flox}$ mice and $LysM^{cre/+}$ mice (purchased from Jackson labs), to deplete syk expression in myeloid cell populations. Preliminary results show that these mice are still capable of curdlan-induced regeneration (**Fig. 3.14**). This result is not entirely surprising, as a previous study demonstrated that $LysM^{cre}$ mice show efficient recombination in only 80% of blood-derived myeloid cell populations, and in less than 50% of microglia (Goldmann et al., 2013). As better tools become available, it will be interesting to deplete dectin-1 and/or syk in individual myeloid cell populations, such as microglia, neutrophils, and monocytes/macrophages, to determine which individual cell types are necessary for curdlan-elicited regeneration.

Do distinct subsets of myeloid cells promote regeneration?

Intraocular injection of zymosan or curdlan causes a large and diverse population of immune cells to infiltrate the eye. As detailed in the discussion section above, macrophages can be polarized along a continuum of activation states including the well-known proinflmmatiory (M1-like) and anti-inflammatory (M2-like) phenotypes. To assess whether macrophage polarization may be involved in immune-mediated neurorepair, we examined the surface expression of M2 markers on macrophages infiltrating the eye following i.o. injection of zymosan or LPS. In zymosan-injected eyes, a significantly higher percentage of infiltrating macrophages stained positively for the M2 markers arginase-1 (ARG-1) and IL4 receptor-α (IL4Rα) compared to LPS injected eyes (**Figure 3.15**). This data is correlative, but suggests that zymosan may facilitate the polarization of macrophages towards an M2-like phenotype. Additional follow up studies are also examining whether distinct subsets of neutrophils may facilitate immune-mediated regeneration.

Examination of downstream signaling pathways

Biochemical analysis of whole eye lysates demonstrates that intraocular injection of curdlan induces phosphorylation of ERK and CREB in a dectin-1-dependent manner. While this finding implicates the involvement of ERK/CREB signaling in immune-mediated regeneration, the data are correlative at this point. Follow-up studies are necessary to determine whether activation of ERK/CREB signaling downstream of dectin-1 is necessary for immune-mediated regeneration. Intraperitoneal administration of MEK or ERK inhibitors may be an effective strategy to block ERK activation following i.o. curdlan injection. Application of these inhibitors immediately before, and for several days following ONC and i.o. injection will be necessary for complete inhibition. Regeneration can then be assessed under these conditions. Whole eye lysates can also be collected at various time points to verify by western blot that ERK phosphorylation is effectively blocked. Additional strategies may include adoptive transfer of peritoneal immune cells or bone-marrow-derived cultured immune cells in which ERK or CREB signaling has been virally manipulated, though this strategy is complicated by the fact that adoptively transferred cells recruit host immune cells to the site of injection.

A recent study demonstrated an important role for osteopontin (OPN), a secreted phosphoprotein, in promoting regeneration of specific subtypes of RGCs, termed alpha-RGCs (αRGCs) (Duan et al., 2015). OPN is capable of stimulating mTOR activity, and αRGCs express high levels of mTOR and OPN. When regeneration is enhanced through deletion of PTEN, αRGCs account for nearly all of the regenerating axons. OPN is found as both a secreted (sOPN) and intracellular protein (iOPN). Interestingly, OPN is expressed in several types of immune cells, including macrophages, neutrophils, and dendritic cells (Wang and Denhardt, 2008). In immune cells, iOPN functions downstream of dectin-1 and TLR2 to promote cytokine production, and may be involved in zymosan-mediated activation of ERK (Inoue et al., 2011). Whether OPN could be a molecular link between the two most robust paradigms for eliciting optic nerve regeneration (PTEN deletion, and immune-mediated regeneration) will be interesting to explore. OPN knockout mice are available, and should be utilized for these studies.

RNA sequencing and cytokine profiling

The dissociation of regeneration and inflammation in the dectin-1/TLR2 compound mutant mice provides a ripe opportunity to separate the beneficial aspects of intraocular inflammation from the concurrent toxic effects. The immune cells present in the eye following zymosan injection of WT mice can be compared with the immune cells in the eyes of *dectin-1/TLR2* compound mutant mice after i.o.nzymosan injection. Any differences in gene expression, cytokine expression, or immune cell composition can be further validated as a potential causative agent for immune-mediated regeneration.

Different sources of beta-glucans promote regeneration

In an effort to identify commercially available substances that promote regenerative growth without the concurrent toxicity of zymosan or curdlan, I have tested a few other sources of beta-glucans. I assessed them both for feasibility of i.o. injection, and for their ability to promote regenerative growth. Scleroglucan (Invivogen #tlrl-scg) is a high molecular weight (>1000 kDa) fungal beta-glucan, consisting of a linear β(1-3) D-glucose backbone with one β(1-6) D-glucose side chain every three main residues. Schizophyllan (Invivogen #tlrl-spg) is another fungal beta-glucan sharing the same structure as scleroglucan, but with a smaller, though still quite large, molecular weight (450 kDa). Both schizophyllan and scleroglucan are gel forming beta-glucans that become difficult to work with in solution, and are thus very challenging to inject into the eye. Mechanical refinement does not ease this process, as is the case with curdlan. While both of these beta-glucans are capable of eliciting regeneration (**Fig. 3.16c,d**), the difficulty of i.o. injection makes them poor candidates for future studies.

A particulate form of whole glucan particles (WGP® Dispersible, Biothera) also known as Wellmune, is obtained from yeast cell walls following a series of alkaline and acid extractions (Li et al., 2007). WGP-dispersible binds and activates dectin-1, but not TLR2 (Goodridge et al., 2011). Injection of WGP-dispersible into the eye is somewhat challenging, as WGP-dispersible does not dissolve in solution. A curdlan suspension in PBS as looks like large granules of sugar that don't dissolve, whereas WGP-dispersible in PBS looks like soft floating discs. These discs are not easily taken up by a 30 gauge needle. However, since they are not rigid, they can be backloaded into the syringe and forced through a 30 gauge needle with relative ease. Injection of WGP-dispersible into the eye is capable of promoting regeneration (**Fig. 3.16a**), though to a lesser extent than zymosan or curdlan. Interestingly, a soluble form of WGP, which is supposed to function as a dectin-1 antagonist, is also capable of promoting a robust regenerative response (**Fig. 3.16b**). Future studies are required with both the dispersible and soluble forms of WGP to determine whether consistent regeneration is achieved, and whether a higher dosage can further enhance regeneration. Subsequent analysis of retinal pathology is needed to determine whether any of these options show reduced toxicity.

With any form of beta-glucan that is injected into the eye, each new lot/preparation must be tested and compared with previous lots. This is particularly important with zymosan. **Figure 3.17** show examples of zymosan-induced regeneration with four different lots of zymosan from two different companies. To obtain accurate results in regeneration studies, experimental groups must always be compared to control groups treated with the exact same lot of zymosan.

3.6 Methods

Transgenic mice: All animal handling and surgical procedures were performed in compliance with local and national animal care guidelines and approved by the University of Michigan Committee on Use and Care of Animals (UCUCA). *Dectin-1 (Saijo et al., 2007), CARD9 (Hsu et al., 2007) ,* and *MyD88 (Adachi et al., 1998)* mutant mice on a C57BL/6 background were kindly provided by Tobias Hohl (Sloan Kettering Cancer Center, New York). *CR3 (CD11b/CD18)* mutants (Rosenkranz et al., 1998), *TLR2* mutants, $CX3CR1^{GFP/+}$ reporter mice (Mizutani et al., 2012), $LysM^{cre/+}$, $Syk^{flox/flox}$, and C57BL/6 wild-type controls either CD45.1 or CD45.2 were purchased from Jackson Laboratories. Mice were group housed in a 12 hour light/dark cycle with access to food and water ad libitum. Breeding pairs of *dectin-1;MyD88* compound mutant mice were kept on enrofloxacin-treated water (1.9 ml of Baytril Injectable (22 mg/ml) per 250 ml water bottle) to compensate for severe immunodeficiency.

Preparation of PAMPs: Zymosan (Di Carlo and Fiore, 1958) and depleted zymosan (Ikeda et al., 2008) from *Saccharomyces cerevisiae* (Invivogen) were suspended in PBS at a concentration of 12.5µg/µl by incubating at 37ºC for 10 min and vortexing. Aliquots were stored at 4 ºC. Lipopolysaccharide (LPS) from *E. coli* (Sigma) was dissolved in PBS (5µg/µl). Curdlan, a particulate β-(1,3)glucan and FDA approved food additive (Zhan et al., 2012) (Wako Chemicals USA), was obtained in powder form, and was mechanically refined using a mortar and pestle continuously for 5 minutes, within 24 hours before use. Immediately before use, refined curdlan was suspended at 25µg/µl in sterile PBS by vortexing for 2 minutes. Immediately before eye injections, the solution was vigorously shaken to resuspend the curdlan. After drawing up the suspension into a syringe, the syringe was visually inspected to insure curdlan particles were present, and that the needle had not been blocked by larger particles. The syringe was rinsed thoroughly with PBS after each injection.

Optic nerve crush (ONC) surgery: Adult male and female mice (6-12 weeks of age) were used for surgical procedures (Dickendesher et al., 2012). Mice were anesthetized with 100mg/kg ketamine and 10mg/kg xylazine i.p., the optic nerve exposed through an incision in the conjunctiva and compressed for 10 seconds with curved forceps (Dumont #5, Roboz) approximately 1-2 mm behind the eye. Immediately after ONC, a Hamilton syringe with a 30 gauge removable needle was used for intraocular (i.o.) injections of ~5 µl of PAMP, including zymosan (12.5µg/µl in PBS), depleted zymosan (12.5µg/µl in PBS), curdlan (25µg/µl in PBS), ~3 µl of LPS (5µg/ul in PBS), or 5µl saline (PBS). After ONC and PAMP injection, eyes were rinsed with a few drops of sterile PBS, and ophthalmic ointment (Puralube) was applied on the operated eye. Two weeks following surgery, mice were given a lethal dose of ketamine/xylazine i.p. and perfused transcardially with PBS (2 min) followed by ice-cold 4% paraformaldehyde in PBS (5 min).

Histochemical Studies: To visualize regenerating RGC axons, animals were perfused, optic nerves dissected and post-fixed in 4% paraformaldehyde in PBS overnight at 4ºC. For cryoprotection, nerves were transferred to a 30% sucrose/PBS solution and kept at 4ºC for at least two hours, and up to two weeks (Winters et al., 2011). Optic nerves were imbedded in

OCT Tissue-Tek Medium and stored at -20°C. Longitudinal sections (14µm thick) were cut with a cryostat, mounted on superfrost^{+} microscope slides (Fisher), and stained with a sheep polyclonal anti-GAP43 antibody (Leon et al., 2000, Dickendesher et al., 2012). Alexa-Fluor488 conjugated donkey anti-sheep secondary antibody (Invitrogen) was used for fluorescent labeling. For immunofluorescence labeling of the retina, eyes were dissected, post-fixed as described above, cryoprotected and sectioned at 25µm. Sections were mounted on superfrost^{+} microscope slides and stained with anti-dectin-1 (Serotec) and anti-GFAP (eBiosciences) antibodies followed by application of the appropriate Alexa-Fluor-conjugated secondary antibody. Nuclear staining with DAPI (4',6-Diamidino-2-Phenylindole, Dilactate at 300 nM) was used to counterstain sections. Images were acquired using an inverted microscope (IX71; Olympus) attached to a digital camera (DP72; Olympus).

Flow Cytometry: For the analysis of immune cells in the eye, mice were euthanized by isofluorane overdose at 7 days after ONC, perfused transcardially with PBS, eyes dissected and the vitreous fluid and retinae harvested. Retinae and vitreous fluid were pooled, homogenized, incubated in collagenase D (1 mg/ml, Fisher Scientific) for 60 min at 37°C, and rinsed in PBS prior to incubation with fluorochrome-conjugated antibodies (CD11b, CD45, CD45.1, CD45.2, CD11c, TLR2, Dectin-1, CD3, CD4, CD8, B220, NK1.1, and F4/80 were purchased from eBiosciences, Ly6C and Ly6G from Pharmingen). Dihydroethidium (Sigma) was added at 0.1 mM concentration to stain cells for ROS production. The spleen was dissected and splenocytes were passed through a 70-µm cell strainer. Red blood cells in spleens and blood were lysed with ACK (Ammonium-Chloride-Potassium) Lysing Buffer (Quality Biological). Flow cytometry was performed using a BD FacsCanto II (BD Biosciences). Cells were gated on forward and side scatter after doublet exclusion. Immune cells were identified as follows: monocytes/macrophages (CD45+ CD11b+ Ly6C+ Ly6G-), neutrophils (CD45+ CD11b+ Ly6C+ Ly6G+), DCs (CD45+ CD11b+ CD11c+), B-cells (CD45+ CD11b- B220+), T-cells (CD45+ CD11b- CD3+ CD4+ or CD8+), NK cells (CD45+ CD11b- NK1.1+), microglia (CD45^{low} CD11b+ CX3CR1+). All flow cytometry experiments were carried out with at least 6 mice (both eyes receiving the same treatment and pooled) per group, with the exception of *dectin-1*$^{-/-}$;*TLR2*$^{-/-}$ double-mutants (n= 3 mice).

Labeled Zymosan: At the time of ONC, Alexa-555 labeled zymosan (Life Technologies) was injected into one eye (5µl, 12.5µg/µl) of adult CX3CR1$^{+/GFP}$ mice. Animals were killed at 2, 6, and 18 hours after ONC, and eyeballs collected for flow cytometry of retina resident microglia and blood-derived neutrophils. Some retinae were cryosectioned and analyzed by confocal microscopy for the presence of GFP^{+} microglia that have taken up Alexa-555 labeled zymosan particles.

Western-blot Analysis: To examine activation of signaling pathways downstream of dectin-1, adult mice were subjected to ONC and i.o. injection of curdlan (25ug/µl, 5µl), PBS (5µl), or LPS (5µg/ul, 3µl). After 6 hours, mice were euthanized with CO_2, and eyes were extracted and snap frozen in dry ice cooled 2-methylbutane. Eyes were stored at -80ºC overnight. Lysates were prepared by homogenizing frozen eyes in ice-cold RIPA (50mM Tris-HCl pH 8.0, 150mM NaCl, 0.1% SDS, 0.5% sodium deoxycholate, 1% NP-40) buffer containing 50 mM beta-glycerophosphate and 100 µM sodium orthovanadate to inhibit phosphatases, and Sigma Protease Inhibitor Cocktail (diluted 1:100). Non-dissolved components were spun down at 14,000 rpm for 5min, supernatants collected, and the protein concentration of the supernatant was measured (BioRad BCA Kit). Supernatants were combined with 2x Laemmli buffer, boiled for 10min, separated by SDS-PAGE (40 µg of protein loaded per lane), and transferred to PVDF membrane (Millipore). PVDF membranes were blocked with 2% milk (BioRad) in TBS-T (Tris-buffered saline pH 7.4, containing 0.1% Tween-20) and probed with antibodies specific for pERK (1:2000, Cell Signaling), ERK (1:2000, Cell Signaling), pSyk (1:1000, Cell Signaling), Syk (1:1000, Cell Signaling), pCREB (1:1000, Upstate), CREB (1:1000, Cell Signaling), and β-actin (1:5000, Sigma). Anti-mouse or anti-rabbit IgG-HRP (Millipore) were used, along with West Pico Substrate or West Femto Substrate (Thermo Scientific) to detect primary antibodies. Protein bands were visualized and quantified with a LI-COR C-Digit and Image Studio software. Western blot band intensity in the linear range was measured with Image Studio software. For quantification, pERK levels were normalized to total ERK levels, pCREB levels to total CREB levels, and pSyk levels to total Syk and actin levels.

Generation of Dectin-1 Bone Marrow Chimeras: Chimeric mice were generated as previously described (King et al., 2010). Briefly, five-to-six week old recipient mice were lethally irradiated

(13 Gy, split dose) and given congenic (CD45.1 or CD45.2) bone marrow (BM) from donor mice (5 million cells in 300µl) via tail vein injection. Six weeks after BM transplant, ONC surgery was performed along with i.o. injection of ~5µl of curdlan (25µg/µl) or PBS. One group of animals (26 mice in total) was sacrificed 14 days after ONC surgery. A second group of BM chimeric mice (21 mice in total) was sacrificed at 7 days after ONC surgery and i.o. injection of ~5µl of curdlan (25µg/µl) or PBS. Nerves were isolated and assessed for RGC axon regeneration by anti-GAP43 labeling. Eyes were processed to assess the composition of the immune infiltrate by flow cytometry. Congenic markers (CD45.1 and CD45.2) were used to assess degree of chimerism. All BM chimeras had >97% chimerism in the myeloid compartment.

Statistical Analysis: For quantification of RGC regeneration, $GAP43^+$ axons in optic nerve sections were counted at every 0.2 mm interval past the injury site up to 1.6 mm. For each nerve, at least three sections were quantified. The number of labeled axons per section was normalized to the width of the section and converted to the total number of regenerating axons per optic nerve, as described previously (Leon et al., 2000). All optic nerve data were analyzed using one-way ANOVA followed by Tukey's post hoc comparison in Graphpad Prism 6.0. Unpaired Students t-test was used to analyze flow cytometric data with only two groups, and one-way ANOVA followed by Tukey's post hoc was used to analyze flow cytometric data with more than two groups.

3.7 Acknowledgements

Portions of this work have been published (see citation below) and are used here in agreement with the Author Rights and Permissions Policy of PNAS.

Baldwin KT*, Carbajal KS*, Segal BM, Giger RJ (2015) Neuroinflammation triggered by by β-glucan/dectin-1 signaling enables CNS axon regeneration. *Proc Natl Acad Sci USA* 112(8):2581-6 (*Equal contribution)

This work was supported by the Charles A. Dana Foundation (B.M.S. and R.J.G), the Cellular and Molecular Biology Training Grant T32GM007315 (K.T.B.), the Ruth Kirschstein Fellowship F31NS081852 (K.T.B.), Training Grant 3T32NS007222-31S1 (K.S.C.), the Dr. Miriam and Sheldon G. Adelson Medical Foundation on Neural Repair and Rehabilitation

(R.J.G.), the Veteran's Administration Merit Review Awards 1I01RX000416 and 1I01BX001387 (R.J.G. and B.M.S.), R01NS081281 (R.J.G.) and R01NS057670 (B.M.S.). We thank Tobias Hohl for *dectin-1;MyD88* and *CARD9* mice, Larry Benowitz for anti-GAP43 and Zhigang He for AAV-shPTEN-GFP.

3.8 Author Contributions

Katherine T. Baldwin (KTB), Kevin S. Carbajal (KSC), Benjmain M Segal (BMS), and Roman J. Giger (RJG) designed experiments; KTB and KSC performed the experiments, analyzed data, and prepared figures; KTB, KSC, BMS, and RJG wrote the manuscript.

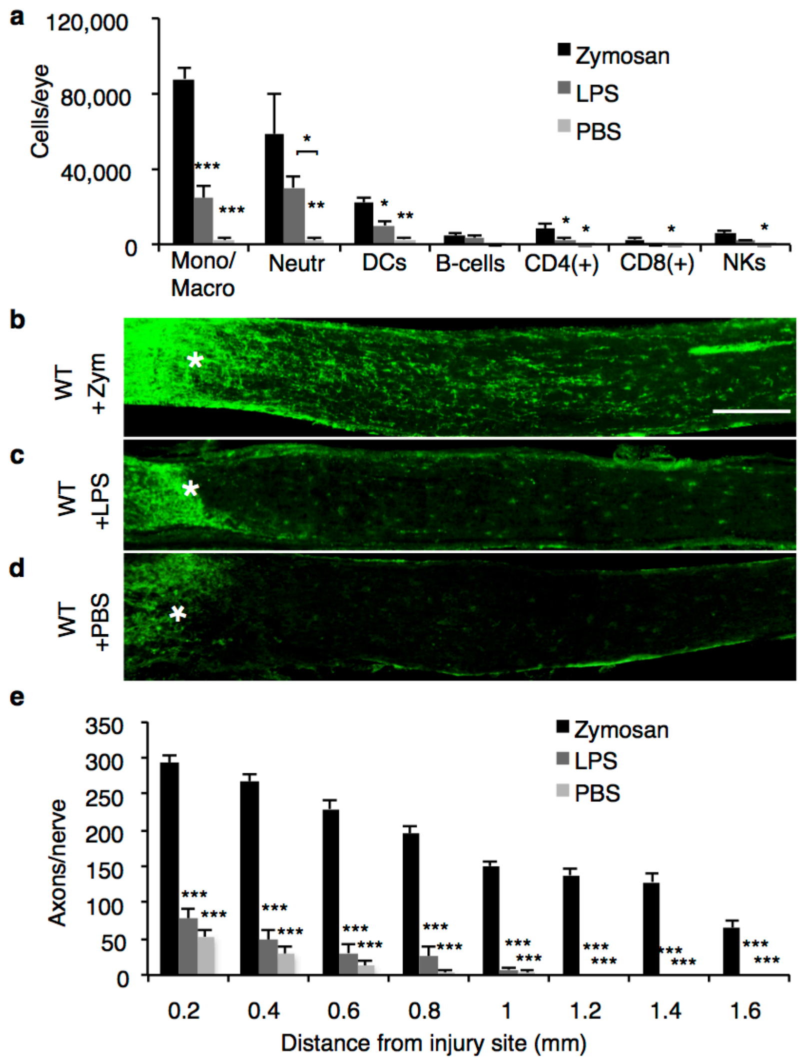

Figure 3.1: Zymosan, but not LPS enables immune-mediated axon regeneration
(**a**) Flow cytometric analysis of immune cells accumulating in the eye of wild-type (WT) mice at 7 days post-ONC and i.o. zymosan (5µl, 12.5µg/µl) injection (n= 5 mice), i.o. LPS (3µl, 5µg/µl) injection (n = 3 mice), or i.o. PBS (5ul) injection. (**b-d**) Longitudinal sections of WT mouse optic nerves at two weeks following ONC and i.o. injection. Regenerating axons are visualized by anti-GAP43 immunofluorescence labeling. The injury site is marked with an asterisk. Scale bar: 200 µm. **(b)** WT mice with i.o. zymosan (n = 6) show robust axon regeneration. No significant regeneration is observed in **(c)** WT mice with i.o. LPS (n = 4), or **(d)** WT mice with i.o. PBS (n = 5). (**e**) Quantification of the number of $GAP43^+$ axons per nerve at 0.2-1.6 mm distal to the injury site. Asterisks indicate a significant difference from zymosan-induced regeneration. Results are presented as mean ± SEM. *** p<0.001, ** p<0.01, * p<0.05 (one-way ANOVA, Tukey's post hoc).

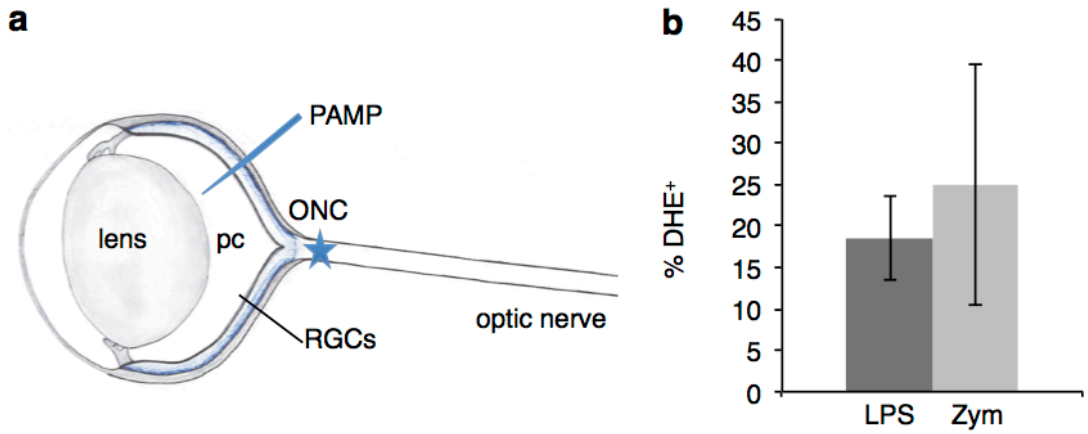

Figure 3.2: Zymosan and LPS produce similar ROS levels in the eye
(**a**) Diagram of mouse optic nerve crush (ONC) injury model. The optic nerve is crushed at 1-2 mm behind the eye ball (ONC, asterisk). PAMPs are injected into the posterior chamber (pc) of the eye to elicit an inflammatory response near the cell soma of RGCs. **(b)** Adult WT mice were subjected to ONC and i.o. injection of LPS or zymosan. Reactive oxygen species (ROS) production by macrophages was assessed by flow cytometry combined with dihyroethidium (DHE) staining at 7 days after ONC. The fraction of ROS producing (DHE^+) cells was not significantly different between LPS and zymosan injected eyes. Values represent the mean ± S.E.M. n = 4 mice (LPS) and n = 4 mice (zymosan), from two independent sets of experiments.

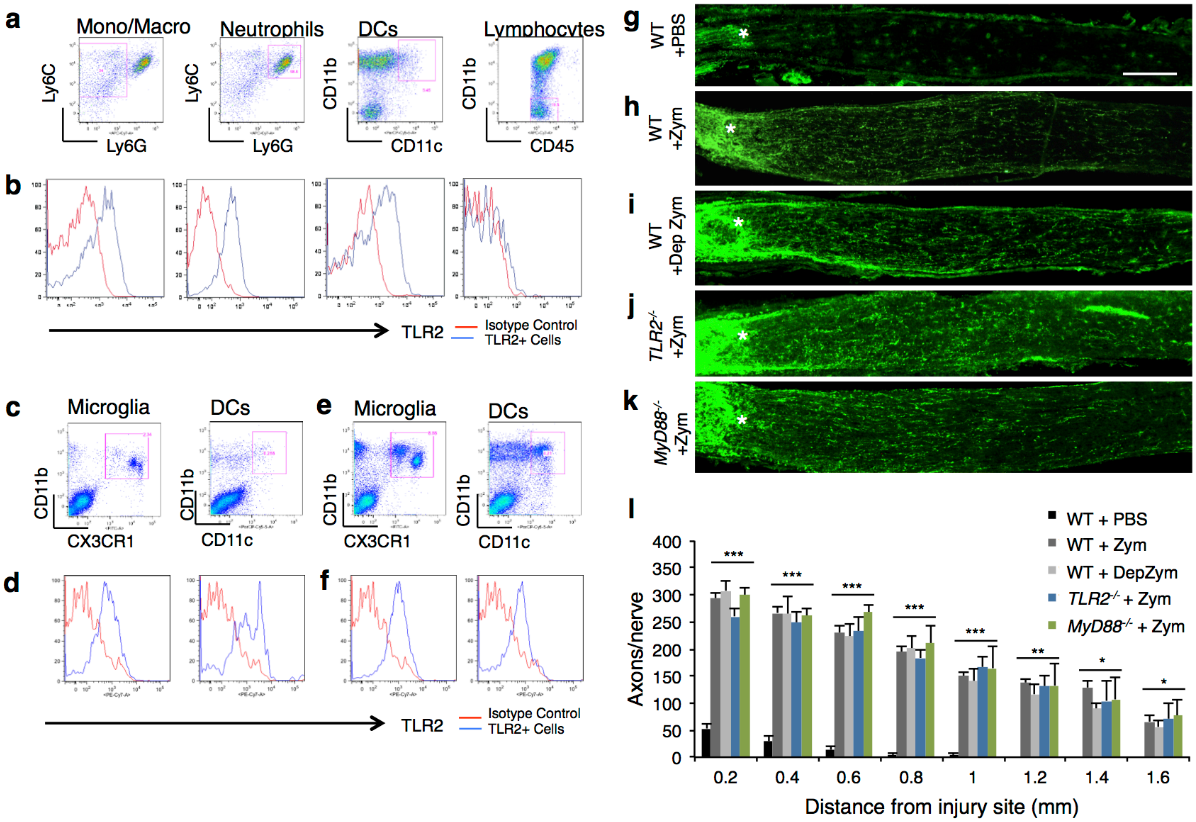

Figure 3.3 TLR2 is expressed on retina-resident and blood-derived immune cells in the eye, but is not necessary for zymosan-induced RGC axon regeneration

(a) Flow cytometic analysis of immune cells accumulating in the eye at 7 days post-ONC and i.o. zymosan injection. Representative dot plots of monocytes/macrophages ($CD45^+/CD11b^+/Ly6C^+/LyG^-$), neutrophils ($CD45^+/CD11b^+/Ly6C^+/LyG^+$), dendritic cells (DCs) ($CD45^+/CD11b^+/CD11c^+$), and lymphocytes ($CD45^+/CD11b^-$). **(b)** Histograms represent TLR2 (blue) or isotype control (red) staining for the gated cell populations. **(c)** In the naïve retina, microglia ($CD45^+/CD11b^+/CX3CR1^+$) and DCs are present, and **(d)** express TLR2. **(e)** At 7 days post-ONC (without i.o. zymosan) cell counts for microglia increase from ~6,000 to ~24,000 and for DCs from ~700 to ~10,000. **(f)** TLR2 expression on microglia and DCs at 7 days post-ONC. Plots and histograms are representative of 2 independent experiments. **(g-k)** Longitudinal sections of optic nerves at 14 days post-ONC stained with anti-GAP43. The injury site is marked with an asterisk. Scale bar: 200 µm. **(g)** Wild-type (WT) mice receiving i.o. PBS (5µl) at the time of injury show very little regenerative growth. **(h)** WT mice with i.o. zymosan (Zym, 5µl, 12.5µg/µl) or **(i)** i.o. depleted zymosan (Dep. Zym, 5µl, 12.5µg/µl) show robust RGC axon regeneration. **(j)** *TLR2*$^{-/-}$ mice with i.o. zymosan, and **(k)** *MyD88*$^{-/-}$ mice with i.o. zymosan show robust regeneration. **(l)** Quantification of the number of GAP43+ axons per optic nerve at 0.2-1.6 mm distal to the injury site: WT + PBS, n=5 nerves, 5 mice; WT + zymosan, n=6 nerves, 6 mice; WT + dep. zymosan, n=4 nerves, 4 mice; *TLR2*$^{-/-}$ + zymosan, n=4 nerves, 4 mice; *MyD88*$^{-/-}$ + zymosan, n=4 nerves, 4 mice. Data are presented as mean ± s.e.m. Regeneration is significantly enhanced in all groups in comparison to WT + PBS. ***$p<0.001$, **$p<0.01$, *$p<0.05$ (one-way ANOVA, Tukey's post hoc).

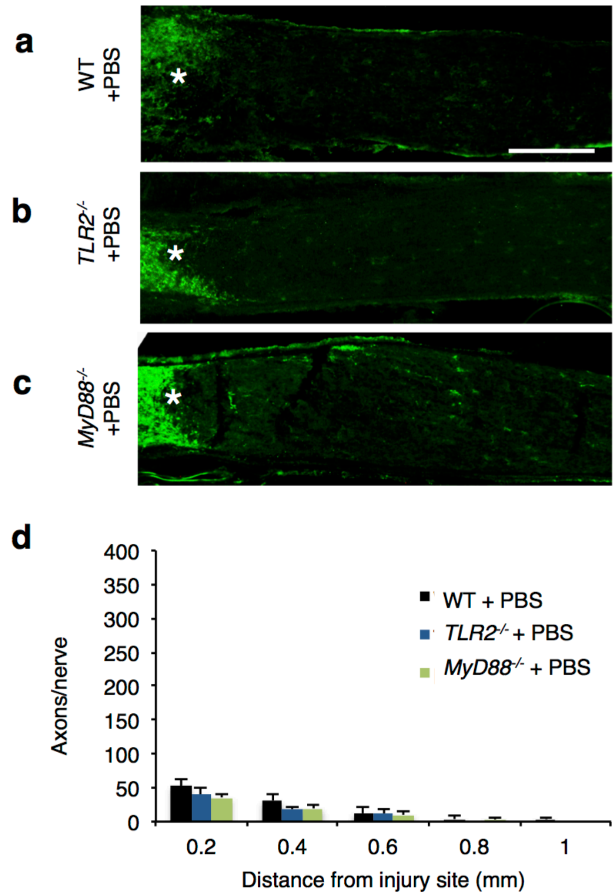

Figure 3.4: Loss of *TLR2* or *MyD88* does not alter RGC axon regeneration
(a) Wild type (WT) mice with i.o. PBS (5µl) show minimal RGC axon regeneration two weeks after ONC, as assessed by anti-GAP43 staining of longitudinal optic nerve sections. The injury site in the nerve is marked with an asterisk. Scale bar: 200 µm. When compared to WT mice, no significant difference in regeneration is observed in **(b)** *TLR2*$^{-/-}$ (n = 4 nerves, 4 mice) or **(c)** *MyD88*$^{-/-}$ mice (n = 3 nerves, 3 mice) subjected to i.o. PBS injection. **(d)** Quantification of GAP43^{+} axons at 0.2 – 1.0 mm distal to the injury site. Results are presented as mean number of axons per nerve ± s.e.m.

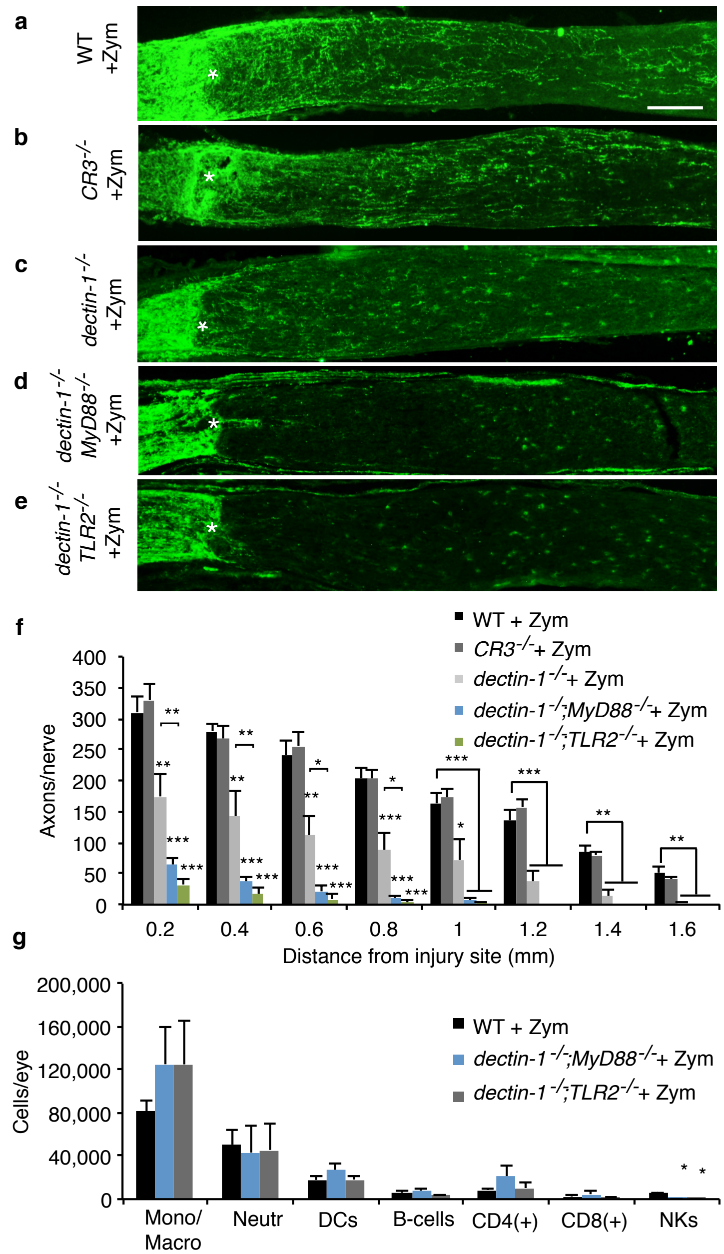

Figure 3.5: Dectin-1 and TLR2 operate as partially redundant zymosan receptors
(a-e) Longitudinal sections of mouse optic nerves at two weeks following ONC and i.o. injection of zymosan stained with anti-GAP43. Injury site marked with an asterisk. Scale bar: 200 µm. **(a)** WT mice with i.o. zymosan (n = 5), and **(b)** complement receptor 3 null mice (*CR3*$^{-/-}$) with i.o. zymosan (n = 3) show robust and comparable axon regeneration. **(c)** In *dectin-1*$^{-/-}$ mice, i.o. zymosan (n = 5) results in significantly reduced regeneration. **(d-e)** I.o. zymosan fails to induce axon regeneration in *dectin-1*$^{-/-}$*;MyD88*$^{-/-}$ compound mutants (n = 7) and *dectin-1*$^{-/-}$*;TLR2*$^{-/-}$ compound mutants (n = 6). **(f)** Quantification of the number of GAP43^{+} axons per nerve at 0.2-1.6 mm distal to the injury site. Data are presented as mean ± s.e.m. Asterisks directly above individual bars indicate a significant difference compared to WT + zymosan. *** p<0.001, ** p<0.01, * p<0.05 (one-way ANOVA, Tukey's post hoc). **(g)** Comparison of the cellular

composite of zymosan-induced inflammation in WT (n = 6 mice), *dectin-1*$^{-/-}$*;MyD88*$^{-/-}$ (n = 6 mice) and *dectin-1*$^{-/-}$*;TLR2*$^{-/-}$ (n = 3 mice) compound mutants. Independent of mouse genotype, similar numbers of macrophages/ monocytes, neutrophils, DCs, B-cells, CD4^{+} and CD8^{+} T-cells, but not NKs were identified in the vitreous.

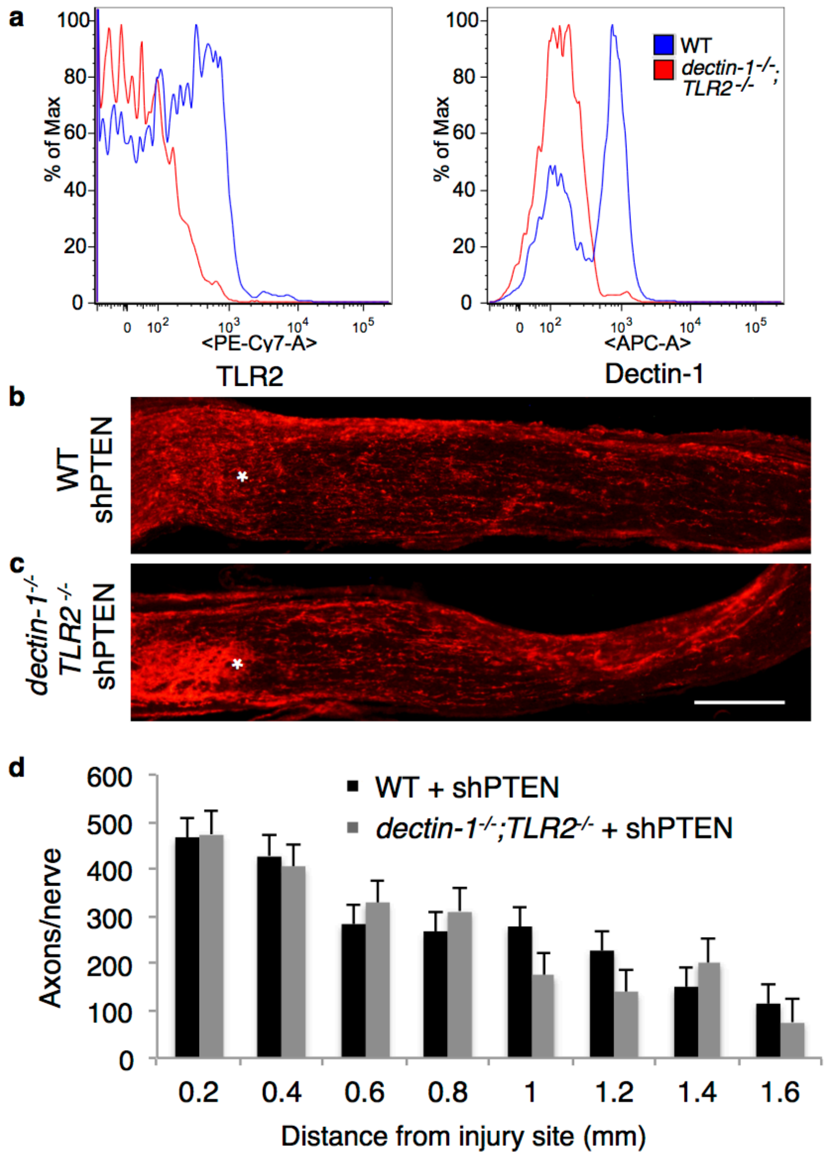

Figure 3.6: Characterization of *dectin-1/TLR2* compound mutant mice

(a) As an independent confirmation that *dectin-1/TLR2* compound mutants are null for the PRRs dectin-1 and TLR2, we carried out flow cytometric analysis of Ly6C^{+} myeloid cells isolated from the blood. Cells from double mutant mice (red line) are negative for TLR2 and dectin-1. Cells from WT mice (blue line) express TLR2 and dectin-1 on their surface. **(b-d)** To verify that *dectin-1/TLR2* compound mutant mice are capable of RGC axon regeneration in a PAMP-independent context, PTEN expression in WT and *dectin-1/TLR2* mice was knocked-down by i.o. injection of AAV2-shPTEN-GFP 14 days before ONC (Zukor et al., 2013). **(b)** Knockdown of *PTEN* elicits robust RGC axon regeneration in WT mice at 14 days following ONC, as assessed by anti-GAP43 staining. **(c)** Similarly robust RGC axon regeneration is observed in *dectin-1/TLR2* mutant mice following PTEN knockdown. **(d)** Quantification of the number of GAP43+ axons per nerve at 0.2-1.6 mm distal to the injury site. Results are presented as mean ± s.e.m. from at least 3 nerves per condition.

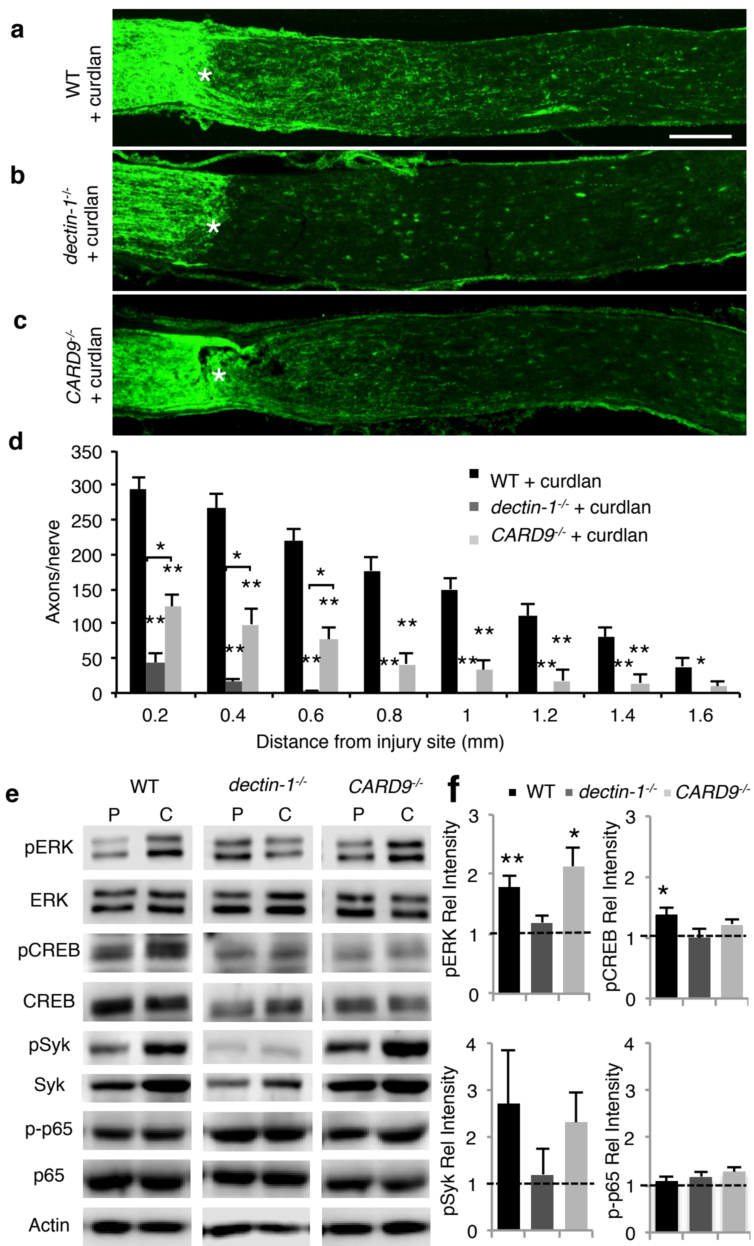

Figure 3.7: β-(1,3)glucan promotes *dectin-1*-dependent long-distance axon regeneration
(a-c) Longitudinal sections of mouse optic nerves at two weeks following ONC and i.o. curdlan (5µl, 25µg/µl) stained with anti-GAP43. Injury site marked with an asterisk. Scale bar: 200 µm. **(a)** WT mice with i.o. curdlan (n = 7) show robust axon regeneration. **(b)** In *dectin-1*$^{-/-}$ mice (n = 12), i.o. curdlan fails to elicit a regenerative response. **(c)** In *CARD9*$^{-/-}$ mice with i.o. curdlan (n = 9), axon regeneration is significantly reduced, yet increased compared to *dectin-1*$^{-/-}$ mice at 0.2 - 0.6 mm distal to the injury site. **(d)** Quantification of GAP43^{+} axons at 0.2-1.6 mm distal to the injury site. Results are presented as mean ± s.e.m. Asterisks directly above individual bars indicate a significance compared to WT + curdlan. **$p<0.001$, *$p<0.05$ (one-way ANOVA, Tukey's post hoc). **(e)** Western blot analysis of adult mouse eye extracts at 6 hours after ONC and i.o. injection of PBS, or curdlan. **(f)** Quantification of western blot band intensity relative to

respective PBS-injected eye. Compared to PBS-injected eyes, curdlan induces a significant increase in levels of pERK and pSyk in WT and *CARD9*$^{-/-}$ eyes, but not in *dectin-1*$^{-/-}$ eyes. Curdlan significantly increases pCREB (S133) levels in WT, but not in *dectin-1*$^{-/-}$ or *CARD9*$^{-/-}$ eyes. Curdlan does not increase phosphorylation of the NF-kB subunit p65 (S536) in any of the genotypes examined. A total of 3-5 eyes from two separate experiments were analyzed for each condition and genotype. Data shown are mean ±S.E.M. ** $p<0.01$, * $p<0.05$.

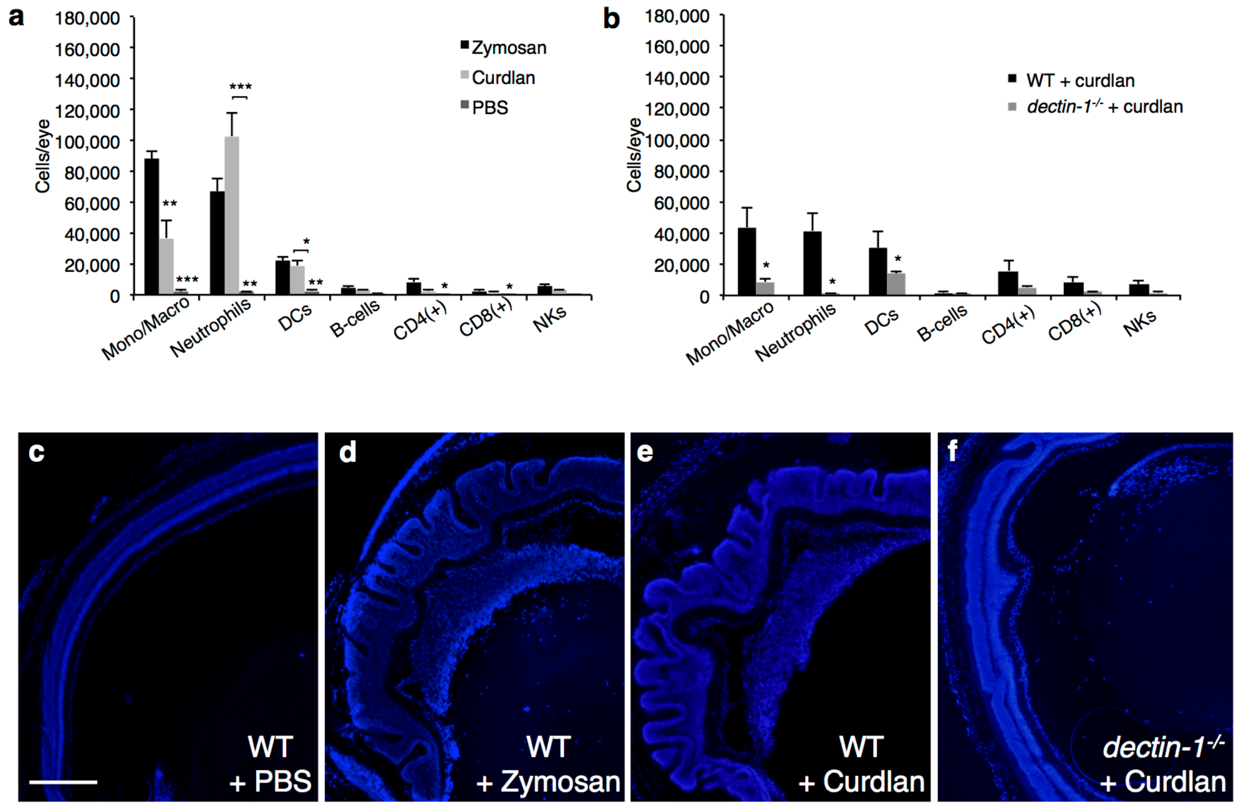

Figure 3.8: Intraocular curdlan-elicited inflammation is associated with retinal damage
Flow cytometric analysis of immune cells accumulating in the eye at 7 days post-ONC and i.o. PAMP injection. **(a)** Injection of zymosan (5µl, 12.5µg/µl) (n = 4 mice) or curdlan (5µl, 25µg/ul) (n = 3 mice) recruits monocytes/macrophages, neutrophils, DCs, and a small number of B-cells, $CD4^+$ T cells, $CD8^+$ T cells, and NKs. With exception of the decreased number of monocytes/macrophages in curdlan-treated animals, the cellular composite is very comparable. Differences between zymosan and curdlan-elicited inflammation likely reflect the fact that these two PAMPs employ partially overlapping, yet distinct receptor mechanisms to trigger inflammation. In contrast to zymosan or curdlan, i.o. injection of PBS (5µl) (n = 6 mice) recruits few immune cells to the vitreous. For statistical analysis, the number of cells was compared to zymosan-injected eyes. Values are shown as mean ± S.E.M. *** p<0.001, ** p<0.01, * p<0.05 (one-way ANOVA, Tukey's post hoc). **(b)** Flow cytometric analysis of infiltrating immune cells in the eye at 7 days post-ONC and i.o. curdlan injection. When compared to WT mice (n = 12 eyes), *dectin-1*$^{-/-}$ mice (n = 12 eyes) show a significant reduction in the number of macrophages/monocytes (from 43,600± 12,000 to 8,800 ± 2,000), neutrophils (from 41,400 ± 11,100 to 1,300 ± 200), and DCs (19,000± 3,100 to 2,600± 500). The number of lymphocytes is not significantly altered. * p<0.05 (unpaired Student's *t* test). **(c-f)** Cross sections of whole eyes stained with Hoechst at 14 days after ONC and i.o. injection of PBS or curldan. The retina is labeled with an "r" and the accumulation of inflammatory cells in the vitreous is labeled with an 'i.' Scale bar represents 100µm. **(c)** The retinal morphology of WT mice with ONC and i.o. PBS appears largely normal after 14 days. In contrast, **(d)** i.o. zymosan, or **(e)** i.o. curdlan causes choroid detachment and extensive retinal folding. The accumulation of immune cells in the

vitreous is clearly visible (indicated by the letter ‘i’). **(f)** In marked contrast, i.o. curdlan does not induce noticeable retinal pathology in *dectin-1*$^{-/-}$ mice, indicating that dectin-1 activation underlies both the beneficial (pro-regenerative) and detrimental (toxic) aspects of i.o. inflammation.

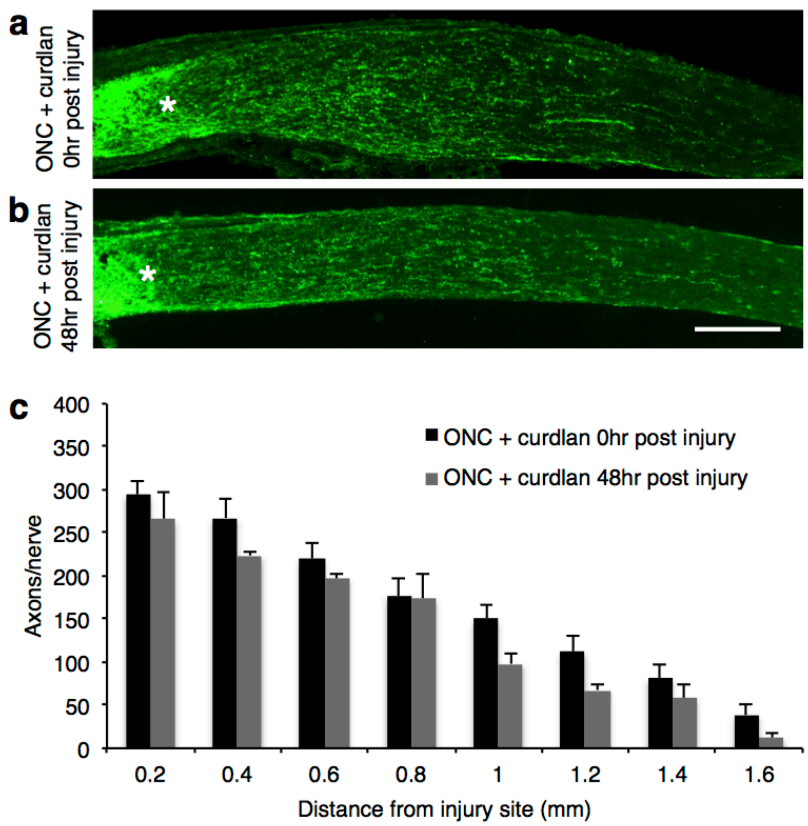

Figure 3.9: Curdlan has a therapeutic window of at least 48 hours

To assess the therapeutic window of i.o. curdlan-elicited RGC axon regeneration, ONC surgery was performed and administration of curdlan delayed for two days. **(a,b)** Longitudinal sections of mouse optic nerves at two weeks following ONC injury. Regenerating axons are stained by anti-GAP43 immunofluorescence labeling. The injury site in the nerve is marked with an asterisk. Scale bar: 200 µm. Intraocular curdlan (5µl, 25µg/µl) was administrated at **(a)** 0 hours following ONC or at **(b)** 48 hours following ONC. Robust regeneration beyond the injury site was observed for both conditions. **(c)** Quantification of GAP43^{+} axons at 0.2 – 1.6 mm distal to the injury site. Results are presented as mean ± s.e.m. from at least 4 nerves per condition.

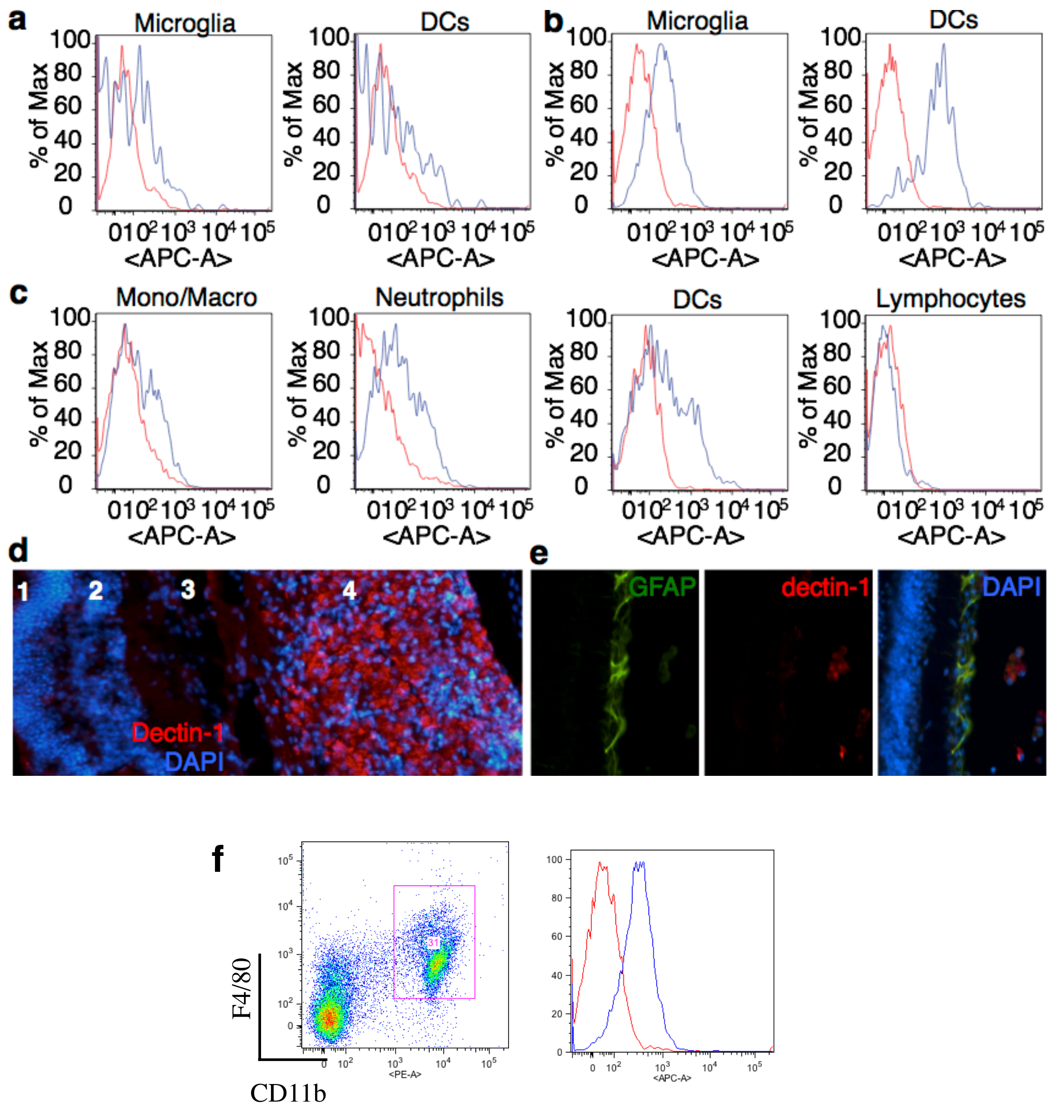

Figure 3.10: Dectin-1 is expressed on retina-resident and blood-derived myeloid cells
Flow cytometic analysis of dectin-1 expression in the eye (blue line), compared to an isotype control (red line). (**a**) Histogram of dectin-1$^+$ microglia and DCs in the eyes of naïve mice and (**b**) 7 days post-ONC in the absence of zymosan. (**c**) Analysis of dectin-1$^+$ cells in the eye at 7 days post-ONC and i.o. zymosan. (**d**) Cross-section through the eye at 14 days post-ONC and i.o. zymosan stained with anti-dectin-1 (red) and DAPI (blue) . Many dectin-1$^+$ cells are found in the vitreous (4), but not in the retina, including the outer nuclear layer (1), the inner nuclear layer (2), or the RGC layer (3). (**e**) Anti-dectin-1 immunolabeling is not observed on GFAP$^+$ retinal cells. Scale bar: 100 µm. **(f)** Analysis of dectin-1$^+$ cells in the optic nerve at 7 days post-ONC.

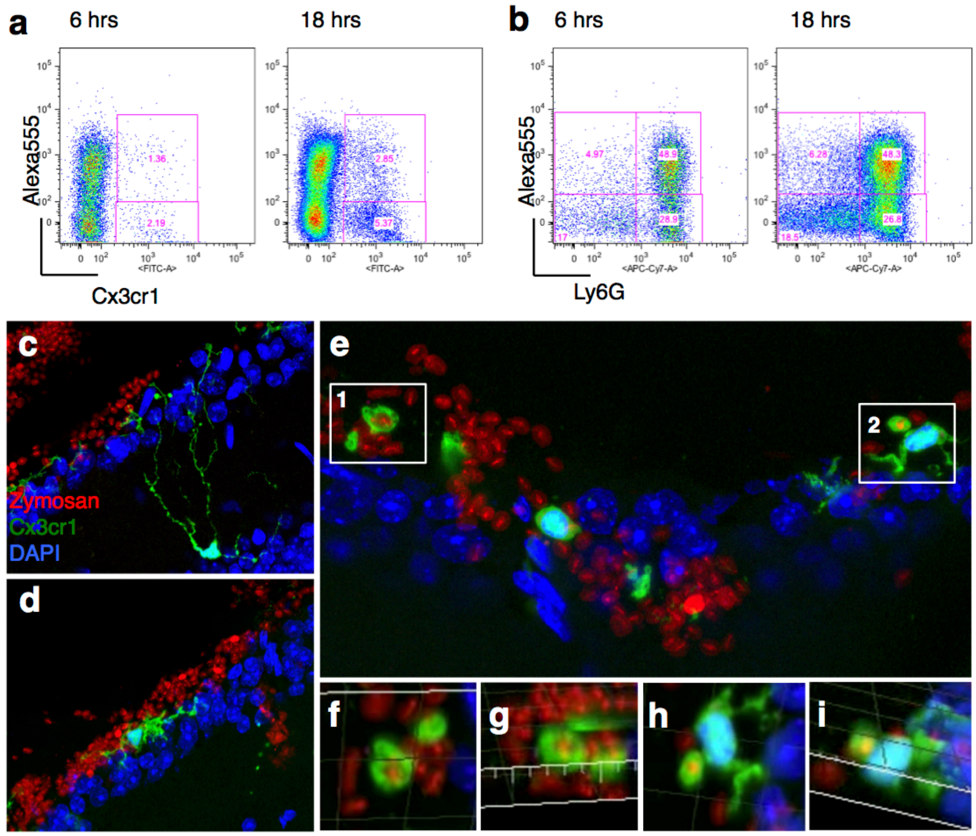

Figure 3.11: Retina-resident microglia and infiltrating neutrophils rapidly phagocytose zymosan particles

(a,b) Alexa555-conjugated zymosan particles were injected into the eye at the time of ONC and zymosan-labeled cells quantified by flow cytometry. (**a**) Dot plot of zymosan-labeled microglia at 6 and 18 hours post-ONC and i.o. zymosan injection. At both time points ~ 40% of CX3CR1$^+$ microglia are positive for zymosan. **(b)** Ly6G$^+$ neutrophils are abundantly found in the vitreous at both 6 and 18 hours following ONC and i.o. zymosan injection. Approximately 50% of neutrophils are positive for zymosan at both 6 and 18 hour time points. Data are representative of at least 2 independent experiments. (**c-i**) Confocal images of retina of CX3CR1$^{GFP/+}$ reporter mice after-ONC and i.o. injection of Alexa555-conjugated zymosan. Scale bar represents 20µm. (**c,d**) At 2 hours after zymosan injection, CX3CR1$^{GFP/+}$ microglia are highly branched, and phagocytosis of zymosan particles (red) is not observed. **(e)** At 6 hours after zymosan injection, CX3CR1$^{GFP/+}$ microglia acquire a more rounded morphology and are positive for zymosan. **(f, g)** Confocal images of double-labeled cells (box 1 in panel e) were rotated and magnified to show that zymosan particles are located within CX3CR1$^{GFP/+}$ microglia. **(h, i)** Rotated close ups of box 2, to demonstrate that zymosan particles are located within CX3CR1$^{GFP/+}$ microglia.

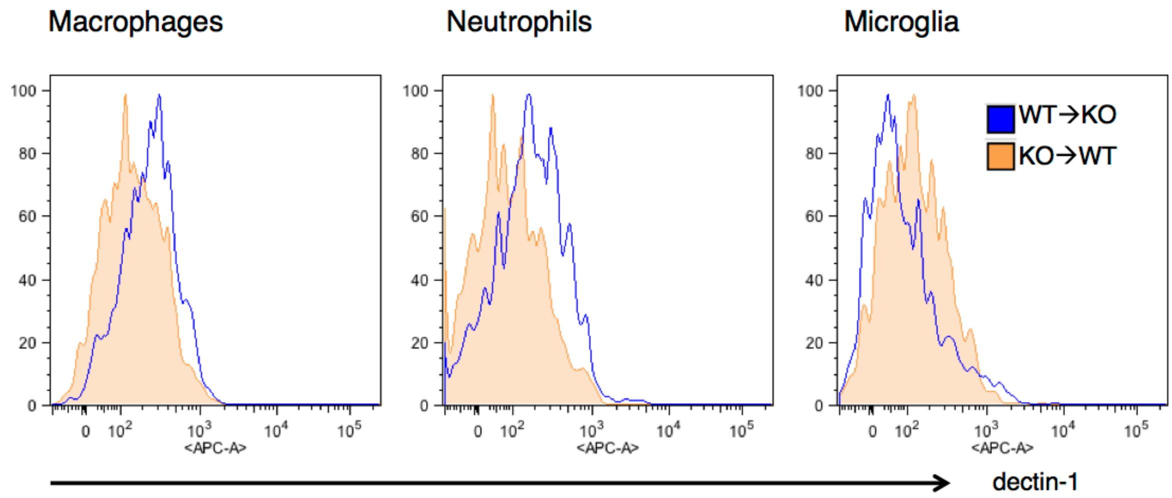

Figure 3.12: Bone marrow chimeric mice are chimeric for dectin-1 expression
Flow cytometry was used to show that transplantation of WT bone marrow into *dectin-1-/-* (KO) recipients [WT→KO] results in mice that express dectin-1 on blood-derived macrophages and neutrophils, but not on retina-resident microglia. Conversely, KO→WT chimeric mice lack dectin-1 on blood-derived immune cells, but express dectin-1 on retina resident microglia.

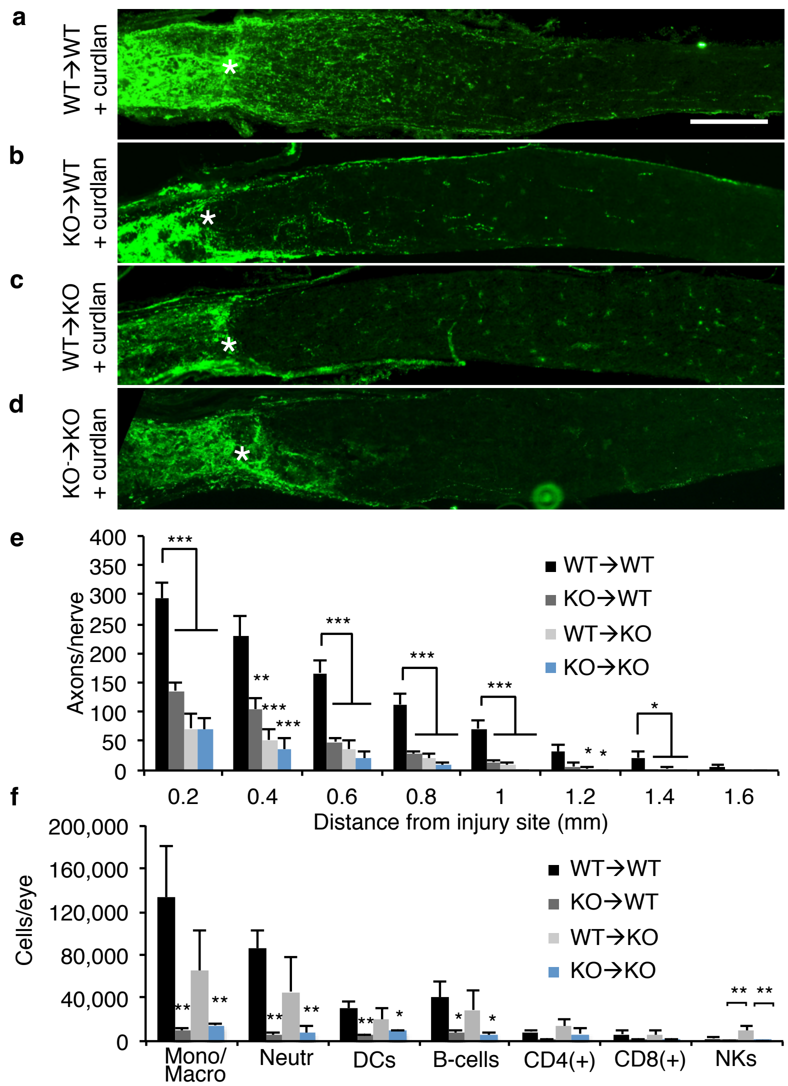

Figure 3.13: Dectin-1 expression is necessary on both radioresistant retinal cells and bone-marrow derived infiltrating cells for curdlan-induced axon regeneration

Reciprocal bone marrow chimeric mice we subjected to i.o. curdlan injection (5µl, 25µg/µl) and regeneration was assessed two weeks later by anti-GAP43 labeling. The injury site is marked with an asterisk. Scale bar: 200 µm. **(a)** WT mice that received WT donor BM (WT→WT) show robust curdlan-induced axon regeneration. **(b)** In contrast, WT mice that received *dectin-1*$^{-/-}$ BM (KO→WT) showed significantly less regeneration, comparable to **(c)** *dectin-1*$^{-/-}$ mice that received WT BM (WT→KO), and **(d)** *dectin-1*$^{-/-}$ mice that received *dectin-1*$^{-/-}$ BM (KO→KO) **(e)** Quantification of GAP43^{+} fibers at 0.2-1.6 mm distal to the injury site (WT→WT + curdlan, n = 6 nerves, 6 mice; KO→WT + curdlan, n = 8 nerves, 5 mice; WT→KO + curdlan, n = 12 nerves, 8 mice; KO→KO + curdlan, n = 6 nerves, 4 mice). **(f)** Flow cytometric analysis of intraocular inflammation at 7 days post i.o. curdlan and ONC. Inflammation in WT→WT and WT→KO mice is comparable. Significantly decreased inflammation is observed in KO→WT and KO→KO mice. Results are presented as mean ± s.e.m. Asterisks indicate a significant difference from WT→WT. *** $p<0.001$, ** $p<0.01$, * $p<0.05$, (one-way ANOVA, Tukey's post hoc).

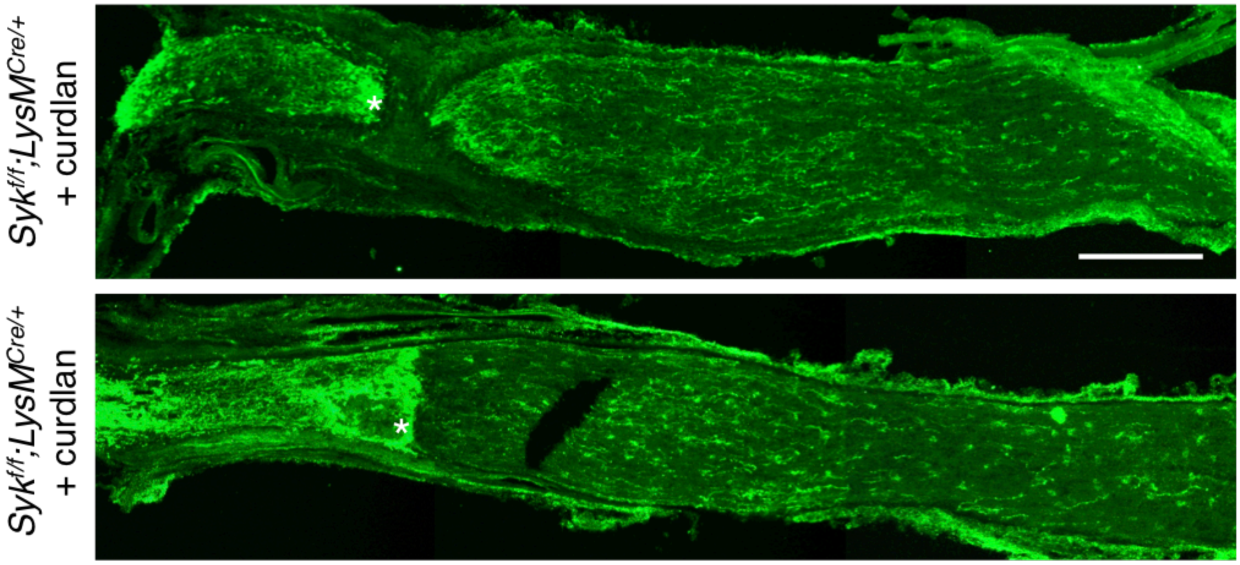

Figure 3.14: Curdlan induces regeneration in Syk$^{f/f}$;LysM$^{Cre/+}$ mice
Longitudinal sections of *Syk$^{f/f}$;LysM$^{Cre/+}$* mouse optic nerves at two weeks following ONC and i.o. injection. Regenerating axons are visualized by anti-GAP43 immunofluorescence labeling. The injury site is marked with an asterisk. Scale bar: 200 µm. Representative images from two different mice are shown.

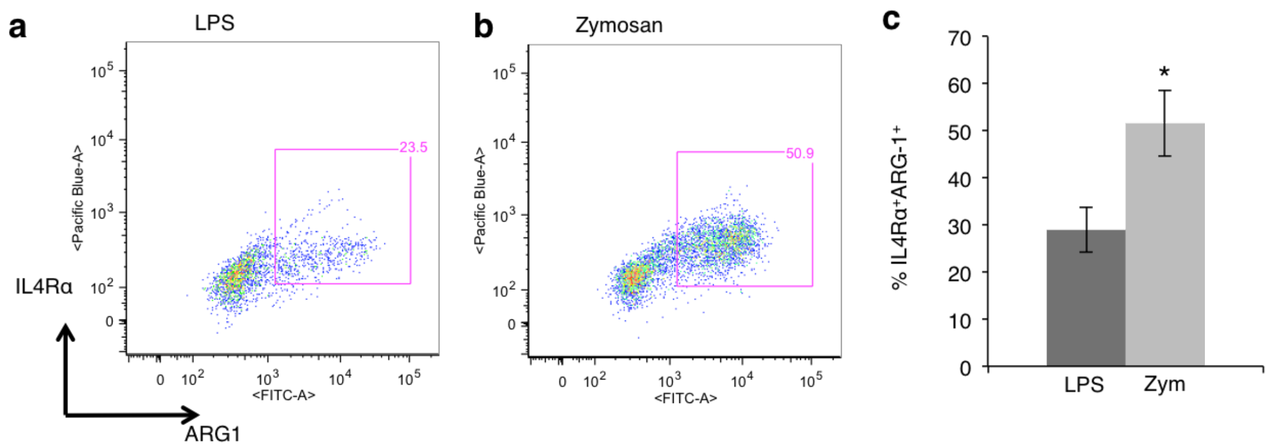

Figure 3.15: Intraocular injection of LPS and zymosan differentially affects macrophage polarization

(a,b) Flow cytometic analysis of monocytes/macrophages isolated from LPS or zymosan injected eyes. At 7 days after injection, expression of the "M2-type" markers arginase-1 (ARG-1) and IL4 receptor-α (IL4Rα) is more abundant in zymosan injected mice. **(c)** Quantification of the fraction of IL4Rα and ARG-1 double positive monocytes/macrophages revealed a significant increase zymosan versus LPS injected eyes. Values represent the mean ± S.E.M. * $p<0.05$ ** $p<0.01$ (unpaired t test) n= 4 mice (LPS) and n = 4 mice (zymosan), from two independent sets of experiments.

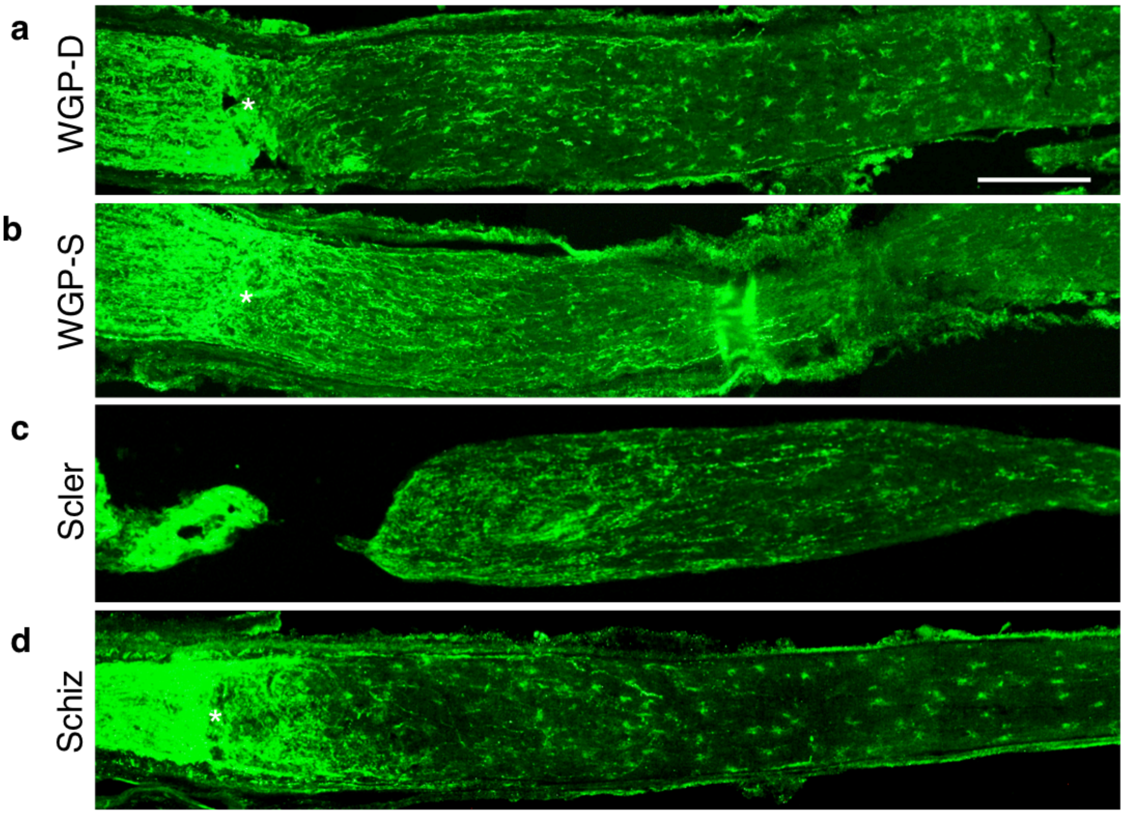

Figure 3.16: Different sources of β-glucans promote CNS axon regeneration
(a-d) Longitudinal sections of WT mouse optic nerves at two weeks following ONC and i.o. injection. Regenerating axons are visualized by anti-GAP43 immunofluorescence labeling. The injury site is marked with an asterisk. Scale bar: 200 µm. **(a)** i.o injection of 5ul (12.5ug/ul) of whole glucan particle dispersable (WGP-D) or **(b)** WGP soluble (WGP-S) from *S. cerevisiae* stimulates optic nerve regeneration. **(c)** Injection of scleroglucan (5ul, 12.5ug/ul) from the filamentous fungus Sclerotium rolfsii elicits robust regeneneration **(d)** Modest regeneration is observed following i.o. injection of Schizophyllin (5ul, 12.5ug/ul) from the fungus Schizophyllum commune.

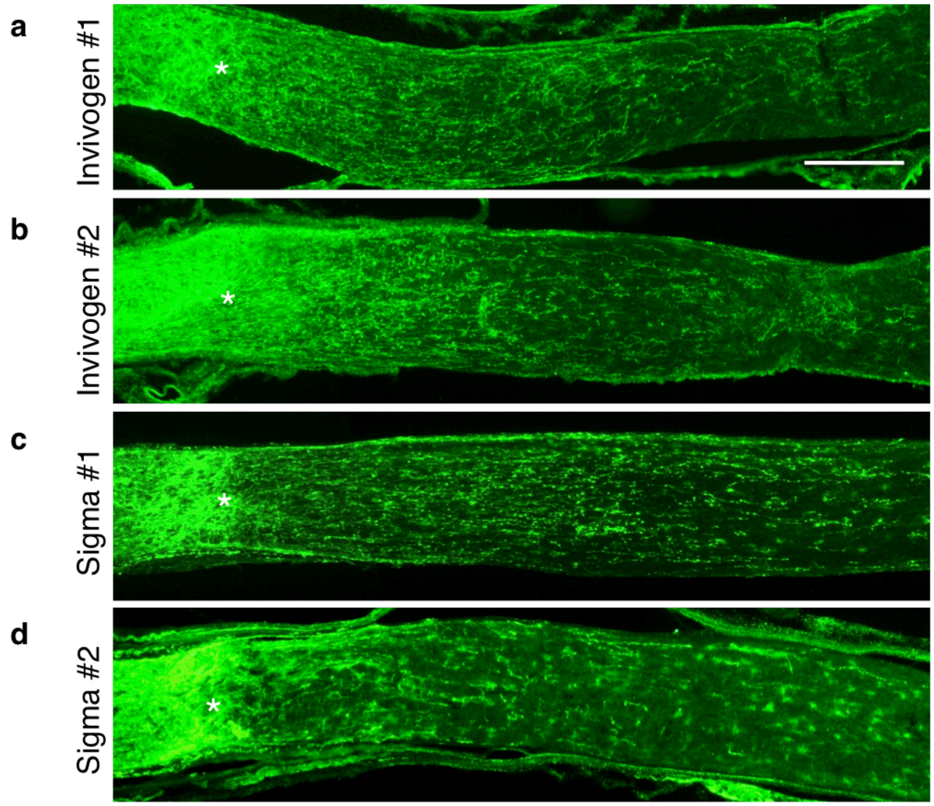

Figure 3.17: Variability in zymosan-induced regeneration among different lots and sources of zymosan

(a-d) Longitudinal sections of WT mouse optic nerves at two weeks following ONC and i.o. injection. Regenerating axons are visualized by anti-GAP43 immunofluorescence labeling. The injury site is marked with an asterisk. Scale bar: 200 µm. **(a-b)** Two different lots of zymosan purchased from Invivogen show a robust and comparable regenerative response. **(c)** A batch of zymosan from Sigma, purchased in November 2010 (Sigma #1) shows equally robust regeneration. **(d)** A subsequent batch purchased from Sigma in January 2013 (Sigma #2) is not as potent, and elicits significantly less robust regeneration.

3.9 References

Adachi O, Kawai T, Takeda K, Matsumoto M, Tsutsui H, Sakagami M, Nakanishi K, Akira S (1998) Targeted disruption of the MyD88 gene results in loss of IL-1- and IL-18-mediated function. Immunity 9:143-150.

Benowitz LI, Popovich PG (2011) Inflammation and axon regeneration. Curr Opin Neurol 24:577-583.

Choi H, Lee RH, Bazhanov N, Oh JY, Prockop DJ (2011) Anti-inflammatory protein TSG-6 secreted by activated MSCs attenuates zymosan-induced mouse peritonitis by decreasing TLR2/NF-kappaB signaling in resident macrophages. Blood 118:330-338.

del Fresno C, Soulat D, Roth S, Blazek K, Udalova I, Sancho D, Ruland J, Ardavin C (2013) Interferon-beta production via Dectin-1-Syk-IRF5 signaling in dendritic cells is crucial for immunity to C. albicans. Immunity 38:1176-1186.

Di Carlo FJ, Fiore JV (1958) On the composition of zymosan. Science 127:756-757.

Dickendesher TL, Baldwin KT, Mironova YA, Koriyama Y, Raiker SJ, Askew KL, Wood A, Geoffroy CG, Zheng B, Liepmann CD, Katagiri Y, Benowitz LI, Geller HM, Giger RJ (2012) NgR1 and NgR3 are receptors for chondroitin sulfate proteoglycans. Nature neuroscience 15:703-712.

Duan X, Qiao M, Bei F, Kim IJ, He Z, Sanes JR (2015) Subtype-Specific Regeneration of Retinal Ganglion Cells following Axotomy: Effects of Osteopontin and mTOR Signaling. Neuron 85:1244-1256.

Elcombe SE, Naqvi S, Van Den Bosch MW, MacKenzie KF, Cianfanelli F, Brown GD, Arthur JS (2013) Dectin-1 regulates IL-10 production via a MSK1/2 and CREB dependent pathway and promotes the induction of regulatory macrophage markers. PLoS One 8:e60086.

Fawcett JW, Schwab ME, Montani L, Brazda N, Muller HW (2012) Defeating inhibition of regeneration by scar and myelin components. Handb Clin Neurol 109:503-522.

Forrester JV, Klaska IP, Yu T, Kuffova L (2013) Uveitis in mouse and man. International reviews of immunology 32:76-96.

Frasnelli ME, Tarussio D, Chobaz-Peclat V, Busso N, So A (2005) TLR2 modulates inflammation in zymosan-induced arthritis in mice. Arthritis research & therapy 7:R370-379.

Gensel JC, Kigerl KA, Mandrekar-Colucci SS, Gaudet AD, Popovich PG (2012) Achieving CNS axon regeneration by manipulating convergent neuro-immune signaling. Cell Tissue Res 349:201-213.

Gensel JC, Nakamura S, Guan Z, van Rooijen N, Ankeny DP, Popovich PG (2009) Macrophages promote axon regeneration with concurrent neurotoxicity. The Journal of neuroscience : the official journal of the Society for Neuroscience 29:3956-3968.

Goldmann T, Wieghofer P, Muller PF, Wolf Y, Varol D, Yona S, Brendecke SM, Kierdorf K, Staszewski O, Datta M, Luedde T, Heikenwalder M, Jung S, Prinz M (2013) A new type of microglia gene targeting shows TAK1 to be pivotal in CNS autoimmune inflammation. Nat Neurosci 16:1618-1626.

Goodridge HS, Reyes CN, Becker CA, Katsumoto TR, Ma J, Wolf AJ, Bose N, Chan AS, Magee AS, Danielson ME, Weiss A, Vasilakos JP, Underhill DM (2011) Activation of the innate

immune receptor Dectin-1 upon formation of a 'phagocytic synapse'. Nature 472:471-475.
Gordon S, Martinez FO (2010) Alternative activation of macrophages: mechanism and functions. Immunity 32:593-604.
Gringhuis SI, den Dunnen J, Litjens M, van der Vlist M, Wevers B, Bruijns SC, Geijtenbeek TB (2009) Dectin-1 directs T helper cell differentiation by controlling noncanonical NF-kappaB activation through Raf-1 and Syk. Nat Immunol 10:203-213.
Gross O, Gewies A, Finger K, Schafer M, Sparwasser T, Peschel C, Forster I, Ruland J (2006) Card9 controls a non-TLR signalling pathway for innate anti-fungal immunity. Nature 442:651-656.
Hauk TG, Leibinger M, Muller A, Andreadaki A, Knippschild U, Fischer D (2010) Stimulation of axon regeneration in the mature optic nerve by intravitreal application of the toll-like receptor 2 agonist Pam3Cys. Invest Ophthalmol Vis Sci 51:459-464.
Hsu YM, Zhang Y, You Y, Wang D, Li H, Duramad O, Qin XF, Dong C, Lin X (2007) The adaptor protein CARD9 is required for innate immune responses to intracellular pathogens. Nat Immunol 8:198-205.
Ikeda Y, Adachi Y, Ishii T, Miura N, Tamura H, Ohno N (2008) Dissociation of Toll-like receptor 2-mediated innate immune response to Zymosan by organic solvent-treatment without loss of Dectin-1 reactivity. Biol Pharm Bull 31:13-18.
Inoue M, Moriwaki Y, Arikawa T, Chen YH, Oh YJ, Oliver T, Shinohara ML (2011) Cutting edge: critical role of intracellular osteopontin in antifungal innate immune responses. J Immunol 186:19-23.
Jia XM, Tang B, Zhu LL, Liu YH, Zhao XQ, Gorjestani S, Hsu YM, Yang L, Guan JH, Xu GT, Lin X (2014) CARD9 mediates Dectin-1-induced ERK activation by linking Ras-GRF1 to H-Ras for antifungal immunity. J Exp Med 211:2307-2321.
Kelly EK, Wang L, Ivashkiv LB (2010) Calcium-activated pathways and oxidative burst mediate zymosan-induced signaling and IL-10 production in human macrophages. J Immunol 184:5545-5552.
Kigerl KA, Gensel JC, Ankeny DP, Alexander JK, Donnelly DJ, Popovich PG (2009) Identification of two distinct macrophage subsets with divergent effects causing either neurotoxicity or regeneration in the injured mouse spinal cord. J Neurosci 29:13435-13444.
King IL, Kroenke MA, Segal BM (2010) GM-CSF-dependent, CD103+ dermal dendritic cells play a critical role in Th effector cell differentiation after subcutaneous immunization. J Exp Med 207:953-961.
Kroner A, Greenhalgh AD, Zarruk JG, Passos Dos Santos R, Gaestel M, David S (2014) TNF and increased intracellular iron alter macrophage polarization to a detrimental M1 phenotype in the injured spinal cord. Neuron 83:1098-1116.
Kurimoto T, Yin Y, Habboub G, Gilbert HY, Li Y, Nakao S, Hafezi-Moghadam A, Benowitz LI (2013) Neutrophils express oncomodulin and promote optic nerve regeneration. The Journal of neuroscience : the official journal of the Society for Neuroscience 33:14816-14824.
Lawrence T, Natoli G (2011) Transcriptional regulation of macrophage polarization: enabling diversity with identity. Nature reviews Immunology 11:750-761.
Leibinger M, Muller A, Andreadaki A, Hauk TG, Kirsch M, Fischer D (2009) Neuroprotective and axon growth-promoting effects following inflammatory stimulation on mature retinal

ganglion cells in mice depend on ciliary neurotrophic factor and leukemia inhibitory factor. The Journal of neuroscience : the official journal of the Society for Neuroscience 29:14334-14341.
Leon S, Yin Y, Nguyen J, Irwin N, Benowitz LI (2000) Lens injury stimulates axon regeneration in the mature rat optic nerve. J Neurosci 20:4615-4626.
Li B, Cramer D, Wagner S, Hansen R, King C, Kakar S, Ding C, Yan J (2007) Yeast glucan particles activate murine resident macrophages to secrete proinflammatory cytokines via MyD88- and Syk kinase-dependent pathways. Clin Immunol 124:170-181.
Magnus T, Schreiner B, Korn T, Jack C, Guo H, Antel J, Ifergan I, Chen L, Bischof F, Bar-Or A, Wiendl H (2005) Microglial expression of the B7 family member B7 homolog 1 confers strong immune inhibition: implications for immune responses and autoimmunity in the CNS. J Neurosci 25:2537-2546.
McGettrick AF, O'Neill LA (2010) Regulators of TLR4 signaling by endotoxins. Sub-cellular biochemistry 53:153-171.
Miron VE, Franklin RJ (2014) Macrophages and CNS remyelination. Journal of neurochemistry 130:165-171.
Mizutani M, Pino PA, Saederup N, Charo IF, Ransohoff RM, Cardona AE (2012) The fractalkine receptor but not CCR2 is present on microglia from embryonic development throughout adulthood. J Immunol 188:29-36.
Muller A, Hauk TG, Fischer D (2007) Astrocyte-derived CNTF switches mature RGCs to a regenerative state following inflammatory stimulation. Brain : a journal of neurology 130:3308-3320.
Murray PJ, Allen JE, Biswas SK, Fisher EA, Gilroy DW, Goerdt S, Gordon S, Hamilton JA, Ivashkiv LB, Lawrence T, Locati M, Mantovani A, Martinez FO, Mege JL, Mosser DM, Natoli G, Saeij JP, Schultze JL, Shirey KA, Sica A, Suttles J, Udalova I, van Ginderachter JA, Vogel SN, Wynn TA (2014) Macrophage activation and polarization: nomenclature and experimental guidelines. Immunity 41:14-20.
Okada T, Ichikawa M, Tokita Y, Horie H, Saito K, Yoshida J, Watanabe M (2005) Intravitreal macrophage activation enables cat retinal ganglion cells to regenerate injured axons into the mature optic nerve. Experimental neurology 196:153-163.
Rosenkranz AR, Coxon A, Maurer M, Gurish MF, Austen KF, Friend DS, Galli SJ, Mayadas TN (1998) Impaired mast cell development and innate immunity in Mac-1 (CD11b/CD18, CR3)-deficient mice. J Immunol 161:6463-6467.
Roth S, Ruland J (2013) Caspase recruitment domain-containing protein 9 signaling in innate immunity and inflammation. Trends Immunol 34:243-250.
Ruffell D, Mourkioti F, Gambardella A, Kirstetter P, Lopez RG, Rosenthal N, Nerlov C (2009) A CREB-C/EBPbeta cascade induces M2 macrophage-specific gene expression and promotes muscle injury repair. Proc Natl Acad Sci U S A 106:17475-17480.
Ruland J (2008) CARD9 signaling in the innate immune response. Ann N Y Acad Sci 1143:35-44.
Saijo S, Fujikado N, Furuta T, Chung SH, Kotaki H, Seki K, Sudo K, Akira S, Adachi Y, Ohno N, Kinjo T, Nakamura K, Kawakami K, Iwakura Y (2007) Dectin-1 is required for host defense against Pneumocystis carinii but not against Candida albicans. Nat Immunol 8:39-46.
Shechter R, London A, Varol C, Raposo C, Cusimano M, Yovel G, Rolls A, Mack M, Pluchino S, Martino G, Jung S, Schwartz M (2009) Infiltrating blood-derived macrophages are

vital cells playing an anti-inflammatory role in recovery from spinal cord injury in mice. PLoS medicine 6:e1000113.
Steinmetz MP, Horn KP, Tom VJ, Miller JH, Busch SA, Nair D, Silver DJ, Silver J (2005) Chronic enhancement of the intrinsic growth capacity of sensory neurons combined with the degradation of inhibitory proteoglycans allows functional regeneration of sensory axons through the dorsal root entry zone in the mammalian spinal cord. The Journal of neuroscience : the official journal of the Society for Neuroscience 25:8066-8076.
Sun F, Park KK, Belin S, Wang D, Lu T, Chen G, Zhang K, Yeung C, Feng G, Yankner BA, He Z (2011) Sustained axon regeneration induced by co-deletion of PTEN and SOCS3. Nature 480:372-375.
Thornton BP, Vetvicka V, Pitman M, Goldman RC, Ross GD (1996) Analysis of the sugar specificity and molecular location of the beta-glucan-binding lectin site of complement receptor type 3 (CD11b/CD18). J Immunol 156:1235-1246.
Tsoni SV, Brown GD (2008) beta-Glucans and dectin-1. Ann N Y Acad Sci 1143:45-60.
Underhill DM, Ozinsky A, Hajjar AM, Stevens A, Wilson CB, Bassetti M, Aderem A (1999) The Toll-like receptor 2 is recruited to macrophage phagosomes and discriminates between pathogens. Nature 401:811-815.
Vidal PM, Lemmens E, Dooley D, Hendrix S (2013) The role of "anti-inflammatory" cytokines in axon regeneration. Cytokine Growth Factor Rev 24:1-12.
Wang KX, Denhardt DT (2008) Osteopontin: role in immune regulation and stress responses. Cytokine Growth Factor Rev 19:333-345.
Winters JJ, Ferguson CJ, Lenk GM, Giger-Mateeva VI, Shrager P, Meisler MH, Giger RJ (2011) Congenital CNS hypomyelination in the Fig4 null mouse is rescued by neuronal expression of the PI(3,5)P(2) phosphatase Fig4. The Journal of neuroscience : the official journal of the Society for Neuroscience 31:17736-17751.
Yin Y, Cui Q, Li Y, Irwin N, Fischer D, Harvey AR, Benowitz LI (2003) Macrophage-derived factors stimulate optic nerve regeneration. The Journal of neuroscience : the official journal of the Society for Neuroscience 23:2284-2293.
Zhan XB, Lin CC, Zhang HT (2012) Recent advances in curdlan biosynthesis, biotechnological production, and applications. Appl Microbiol Biotechnol 93:525-531.
Zukor K, Belin S, Wang C, Keelan N, Wang X, He Z (2013) Short hairpin RNA against PTEN enhances regenerative growth of corticospinal tract axons after spinal cord injury. J Neurosci 33:15350-15361.

CHAPTER IV:

Discussion: Interpretation of Results, and the Future of CNS Repair

Over the past few decades, our understanding of the molecular and cellular mechanisms that restrict or promote regeneration in the injured adult mammalian CNS has improved substantially. Neurite outgrowth assays revealed that injured CNS tissue contains a diverse array of inhibitory ligands that bind axonal surface receptors to restrict growth and plasticity *in vitro* (Giger et al., 2010). However, blocking inhibitory mechanisms *in vivo* has met with only minimal success in promoting regenerative growth (Lee et al., 2010, Dickendesher et al., 2012). Conversely, genetic manipulation of neuron intrinsic pathways to promote cell growth and survival elicits a robust regenerative response *in vivo* (Sun et al., 2011). A major caveat for many of these studies, however, is that genetic manipulation done prior to injury yields more robust regeneration than manipulation after injury, diminishing the therapeutic potential of these studies. Furthermore, knockdown of tumor suppressor genes, such as PTEN, may have undesirable long-term consequences. Several studies have shown that a local inflammatory response initiated after injury significantly enhances neuronal survival and regenerative growth. Until recently, the nature of this inflammatory response, and the underlying molecular mechanisms were unknown. Our studies provide the first insights into the cellular and molecular mechanisms of immune-mediated regeneration. Since an immune response initiated two days after injury promotes regeneration to a similar extent as one initiated at the time of injury, exploitation of immunomodulatory mechanisms to promote regeneration holds great promise therapeutically.

4. 1 Uncoupling Immune-Mediate Regeneration and Toxicity

We have identified a ligand-receptor system capable of promoting robust regeneration in the injured rodent CNS. Ligation of β1,3-glucan with dectin-1 on cells of the innate immune system is sufficient to elicit robust regeneration in the mouse optic nerve. β-glucans from several different sources, including fungal (zymosan, scleroglucan, WGP) and bacterial (curdlan), successfully promote regeneration. Conversely, other inflammatory compounds, such as the TLR4 ligand LPS, do not promote regeneration, despite causing intraocular inflammation, indicating that only activation of certain immune pathways leads to regenerative axonal growth. Unfortunately, this enhanced regeneration is accompanied by concurrent toxicity. In both curdlan and zymosan-injected eyes, the retina is severely buckled and detached from the pigmented epithelium. Curdlan-induced retinal pathology is dectin-1-dependent, as i.o. curdlan fails to induce retinal pathology in *dectin-1* knockout mice. With our current level of understanding of the signaling pathways important for immune-mediated regeneration downstream of dectin-1, we cannot uncouple regeneration from toxicity. Separating these two aspects will be vital for the development of therapeutic strategies, as the detrimental aspects of neuroinflammation may damage existing structures and complicate repair efforts.

Opportunities to uncouple immune-mediated regeneration from toxicity could exist at several different points. Is it possible to activate dectin-1 signaling with a ligand that promotes regeneration, but not toxicity? Since curdlan is bacterial in origin, there is a possibility of LPS contamination. Perhaps different forms and/or sources of β-glucan are less toxic, but still able to promote robust regeneration. Any additional molecules or compounds that are known dectin-1 agonists can easily be screened for their efficacy in promoting regeneration and/or toxicity using the optic nerve crush injury model. One study demonstrated that binding of particulate β-glucans to dectin-1 on cultured macrophages promotes formation of a "phagocytic synapse" (Goodridge, et al., 2011). Specifically, particulate β-glucan promotes the clustering of dectin-1 receptors, thereby excluding the regulatory tyrosine phosphatases CD45 and CD148 from sites of β-glucan contact, and allowing productive signaling of Src family and Syk kinases (Goodridge et al., 2011). We observed that intraocular injection of soluble β-glucan (WGP-S) promotes optic nerve regeneration, suggesting that formation of a phagocytic synapse may not be necessary for dectin-1-mediated regeneration, and perhaps is only needed for recruitment of pro-inflammatory factors that mediate a classical/toxic immune response.

Separating immune-mediated regeneration from toxicity at the receptor level may not be possible. Unraveling the molecular mechanism downstream of dectin-1 will likely be necessary to fully understand the diverse effects of dectin-1 activation. Our data show that curdlan-induced regeneration correlates with increased phosphorylation of ERK and CREB in a dectin-1-dependent manner. As discussed in Chapter III, follow-up studies are needed to determine whether activation of ERK and CREB in immune cells in the eye is necessary to promote regeneration. If blocking ERK or CREB activation inhibits curdlan-induced regeneration, but not curdlan-induced retinal pathology, this would suggest that alternative pathways downstream of dectin-1 are responsible for the toxicity aspect, making ERK and CREB key targets for therapeutic strategies. However, if blocking ERK or CREB inhibits both regeneration and toxicity, then we will need to probe deeper. Activation of dectin-1 or ERK/CREB signaling in different subtypes of myeloid cells could also have different outcomes. Given the heterogeneity of immune cells that infiltrate the eye, assessing the relative contribution of ERK/CREB signaling in different cell types *in vivo* will be difficult.

Ultimately, uncoupling immune-mediated regeneration may not be possible until much further downstream. Phosphorylated CREB translocates to the nucleus where it participates in regulation of gene transcription (Yamamoto et al., 1988). Downstream of dectin-1, CREB promotes transcription of IL-10 (Elcombe et al., 2013), a cytokine involved in "M2" type macrophage polarization (Martinez et al., 2008). One hypothesis for how innate immunity leads to regenerative growth of RGCs is that activation of ERK/CREB signaling pathways in immune cells promotes transcription of cytokines and other growth factors, which are then released by immune cells into the vitreous of the eye. Zymosan and curdlan may stimulate immune cells to produce a whole cocktail of factors, some required for promoting regeneration, and others required for retinal detachment and buckling. Identifying these factors may be a daunting task, but if accomplished, a specific mixture of factors could be applied post injury to promote regenerative growth with minimal side effects.

4.2 Bridging the Gap Between Inflammation and Regeneration

How does β-glucan/dectin-1 signaling in immune cells result in regenerative growth and survival of injured RGCs? Because dectin-1 expression is not observed on RGCs, curdlan and zymosan-induced neuroprotection and axonal regeneration must occur through a non-cell-autonomous mechanism. As mentioned above, one hypothesis involves CREB-mediated regulation of gene transcription. Ligation of β-glucan with dectin-1 on immune cells may result in a CREB-dependent increase in transcription of a specific set of cytokines and growth promoting factors. These factors could help with recruiting additional types of immune cells that promote regeneration, communicate with other retina-resident cells such as astrocytes, or engage directly with RGCs. A few factors that mediate the beneficial aspects of inflammatory stimulation have already been identified, including ciliary neurotrophic factor (CNTF), leukemia inhibitory factor (LIF), and IL-6 (Leibinger et al., 2009, Leibinger et al., 2013b). Follow lens injury, CNTF is secreted by retinal astrocytes, and contributes to RGC axon regeneration (Leibinger et al., 2009). How lens injury leads to induction of CNTF expression by astrocytes is not known. CNTF-mediated regeneration requires neuronal activation of STAT3 (Leibinger et al., 2013a), providing a link to neuron intrinsic growth programs. Additionally, viral overexpression of CNTF in RGCs promotes regenerative growth, but is hampered by aberrant sprouting and axonal misguidance (Pernet et al., 2013).

Several tools are currently available that allow for unbiased analysis of gene expression and protein content in the eyes of mice following optic nerve crush injury and i.o. injection of inflammatory compounds. RNA sequencing (RNAseq) is a powerful and sensitive tool for quantitative analysis of RNA (mRNAs, miRNAs, lncRNAs) expression. Additionally, RiboTag mice can be used to identify ribosome-associated mRNAs that are actively being transcribed (Sanz et al., 2009). Proteomic analysis of the vitreous of the eye will allow for identification of secreted proteins, including cytokines, chemokines, and growth factors. The dissociation of regeneration and inflammation in dectin-1/TLR2 compound mutant mice provides an excellent opportunity to identify critical players in immune-mediated regeneration. Any mRNA or protein that is similarly expressed in the eyes of WT and *dectin-1/TLR2* mice following i.o. zymosan is likely not sufficient to drive regenerative growth. To further narrow down a list of candidates, we can compare additional positive and negative controls. For example, we can exclude mRNAs and proteins that are similarly expressed in WT eyes injected with LPS. Candidates from this further refined list that show similar expression in curdlan-injected and zymosan-injected eyes will be top candidates for linking neuroinflammation with regenerative growth of RGCs.

Does immune-mediated regeneration ultimately tie into the signaling pathways in RGCs that have been shown to promote CNS regeneration? Combining PTEN deletion with i.o. injection of zymosan further enhances regenerative growth (de Lima et al., 2012), suggesting that these two methods involve different signaling pathways. Still, there may be some amount of overlap, as one study found that blocking mTOR activity reduced the lengthy regeneration achieved with an inflammatory stimulus (Leibinger et al., 2012). As discussed above, CNTF-mediated regeneration requires neuronal activation of STAT3. Work from Zhigang He's laboratory has shown that deletion of SOCS3, an inhibitor of STAT3, promotes robust regeneration in the mouse optic nerve (Sun et al., 2011). Whether CNTF activates STAT3 through suppression of SOCS3 is unknown. As discussed in Chapter 3, osteopontin (OPN) is another potential link between innate immunity and neuron intrinsic signaling pathways. OPN stimulates mTOR activity, and regenerating αRGCs express high levels of mTOR and OPN (Duan et al., 2015). In immune cells, OPN functions downstream of dectin-1 and TLR2 to promote cytokine production, and may be involved in zymosan-mediated activation of ERK (Inoue et al., 2011). Whether OPN may be a molecular link between the two most robust paradigms for eliciting optic nerve regeneration (PTEN deletion, and immune-mediated regeneration) will be interesting to explore.

4.3 What role do microglia play in the injured optic nerve?

Results from studies with bone marrow chimeric mice indicate that dectin-1 expression on radioresistent retina-resident cells, which includes microglia, is necessary for curdlan-induced regeneration in the mouse optic nerve. The role that microglia play in immune-mediated neuronal regeneration is unclear. In the retina, microglia may produce cytokines or growth factors that stimulate growth programs in injured RGCs and support RGC survival. Our studies in bone marrow chimeric mice revealed that dectin-1 expression on microglia is not necessary for recruitment of blood-derived immune cells into the eye. However, this does not rule out the possibility that the composition of blood-derived immune cells is altered when dectin-1 expression on retina-resident immune cells is lost. Dectin-1-expressing microglia may help to recruit specific subtypes of immune cells that are necessary for a robust regenerative response.

Growing evidence suggests that microglia assume distinct phenotypes with different degrees of pro- or anti-inflammatory functions (Orihuela et al., 2015), similar to the idea of macrophage polarization. Following optic nerve crush injury, there is a large number of dectin-1+ microglia in the optic nerve. Could certain types of inflammatory stimulation improve the ability of microglia to phagocytose and clear myelin debris? Improved clearance of myelin debris could decrease myelin-mediated growth inhibition, and allow space for newly regenerating axons. Additionally, the possibility that microglia could interfere with the formation or integrity of the glial scar has not been examined. Since zymosan leads to further enhanced regeneration upon deletion of multiple CSPG receptors, this possibility seems unlikely (Dickendesher et al., 2012). As new tools for microglia manipulation become available, we will be able to explore these ideas and improve our understanding of the role of microglia in immune-mediated regeneration.

4.4 The Long and Winding Road to Functional Recovery

Functional recovery of damaged CNS tissue requires several steps. First and foremost, there must be regenerative growth of injured axons, whether through stimulation of intrinsic growth potential, blockade on extrinsic inhibitory cues, or a combination of both. Second, this regenerative growth must be accompanied with guidance cues to direct growing axons to their proper targets, and prevent them from forming improper or excessive connections. Third, for any regenerative growth to have functional relevance, axons that reach their targets must form functional synapses. Finally, remyelination of regenerated axons is needed for rapid firing of electrical impulses and metabolic support of axons. All of these steps must be accomplished in an environment that potently inhibits aberrant growth and sprouting.

Activation of specific immunomodulatory pathways has proven a successful method for stimulating robust axon regeneration after injury to the rodent CNS. Combining immune-mediated regeneration with activation of neuron intrinsic pathways or neutralization of inhibitory ligands leads to a further enhancement of regenerative growth. In the mouse optic nerve, robust regeneration into optic chiasm is achieved by the combined deletion of PTEN and SOCS3 (Sun et al., 2011). Once at the chiasm, however, many regenerating axons seem to get lost. A portion of regenerating axons make a u-turn and begin to grow into the contralateral (uninjured) nerve. This aberrant path-finding could be due to the absence of embryonic guidance cues that would normally guide growing axons to their appropriate targets.

Manipulation of CNS regeneration inhibitors, such as MAIs, CSPGs, and their receptors, is not as effective as other strategies for promoting regenerative growth in the initial steps towards CNS repair. However, these molecules may have a bigger impact in combinatorial treatments, or at the later stages of repair, including network refinement, proper target finding, and formation of functional synapses. In fact, many CNS regeneration inhibitors play important physiological roles in the development, refinement, and maintenance of synaptic connections in the healthy brain. The Nogo receptor family members NgR1, NgR2, and NgR3 restrict synaptogenesis in the juvenile mouse brain (Wills et al., 2012). NgR1 and Nogo, along with CSPGs, contribute to the closure of the critical period in the developing rodent visual system (Pizzorusso et al., 2002, McGee et al., 2005). NogoA, OMgp, NgR1, and CSPGs, have all been show to negatively regulate activity-dependent synaptic plasticity (Lee et al., 2008, Raiker et al., 2010, Mironova and Giger, 2013). The important function of CNS inhibitory molecules in brain development and plasticity raises important considerations for therapeutic strategies designed to promote neural regeneration following injury. The acquisition of a large number of ligand-receptor systems that restrict neural network plasticity may have been a prerequisite that enabled the evolution of larger and more powerful neural networks. Following injury to the adult CNS, molecules that restrict aberrant growth and plasticity may be detrimental since they limit attempts to modify or rebuild nearby networks to compensate for lost neural circuits. Manipulating these molecules to promote neurorepair could affect the integrity of intact neural networks. Thus, an understanding of the physiological role of these molecules in the uninjured CNS is of great interest both biologically and clinically.

The optic nerve crush injury model is an excellent tool for studying CNS regeneration *in vivo*. In humans, however, injury to the optic nerve is much less common than spinal cord injury (SCI), or other damaging insults to the CNS, such as stroke. Therefore, successful methods for promoting regeneration in the optic nerve need to be assessed for their ability to promote regeneration and repair in the injured brain and spinal cord. While injured axons in the mouse optic nerve can successfully regenerate up to several millimeters, injured axons in the spinal cord need to travel significantly longer distances. With multiple ascending and descending fiber tracts, the spinal cord is much more complex than the optic nerve. There is evidence that immune-mediated repair mechanisms can successfully promote spinal cord regeneration under certain conditions. Intraspinal or dorsal root ganglion (DRG) injection of zymosan activates macrophages, and promotes transient growth of injured ascending sensory axons with concurrent toxicity (Gensel et al., 2009). A conditioning injury to the peripheral branch of DRG sensory neurons promotes regeneration of the central branch of DRG neurons that form the dorsal columns in the spinal cord. Conditioning injury is associated with macrophage accumulation near DRG cell bodies, which may play a vital role in regeneration of the central branch of DRG neurons (Kwon et al., 2013). Additional studies are needed to determine the whether β-glucan/dectin-1-mediated neuroinflammation is capable of promoting spinal cord axon regeneration. Concurrent toxicity must also be evaluated, and must be minimized to make immune-mediated regeneration a viable therapeutic option.

We are still many years away from achieving robust functional recovery of injured CNS networks in humans. Many challenges lies ahead, but regenerative growth of severed axons is a prerequisite for studying the later stages of CNS repair, such as target finding, synapse formation, and remyelination. My dissertation work demonstrates that post-injury manipulation of specific immunomodulatory pathways promotes extensive growth of injured RGC axons. These findings have broad implications for understanding the elaborate cross-talk that occurs between the nervous system and the immune system, and how these pathways can be exploited to promote repair following CNS injury or disease.

4.5 References

de Lima S, Koriyama Y, Kurimoto T, Oliveira JT, Yin Y, Li Y, Gilbert HY, Fagiolini M, Martinez AM, Benowitz L (2012) Full-length axon regeneration in the adult mouse optic nerve and partial recovery of simple visual behaviors. Proc Natl Acad Sci U S A 109:9149-9154.

Dickendesher TL, Baldwin KT, Mironova YA, Koriyama Y, Raiker SJ, Askew KL, Wood A, Geoffroy CG, Zheng B, Liepmann CD, Katagiri Y, Benowitz LI, Geller HM, Giger RJ (2012) NgR1 and NgR3 are receptors for chondroitin sulfate proteoglycans. Nat Neurosci.

Duan X, Qiao M, Bei F, Kim IJ, He Z, Sanes JR (2015) Subtype-Specific Regeneration of Retinal Ganglion Cells following Axotomy: Effects of Osteopontin and mTOR Signaling. Neuron 85:1244-1256.

Elcombe SE, Naqvi S, Van Den Bosch MW, MacKenzie KF, Cianfanelli F, Brown GD, Arthur JS (2013) Dectin-1 regulates IL-10 production via a MSK1/2 and CREB dependent pathway and promotes the induction of regulatory macrophage markers. PLoS One 8:e60086.

Giger RJ, Hollis ER, 2nd, Tuszynski MH (2010) Guidance molecules in axon regeneration. Cold Spring Harb Perspect Biol 2:a001867.

Inoue M, Moriwaki Y, Arikawa T, Chen YH, Oh YJ, Oliver T, Shinohara ML (2011) Cutting edge: critical role of intracellular osteopontin in antifungal innate immune responses. J Immunol 186:19-23.

Lee H, Raiker SJ, Venkatesh K, Geary R, Robak LA, Zhang Y, Yeh HH, Shrager P, Giger RJ (2008) Synaptic function for the Nogo-66 receptor NgR1: regulation of dendritic spine morphology and activity-dependent synaptic strength. The Journal of neuroscience : the official journal of the Society for Neuroscience 28:2753-2765.

Lee JK, Geoffroy CG, Chan AF, Tolentino KE, Crawford MJ, Leal MA, Kang B, Zheng B (2010) Assessing spinal axon regeneration and sprouting in Nogo-, MAG-, and OMgp-deficient mice. Neuron 66:663-670.

Leibinger M, Andreadaki A, Diekmann H, Fischer D (2013a) Neuronal STAT3 activation is essential for CNTF- and inflammatory stimulation-induced CNS axon regeneration. Cell Death Dis 4:e805.

Leibinger M, Andreadaki A, Fischer D (2012) Role of mTOR in neuroprotection and axon regeneration after inflammatory stimulation. Neurobiol Dis 46:314-324.

Leibinger M, Muller A, Andreadaki A, Hauk TG, Kirsch M, Fischer D (2009) Neuroprotective and axon growth-promoting effects following inflammatory stimulation on mature retinal ganglion cells in mice depend on ciliary neurotrophic factor and leukemia inhibitory factor. J Neurosci 29:14334-14341.

Leibinger M, Muller A, Gobrecht P, Diekmann H, Andreadaki A, Fischer D (2013b) Interleukin-6 contributes to CNS axon regeneration upon inflammatory stimulation. Cell Death Dis 4:e609.

Martinez FO, Sica A, Mantovani A, Locati M (2008) Macrophage activation and polarization. Front Biosci 13:453-461.

McGee AW, Yang Y, Fischer QS, Daw NW, Strittmatter SM (2005) Experience-driven plasticity of visual cortex limited by myelin and Nogo receptor. Science 309:2222-2226.

Mironova YA, Giger RJ (2013) Where no synapses go: gatekeepers of circuit remodeling and synaptic strength. Trends Neurosci 36:363-373.
Orihuela R, McPherson CA, Harry GJ (2015) Microglial M1/M2 polarization and metabolic states. Br J Pharmacol.
Pernet V, Joly S, Dalkara D, Jordi N, Schwarz O, Christ F, Schaffer DV, Flannery JG, Schwab ME (2013) Long-distance axonal regeneration induced by CNTF gene transfer is impaired by axonal misguidance in the injured adult optic nerve. Neurobiol Dis 51:202-213.
Pizzorusso T, Medini P, Berardi N, Chierzi S, Fawcett JW, Maffei L (2002) Reactivation of ocular dominance plasticity in the adult visual cortex. Science 298:1248-1251.
Raiker SJ, Lee H, Baldwin KT, Duan Y, Shrager P, Giger RJ (2010) Oligodendrocyte-myelin glycoprotein and Nogo negatively regulate activity-dependent synaptic plasticity. J Neurosci 30:12432-12445.
Sanz E, Yang L, Su T, Morris DR, McKnight GS, Amieux PS (2009) Cell-type-specific isolation of ribosome-associated mRNA from complex tissues. Proc Natl Acad Sci U S A 106:13939-13944.
Sun F, Park KK, Belin S, Wang D, Lu T, Chen G, Zhang K, Yeung C, Feng G, Yankner BA, He Z (2011) Sustained axon regeneration induced by co-deletion of PTEN and SOCS3. Nature 480:372-375.
Yamamoto KK, Gonzalez GA, Biggs WH, 3rd, Montminy MR (1988) Phosphorylation-induced binding and transcriptional efficacy of nuclear factor CREB. Nature 334:494-498.

Appendix:

Does NogoA regulate homeostatic synaptic plasticity?

A.1 Abstract

Plasticity of synaptic connections in the brain is critical for learning, memory formation, and cognitive function. Activity-dependent modifications in synaptic strength occur at individual synapses, and are balanced by homeostatic scaling mechanisms that maintain network stability while preserving relative changes in synaptic strength. Several molecular links between Hebbian forms of synaptic plasticity and homeostatic plasticity have been identified, but the mechanism of how these two distinct forms of neuronal plasticity interact at the molecular level remains poorly understood. NogoA is a membrane-associated reticulon protein that negatively regulates activity-dependent strengthening of synaptic transmission. In this study, we examined whether NogoA plays a concurrent role in homeostatic plasticity. Prolonged changes in network activity lead to down-regulation (TTX) or up-regulation (Bic) of Nogo-A surface levels. The observed bidirectional changes in NogoA on the cell surface shows activity-dependent regulation of Nogo-A. Knockdown of NogoA drastically reduces expression levels of the AMPA receptor subunit GluA1, and the mTORC1 target S6K. Furthermore, loss of NogoA attenuates homeostatic scaling up of surface GluA1 in TTX-treated hippocampal cultures. Collectively, these results suggest that NogoA serves as a point of molecular overlap between Hebbian and homeostatic plasticity. Additional studies are needed to determine the molecular mechanisms of NogoA-mediated regulation of GluA1 expression and homeostatic scaling.

A.2 Introduction

Synaptic transmission occurs at excitatory (glutamatergic) and inhibitory (GABAergic) synaptic connections in the brain. Individual neurons possess finely tuned mechanisms to sense and respond to changes in network activity, while maintaining a proper balance between excitation and inhibition. Synapses have the ability to alter their strength in response to various stimuli, a process known as functional synaptic plasticity. Activity-dependent, or Hebbian, forms of synaptic plasticity, including long-term potentiation (LTP) and long-term depression (LTD) of synaptic transmission, alter the relative strength of individual excitatory synapses (Malenka and Bear, 2004). These activity-dependent changes in synaptic strength are thought to form the cellular basis of learning and memory (Siegelbaum and Kandel, 1991). Another form of synaptic plasticity, homeostatic scaling, alters the strength of many synaptic connections proportionally and in a uniform direction, protecting relative changes in synaptic strength (Turrigiano et al., 1998). Homeostatic scaling functions to maintain neuron firing rates in a stable range, despite concurrent activity-dependent changes at individual synapses and chronic changes in network activity. Homeostatic scaling also occurs at individual synapses (Beique et al., 2011), and global and local plasticity occur simultaneously. How do these different forms of neuronal plasticity interact to maintain network stability while preserving newly encoded alterations in synaptic strength?

Growing evidence indicates that Hebbian and homeostatic plasticity interact at the molecular level, but the underlying mechanisms remain incompletely understood. To alter synaptic strength, LTP, LTD, and homeostatic scaling all involve regulation of the abundance of AMPA-type glutamate receptors (AMPARs) in the postsynaptic membrane. Elegant work from the Huganir laboratory showed that homeostatic scaling induces PKA-mediated changes in phosphorylation of the AMPAR subunit GluA1, interfering with the ability of cortical neurons to express LTP (Diering et al., 2014). In addition to AMPARs, several other molecules have important roles in both Hebbian and homeostatic plasticity. In the rat visual cortex, brain-derived neurotrophic factor (BDNF) enhances LTP and blocks LTD (Akaneya et al., 1996, Akaneya et al., 1997). BDNF also plays a critical role in homeostatic plasticity, mediating the effects of chronic activity blockade on the amplitude of miniature excitatory post-synaptic currents (mEPSCs) (Rutherford et al., 1998). Activation of mTOR complex 1 (mTORC1)-dependent local protein synthesis is critical for certain forms of late-LTP (Tang et al., 2002), and contributes to homeostatic regulation of synaptic function (Henry et al., 2012, Bateup et al., 2013). Collectively, these findings suggest that common molecular targets regulate the interaction of Hebbian and homeostatic plasticity.

NogoA is a membrane-associated protein that belongs to the reticulon family, and was originally identified as a myelin-associated inhibitor of CNS axon regeneration (Huber and Schwab, 2000). NogoA is expressed in neurons, present in synaptic density fractions (Lee et al., 2008), and well-established as a negative regulator of activity-dependent synaptic strength (Raiker et al., 2010, Delekate et al., 2011, Kempf et al., 2014). NogoA restricts LTP at CA3-CA1 synapses in acute hippocampal slices through at least two different inhibitory domains, Nogo-66 and NogoΔ20 (Raiker et al., 2010, Kempf et al., 2014). The molecular mechanisms utilized by NogoA to restrict synaptic strength are not fully understood, though work from our laboratory has shown that acute treatment of Nogo66 suppresses LTP in a NgR1-dependent manner. Furthermore, Nogo66 attenuates BDNF-mediated activation of mTORC1 signaling in cultured hippocampal neurons (Raiker et al., 2010). Chronic depletion of NogoA is associated with cognitive impairment and brain disorders, such as schizophrenia (Willi et al., 2010, Petrasek et al., 2014a, Petrasek et al., 2014b) Whether NogoA is regulated by chronic changes in neuronal activity, or whether NogoA plays a role in the regulation of homeostatic plasticity is not known. Here I investigate the role of NogoA in homeostatic synaptic scaling.

A.3 Results

Surface NogoA levels are regulated by chronic changes in neuronal activity

Chronic manipulations to neuronal activity lead to compensatory changes in expression of synaptic proteins (O'Brien et al., 1998, Ehlers, 2003). Treatment with tetrodotoxin (TTX), a voltage-gated sodium channel blocker, silences neuronal activity, thereby inducing homeostatic scaling up of surface levels of AMPAR subunits GluA1 and GluA2. Conversely, treatment with the $GABA_A$ receptor antagonist bicuculline causes chronic hyperactivity and a compensatory scaling down of surface GluA1 and GluA2 levels (Shepherd et al., 2006). NogoA restricts activity-dependent synaptic plasticity (Raiker et al., 2010), therefore chronic changes in neuronal activity could induce homeostatic changes in NogoA expression as a compensatory mechanism to aid in promoting or restricting synaptic activity. To examine whether NogoA expression is regulated by chronic manipulations to neuronal activity, we treated rat primary hippocampal neurons for 24 or 48 hours with TTX (2μM) or bicuculline (40μM). Immunolabeling of cell surface proteins in primary hippocampal neurons treated with TTX revealed a global increase in the surface expression of GluA1, and a decrease of surface NogoA (**Figure A.1a**). To more accurately assess changes in surface protein levels, we performed cell surface biotinylation followed by streptavidin pull-down and Western blot analysis. Following 24hr TTX treatment, we observed a significant reduction of Nogo-A from the cell surface ($p = 0.0299$) while surface levels of GluA1 were significantly increased (**Figure A.1b,c**). Bicuculline treatment trended towards increasing NogoA surface levels ($p = 0.2936$), while decreasing GluA1 surface levels (**Figure A.1b,c**). Total levels of NogoA were not affected by these manipulations (**Figure A.1c**). These findings demonstrate that surface levels of NogoA are regulated by chronic changes in network activity, and are consistent with a role for NogoA as a negative regulator of synaptic activity.

Loss of NogoA reduces expression of GluA1, GluA2, and S6K

To determine whether manipulations to NogoA protein expression regulate neuronal activity, we treated primary hippocampal cultures at 10 days *in vitro* (10 DIV) with a lentiviral vector (LV) containing a shRNA directed against NogoA (LV-shNogoA) or an empty vector control (LV-control). At 17 DIV, LV-treated cultures were lysed and analyzed by Western blotting. In LV-shNogoA treated cultures, Nogo-A protein levels were significantly reduced (<3% of control levels). Knockdown of NogoA dramatically reduced total protein levels of the AMPA receptor subunits GluA1 and GluA2, but not of the NMDA receptor subunit GluN2B (**Figure A.2a,b**). Levels of PSD95 were unchanged (**Figure A.2a,b**), suggesting that the decrease in AMPAR subunit expression was not due to a reduction in synaptic number or the size of post-synaptic densities. We also observed a significant reduction in levels of total and phosphorylated S6K, a substrate of active mTOR complex 1 (mTORC1) (**Figure A.2a,b**). To verify that changes in protein abundance were not due to off-target effects of the NogoA shRNA, we transduced neurons with LVs containing 3 different NogoA shRNA constructs. Two of the three additional constructs tested successfully knocked down NogoA, and lead to a decrease in GluA1 and S6K protein levels, indicating that these changes in protein expression are not due to off-target effects (**Figure A.2c**).

NogoA regulates AMPAR protein expression independently of known receptors

NogoA restricts activity-dependent synaptic plasticity through at least two separate domains, Nogo-66 and NogoΔ20 (Raiker et al., 2010, Delekate et al., 2011, Kempf et al., 2014). Nogo-66 negatively regulates activity-dependent synaptic plasticity through NgR1, and to a lesser extent, through PirB (Raiker et al., 2010). To determine whether NogoA-mediated regulation of GluA1 protein levels depends on either of these receptors, we repeated NogoA knockdown experiments in mouse hippocampal cultures from mice lacking *NgR1* and *PirB*, as well as mice lacking all three Nogo receptors, *NgR1, NgR2,* and *NgR3*. Both *NgR1/PirB* and *NgR1/NgR2/NgR3* knockout cultures transduced with LV-shNogoA showed a reduction in expression of GluA1, GluA2, and pS6K, comparable to that of WT cultures transduced with LV-shNogoA. This finding demonstrates that NgR1 and PirB are not involved in NogoA-mediated regulation of GluA1, GluA2, and pS6K (**Figure A.2d**). NogoΔ20 was shown to restrict hippocampal LTP through Sphingosine 1 phosphate receptor 2 (S1PR2) (Kempf et al., 2014). Treatment of hippocampal cultures with 5μM JTE-013, and inhibitor of S1PR2, for 24 or 48 hours did not alter surface GluA1 expression (**Figure A.2e,f**). Additional studies may be needed to definitively exclude a role for S1PR2.

NogoA regulates GluA1 expression and synaptic transmission in a cell-autonomous manner

In addition to a reduction in total GluA1 protein levels, surface expression of GluA1 is substantially reduced following NogoA knockdown (**Figure A.3a,b**). To determine whether changes in surface GluA1 expression reflect physiological changes in synaptic transmission, we recorded mini excitatory post-synaptic currents (mEPSCs) from hippocampal neurons transfected with a pSuperior-neo-GFP plasmid containing NogoA shRNA or control shRNA. LV treatment of cultured hippocampal neurons adversely affected whole cell patch clamp recordings independently of the transgene carried by the LV particle, therefore we utilized a Calcium Phosphate (CalPhos) transfection protocol to achieve NogoA knockdown in a small percentage (<1%) of cells. Transfected cells were visualized by GFP expression. Using single cell recording from transfected pyramidal neurons, we analyzed frequency and amplitude of mEPSCs. Loss of NogoA did not alter mEPSC frequency (**Figure A.3d**). In accordance with our biochemical data, loss of NogoA significantly reduced mEPSC amplitude (**Figure A.3e**). Importantly, because of the sparse transfection efficiency achieved with the CalPhos protocol, this finding indicates that NogoA regulates mEPSC amplitude in a cell-autonomous manner. This result also suggests that NogoA regulates expression of GluA1 cell autonomously.

NogoA knockdown attenuates TTX-mediated increase in surface GluA1

Because loss of NogoA results in decreased GluA1 expression and a scaling down of mEPSC amplitude, we hypothesized that NogoA is involved in regulation of homeostatic synaptic scaling. To test whether NogoA is required for upregulation of surface GluA1, we treated primary hippocampal cultures with LV-shNogoA or LV-control at 10 DIV, followed by 24 hour TTX treatment at 16 DIV, and cell surface biotinylation at 17 DIV. As expected, treatment of LV-control neurons with TTX scaled up surface GluA1 levels, and LV-shNogoA cultures had significantly reduced surface GluA1 levels (**Figure A.4**). Interestingly, TTX treatment of LV-shNogoA cultures did not significantly increase surface levels of GluA1(**Figure A.4**). These results indicate that loss of NogoA attenuates TTX-mediated scaling up of chronically inactive neurons, and suggests that NogoA may play an important role in homeostatic scaling mechanisms that increase synaptic strength.

Loss of NogoA selectively impairs BDNF signaling

Loss of NogoA could render neurons incapable of responding to subsequent changes in activity by adversely affecting their health or metabolism, which could account for their inability to scale in response to TTX treatment. To rule out this possibility, we assessed the response of LV-shNogoA cultures to acute treatment with BDNF. We have previously shown that treating primary neurons with BDNF (100ng/ml) for 30 minutes drastically increases phosphorylation of several key signaling molecules, including ERK, AKT (Ser473), and S6K (Raiker et al., 2010). As expected, treatment of LV-control transduced neuronal cultures with BDNF for 30 minutes prior to lysis strongly increased phosphorylation of ERK, AKT, and S6K (**Figure A.5**). In LV-shNogoA transduced cultures, BDNF increased levels of pERK and pAKT, but failed to affect pS6K levels (**Figure A.5**). These results show that loss of NogoA selectively impairs the sensitivity of neurons to BDNF-mediated regulation of S6K phosphorylation, while leaving ERK and AKT singling pathways unaffected.

NogoA knockdown does not impair bicuculline-mediated increase in Arc protein levels

Arc is an immediate early gene that is rapidly induced by increases in neuronal activity (Lyford et al., 1995). Arc plays a critical role in mediating homeostatic plasticity, aiding in removal of AMPARs from the cell surface (Shepherd et al., 2006). Following bicuculline treatment, Arc nuclear expression increases to suppress transcription of GluA1 (Korb et al., 2013). To assess whether activity-mediated induction of Arc expression was perturbed in LV-shNogoA neurons, we examined Arc expression levels following acute treatment with bicuculline for 4hrs. Cultures were lysed with RIPA buffer to ensure that the nuclear membrane was disrupted. In both LV-control and LV-shNogoA transduced neuronal cultures, bicuculline induced a robust increase in Arc expression (**Figure A.6**), indicating that loss of NogoA does not affect activity-induced Arc expression.

Enhancing mTORC1 activity does not rescue expression of GluA1 or S6K in LV-shNogoA neurons

One explanation for the blockade of BDNF-mediated S6K phosphorylation in LV-shNogoA neurons could be the increased activity of signaling pathways that inhibit mTORC1. Tuberous sclerosis 2 (TSC2) is an upstream inhibitor of mTORC1 (Tee et al., 2002). In complex with TSC1, TSC2 functions as a GTPase activating protein (GAP) for the small GTPase Rheb (Inoki et al., 2003, Tee et al., 2003). GTP-bound Rheb activates mTORC1; thus, by stimulating conversion of GTP-Rheb to GDP-Rheb, TSC2 functions to block activation of mTORC1. A recent study from the Sabatini laboratory found that loss of TSC1/TSC2 lead to chronically high mTORC1 activity and hyperexcitability in hippocampal neurons, resulting in homeostatic scaling down of AMPAR surfaces levels, including GluA1 and GluA2, and reduced mEPSC amplitude (Bateup et al., 2013). We examined whether loss of TSC1/TSC2 expression could rescue levels of pS6K in LV-shNogoA neurons by combining knockdown of TSC1 and NogoA.

Treatment of primary hippocampal neurons from $TSC1^{f/f}$ mice with an LV containing a GFP-IRES-Cre construct under the control of a synapsin promoter (LV-synGFPCre) successfully knocked down TSC1, leading to simultaneous destabilization and depletion of TSC2 protein levels (**Figure A.7a**). As a control, $TSC1^{f/f}$ neurons were treated with LV-synGFP. Similar to previously published results, knockdown of TSC1 increased phosphorylation of the mTORC1 targets S6K and 4EBP1, and decreased total GluA1 expression (**Figure A.7a**) (Bateup et al., 2013). In the same cultures we observed an increase in expression of the GABA synthesizing enzyme GAD67, indicative of a scaling up of inhibitory transmission in response to hyperactivity. The combined loss of NogoA and TSC1 yielded GluA1 and pS6K levels similar to that of NogoA knockdown alone, suggesting that TSC1/TSC2 is not required for NogoA-mediated decrease in GluA1, S6K, or pS6K levels (**Figure A.7b,d**). However, the combined knockdown of TSC1 and NogoA did decrease total S6K protein levels to a further extent than NogoA knockdown alone. While the absolute levels of pS6K were not different between these two conditions, there was a net increase in S6K phosphorylation when normalized to total S6K levels (**Figure A.7c**). Levels of 4EBP1 and p4EBP1 were unchanged between NogoA and NogoA/TSC1 knockdown cultures. Interestingly, preliminary evidence suggests that NogoA knockdown attenuates the increase in GAD67 observed in TSC1 knockdown neurons (**Figure A.7a**). This finding suggests that NogoA may be involved in regulating GABAergic inhibitory synaptic transmission.

Loss of NogoA alters gene transcription

Since activation of mTORC1 promotes translation of synaptic proteins (Takei et al., 2004), the decreased levels of pS6K in LV-shNogoA transduced neuronal cultures could decrease translation of GluA1 and GluA2 mRNA. To determine whether the decreased expression of GluA1 protein observed in LV-shNogoA neurons is due to decreased translation of *GluA1* mRNA, or whether it is reflective of changes in gene transcription, we performed qPCR analysis of LV-shNogoA and LV-control transduced hippocampal cultures using RT^2 Profiler

GABA/Glutamate PCR arrays from Qiagen. LV-shNogoA cultures displayed decreased levels of *GluA1* mRNA levels in four separate experiments (**Figure A.8a, Table A.1**), suggesting that loss of NogoA leads to a reduction in *GluA1* gene transcription. LV-shNogoA cultures also showed changes in the mRNA levels of other synaptic proteins, including decreases in $GABA_A$ receptor subunits β1 and β3, mGluR1, and Vgat (**Figure A.8a, Table A.1**). We also used RT^2 Profiler PCR Assays to analyze components of the mTOR signaling pathway. Similar to the biochemical data, LV-shNogoA cultures showed a decrease in *S6K* mRNA (**Figure A.8b, Table A.2**). Interestingly, NogoA knockdown increased *Rheb* mRNA levels (**Figure A.8b**), possibly to compensate for decreased S6K activity. NogoA knockdown also increased mRNA levels of RhoA (**Figure A.8b**), a protein involved in NogoA-mediated inhibition of neurite outgrowth (Niederost et al., 2002). Collectively, qPCR analysis demonstrates that loss of NogoA results in changes in transcription of several genes involved in synaptic plasticity and mTOR signaling. Whether these changes occur directly as a result of loss of NogoA, or indirectly as a compensatory mechanism for other cellular changes caused by loss of NogoA, remains to be determined.

Is the phosphorylation status of NogoA regulated by endogenous BDNF signaling?

Levels of BDNF expression play important roles in both activity-dependent and homeostatic plasticity, as discussed above. Primary hippocampal neurons prepared from E18 rat embryos include astrocytes and produce a certain amount of endogenous BDNF (Lang et al., 2007). An exogenously applied fragment of NogoA (called Nogo66) attenuates BDNF-mediated activation of mTORC1 signaling (Raiker et al., 2010), yet loss of NogoA impairs BDNF/S6K sensitivity of cultured hippocampal neurons (**Figure A.5**). Do BDNF and NogoA cross-talk with one another under basal conditions? At a low dose (200 nM), K252a specifically inhibits activation of trk receptor kinases (Tapley et al., 1992). The prominent ligand-receptor system in hippocampal cultures is the BDNF receptor trkB interaction. Upon treatment of hippocampal neurons with K252a for 2 hours, Western blot analysis of cell lysates revealed a small, but persistent downward shift in the molecular weight (MW) of NogoA (**Figure A.9a,b**). Incubation of hippocampal cultures with lambda phosphatase produced an identical downward shift in the MW of NogoA that was not further shifted upon treatment with K252a (**Figure A.9a**). This suggests that NogoA is a phospho-protein. Interestingly, 24hr treatment with K252a reduced surface levels of both NogoA and GluA1 (**Figure A.9c**). NogoA is ubiquitinated (**Figure A.9d,g**), but not sumoylated, under basal conditions (**Figure A.9i,j**). The K252a-induced MW shift of NogoA was not due to de-ubiquitination of NogoA, as NogoA remained ubiquitinated in K252a-treated cultures (**Figure A.9d**). As an independent approach to assess Nogo-A post-translation modification (PTM), we used affinity purification from primary hippocampal neurons followed by Mass Spectrometry analysis. We found that NogoA undergoes post-translational modification (phosphorylation) at several serine residues under basal conditions (**Table A.3**). Taken together, these results suggest that endogenous BDNF may regulate the phosphorylation status of NogoA. Further experiments are necessary to determine whether NogoA phosphorylation has any functional consequence.

Do changes in activity cause post-translation modification of NogoA?

In addition to the K252a-induced NogoA MW shift, we observed a striking separation of NogoA into two distinct bands following treatment with TTX (**Figure A.9e**). Interestingly, treatment with AMPA (10μM, 1hr) produced a similar NogoA band separation (**Figure A.9b**).

Whether this band separation is indicative of NogoA PTM remains to be determined. Comparison of NogoA phosphorylation sites between untreated cultures and TTX-treated cultures did not reveal any differences (**Table A.3, Table A.4**), though mass spec analysis covered only 80% of the total NogoA protein sequence. TTX-treatment did not increase NogoA ubiquitination (**Figure A.9g**), and NogoA was not observed to be sumoylated (**Figure A.9i,j**). Additional studies are needed to confirm the nature of this band separation, and whether it represents a functionally relevant modification to NogoA protein.

NogoA overexpression is unsuccessful in neuronal cultures

Attempts to overexpress NogoA in cultured hippocampal neurons have thus far been unsuccessful. LV transduction of myc-tagged Human NogoA into HEK293T cells, which normally express very little NogoA, resulted in robust NogoA overexpression (**Figure A.10a**). Transduction of hippocampal neurons with the same LV did not increase expression of NogoA, though a low level of myc signal could be detected via Western blot (**Figure A.10b**). Mutating several C-terminal lysine residues to alanine, in an attempt to block NogoA ubiquitination and degradation, also failed to enhance NogoA expression in neurons (**Figure A.10b**). Do neurons possess mechanisms not present in HEK293T cells that actively repress excessive expression of NogoA? If so, this would suggest that neurons tightly regulate total NogoA protein levels, and perhaps do not tolerate overexpression of NogoA.

A.4 Discussion and Future Directions

The results presented here in the Appendix of my thesis constitute a large amount of data surrounding the physiological role of NogoA in cultured hippocampal neurons. I have shown that NogoA surface expression is regulated bidirectionally by chronic changes in network activity, and that loss of NogoA reduces GluA1 and S6K protein and mRNA levels. Furthermore, loss of NogoA attenuates TTX-mediated scaling up, and alters BDNF-sensitivity. Collectively, these findings suggest that NogoA may play an important role in homeostatic synaptic plasticity. However, there are still many gaps in our knowledge, especially with regard to the underlying molecular mechanisms of how NogoA is involved in these processes. Additional studies will be necessary to complete this story.

The restrictive role of NogoA in synaptic plasticity

The role of NogoA as a negative regulator of activity-dependent synaptic plasticity is well-established (Raiker et al., 2010, Delekate et al., 2011, Kempf et al., 2014). We observed that surface levels of NogoA are significantly decreased in response to chronic inactivity (**Figure A.1b**). Could NogoA function as a molecular break for synaptic activity? If so, then reducing NogoA surface levels would help facilitate synaptic upscaling in response to activity blockade. Furthermore, increasing NogoA surface levels in response to chronic hyperactivity would aid in scaling down of synaptic activity. Following this logic, we should expect that decreasing surface NogoA would cause hyperactivity of neuronal networks, resulting in a compensatory scaling down of synaptic activity. LV-shNogoA cultures displayed decreased expression of GluA1 and S6K (**Figure A.2**), and were impaired in their ability to scale up GluA1 levels following TTX treatment (**Figure A.4**). Furthermore, loss of NogoA in individual neurons decreased mEPSC amplitude (**Figure A.3**). Together, these findings suggest that NogoA regulates homeostatic plasticity by functioning as a molecular break on neuronal activity.

Does NogoA regulate inhibitory synaptic transmission?

Knockdown of NogoA could activate or repress downstream signaling pathways that directly affect the transcription of GluA1. Alternatively, loss of NogoA could result in hyperactivity or an imbalance between excitation and inhibition, leading to the induction of offsetting homeostatic scaling mechanisms that decrease GluA1 expression. Some evidence exists for the latter possibility. Treating acute hippocampal slices with pictrotoxin (PTX) to block $GABA_A$ receptor activity enhances LTP at WT CA3-CA1 synapses. Antibody blockade of NogoA also enhances LTP, but is not further enhanced when combined with PTX treatment (Delekate et al., 2011), suggesting that NogoA may regulate inhibitory synaptic transmission. We observed that loss of TSC1 in primary hippocampal neurons increased levels of GAD67, but this increase was blocked with loss of NogoA (**Figure A.7a**). This finding suggests that NogoA could be involved in promoting inhibitory synaptic transmission. Perhaps loss of NogoA leads to decreased inhibitory synaptic transmission (similar to treatment with bicuculline or PTX), resulting in over-excitation, and initiating homeostatic downscaling mechanisms. RT-PCR analysis revealed that LV-shNogoA transduced cultures have decreased mRNA levels of the $GABA_A$ receptor subunits β1 and β3, and increased levels of $GABA_A$ receptor subunit ε (**Figure A.8a, Table A.1**). Interestingly, a study of $GABA_A$ receptor subunit expression in human brain tissue revealed decreased expression of subunit β1 and increased expression of subunit ε in patients suffering from schizophrenia or major depression (Fatemi et al., 2013).

An important follow-up experiment for our studies is to examine the combined effect of NogoA knockdown and bicuculline treatment. Based on our preliminary results, NogoA knockdown should occlude bicuculline-mediated scaling down of surface GluA1. This would provide further evidence for a role of NogoA in regulating inhibitory synaptic transmission. RT-

PCR results should be confirmed at the protein level, by examining $GABA_A$ receptor expression via Western blot. We can also record mIPSCs from neurons following NogoA knockdown, to determine whether NogoA regulates inhibitory synaptic transmission in a cell autonomous manner. To determine whether NogoA regulates global network activity, LV-shNogoA and LV-control transduced cultures can be examined via multi-electrode array (MEA) recordings.

Differential effects of acute vs. chronic manipulation of NogoA expression

The slow and gradual nature of the LV-mediated shRNA knockdown makes it difficult to observe early cellular events that result from NogoA knockdown. A reduction in NogoA protein levels is not observed until 72hrs after transduction with LV-shNogoA (**Figure A.11**). A much larger decrease in NogoA expression is observed at 7 days after transduction. GluA1 expression gradually decreases with NogoA knockdown. Perhaps acute antibody blockade of NogoA would be more useful in observing the more immediate effects of NogoA knockdown on GluA1 expression and synaptic transmission. One study observed that depletion of NogoA with a mixture of siRNAs lead to an increase in GluA1 expression in cultured hippocampal neurons in an mTORC1-dependent manner (Peng et al., 2011). The mixture of siRNAs used in this study has not been validated for off-target effects, but if these results are real, perhaps the more rapid knockdown achieved with siRNA transfection produces an initial increase in mTORC1 activity. Given our previous finding that acute Nogo-66 treatment blocks BDNF-mediated increase in pS6K levels (Raiker et al., 2010), acute depletion of NogoA may have the opposite effect.

Does NogoA cross-talk with other master regulators of synaptic plasticity?

As discussed above, Arc is a critical regulator of synaptic homeostasis. Arc is dynamically regulated by changes in activity; bicuculline treatment increases Arc expression, while TTX treatment reduces Arc expression (Shepherd et al., 2006). Arc overexpression blocks homeostatic scaling up induced by chronic inactivity, while *Arc* knockout neurons display increased surface expression of AMPARs, similar to TTX-treated neurons (Shepherd et al., 2006). In addition to its established role in removal of AMPARs from the cell surface, Arc was more recently shown to play an important role in the nucleus, decreasing transcription of GluA1 following treatment with bicuculline (Korb et al., 2013). Is Arc responsible for the decreased GluA1 transcription observed in LV-shNogoA cultures? While we did not observe global changes in Arc expression in LV-shNogoA cultures (**Figure A.6**), perhaps Arc nuclear localization or transcriptional activity is altered in some manner that is not visible by Western blot analysis of whole cell lysates. Initial attempts to knockdown Arc expression using LV-shRNAs were unsuccessful, so we need to find alternate constructs to deplete Arc expression, or utilize Arc knockout neurons to determine whether Arc expression is required to decrease transcription of GluA1 in LV-shNogoA cultures.

Multiple lines of evidence suggest that NogoA and BDNF participate in some sort of cross-talk, but the mechanisms are unclear. Acute treatment with Nogo66 blocks BDNF-mediated activation of S6K (Raiker et al., 2010), while loss of NogoA expression selectively impairs BDNF-mediated activation of S6K in primary hippocampal neurons (**Figure A.5**). Endogenous BDNF may regulate the phosphorylation state of NogoA. K252a blocks BDNF signaling, and causes a NogoA MW shift that is mimicked by treatment with lambda phosphatase (**Figure A.9a**). Furthermore, long term (24hr) treatment with K252a reduces surface expression of both GluA1 and NogoA (**Figure A.9c**). Does NogoA act as a sensor of endogenous BDNF levels? Is NogoA phosphorylation functionally significant? To establish that BDNF signaling through TrkB drives phosphorylation of NogoA, we can treat cultured hippocampal neurons with a soluble TrkB-IgG fusion protein to block endogenous BDNF signaling. If successful, this would also rule out the possibility of a K252a off-target effect. To determine whether K252a truly affects the phosphorylation state of NogoA, we can utilize mass spec analysis of NogoA PTM. NogoA phosphopeptides that are not detected in K252a treated cultures will be good candidates for sites that are regulated by BDNF/K252a. Depending on the nature of the phosphorylation site that are identified, we may be able to predict specific kinases and/or phosphatases that regulate phosphorylation at these residues.

Concluding Remarks

Hebbian and homeostatic forms of synaptic plasticity occur simultaneously to maintain balanced network activity, while allowing for activity-dependent modifications in synaptic strength. Proteins such as GluA1, BDNF, and Arc serve as molecular points of contact between these two distinct forms of plasticity. However, our understanding of the cellular and molecular mechanisms that enable this cross-talk is still incomplete. NogoA is well-established as a negative regulator of activity-dependent synaptic plasticity. In the current study, I have shown that NogoA is regulated by chronic changes in neuronal activity, and may participate in regulation of homeostatic plasticity. Additional studies are necessary to determine the cellular and molecular nature of NogoA's involvement in homeostatic plasticity. Since NogoA restricts plasticity in the injured CNS, and has been associated with human brain disorders, such as schizophrenia, an intricate understanding of the physiological role of NogoA is of great interest both biologically and clinically.

A.5 Methods:

Rat Primary Neuronal Culture: Primary hippocampal and cortical neurons were obtained from rat embryos at E18.5 (time pregnant Sprague-Dawley rats, from Charles River). For hippocampal cultures, care was taken to dissect out the entire hippocampus, including the dentate gyrus (DG) and CA1. Dissected tissue was incubated at 37C for 5 minutes (hippocampal) or 10 minutes (cortical) in L15 media containing 1x Trypsin/EDTA (0.05%) and DNaseI. Following trypsin incubation, cells were washed twice in DMEM containing 10% FBS, then resuspended in 1ml of neuronal growth medium (NGM: Neurobasal, B27, Glutamax, Pen/Strep, Glucose) by pipetting up and down 20 times with a P1000 pipet . Cells were pelleted by centrifugation at 800 rpm for 4 minutes, then resuspended in 1mL of NGM, counted, and plated on PDL-coated plates or coverslips (PDL from Sigma #P7886, 100ug/ml in water). For biochemistry, hippocampal neurons were plated at 200,000 cells/well of a 12 well plate, and 600,000 cells/well of a 6 well plate. Cortical neurons were plated at 250,000/well (12 well) and 750,000 (6 well). For imaging, hippocampal neurons were plated on 18mm (100,000 cells) or 12mm (50,000 cells) glass coverslips. One-third of the media was changed every 7 days.

Mouse Primary Neuronal Culture: Primary hippocampal neurons were prepared from WT, *NgR1/PirB*, *NgR1/NgR2/NgR3*, or *TSC1*$^{f/f}$ neonatal mice at P0 or P1. Dissected hippocampi were incubated in HBSS with Trypsin, glucose, and DNase I for 15min at 37˚C to digest tissue. Tissue was pelleted by centrifugation at 100 rcf for 3min, and subjected to 3 washes with HBSS, and resuspended in Mouse-NGM (same recipe as NGM above, but without the glucose). Cells were plated on PDL-coated 12-well plates at 400,000-500,000 cells/well. One-third of the media was changed every 7 days.

Lentiviral Transduction: Every Lentivirus (LV) used in this study was produced by the University of Michigan Vector Core. All LV transductions were performed at least 7 days prior to analysis, with the exception of time course experiments (Figure A.12). Cultures were transduced by adding concentrated LV (either 10x or 500x stock) directly into the media at an amount equal to a 1x working concentration (either 1:10 or 1:500, respectively). 48-72hrs after LV treatment, approximately 1/3 of the medium was replaced with fresh NGM. Treatment with

1x LV resulted in transduction of ~80% of cells in primary hippocampal cultures. For knockdown of NogoA, an shRNA plasmid was obtained from Dr. Christine Bandtlow and cloned into the pLentilox3.7 plasmid (UM vector core) packaged into an LV, and concentrated to a 500x stock. Other shRNA constructs were obtained from commercial sources. See below for sequences. Syn-GFP-IRES-Cre and Syn-GFP containing plasmids were obtained from the Sabatini laboratory. Human NogoA was PCR amplified and cloned into pLentilox EV plasmid obtained from the UM vector core, along with a myc tag.

Sequences of NogoA shRNAs

1: Bandtlow: AAGATTGCTTATGAAAC

2: OpenBiosystems (V2LMM_33110): TCTCTTCCTAGTTTATGTG

3: Origene (TL711619B): CAGCAGTGTCATCCTCAGAAGGAACAATT

4: Origene (TL711619C): GATACCTTGGTAACTTATCAGCAGTGTCA

Pharmacological Treatments: BDNF (Sigma) was prepared as a 500x stock in water (50ug/ul) and stored aliquoted at -20˚C. Cultures were treated with BDNF (100ug/mL) for 30 minutes prior to lysis. K252a (CalBiochem) (200nM) was added to cultures at 2hrs or 24hrs before lysis, depending on the experiment. AMPA (10uM, Sigma) was added to cultures 1hr prior to lysis. TTX (2uM) (Calbiochem), and Bicuculline (Sigma) (40uM) were added to cultures at 48, 24, or 4 hrs prior to lysis, depending on the experiment. JTE-013 (5uM, Tocris) was added to cultures for 24 or 48hr prior to lysis.

Cell Surface Biotinylation: Cell surface biotinylation experiments were performed on primary hippocampal neurons at 17 DIV (days *in vitro*). Neurons were placed on ice and washed 3x with cold PBS containing 100mM $CaCal_2$ and 50mM $MgCl_2$. EZ-Link Sulfo-NHS-LC-Biotin (Life Technologies) was warmed to room temperature and dissolved in PBS (with Ca/Mg) at 1mg/ml. Neurons were incubated in biotin for 30min on ice, and the reaction was quenched by washing 3x in cold Tris-Buffered Saline (50mM Tris, 150mM NaCl, pH 7.4). Neurons were lysed for 20 min on ice using cooled Brij lysis buffer (BLB) (10 mM potassium phosphate, pH 7.2, 1 mM EDTA, 10 mM MgCl2, 50 mM β-glycerophosphate (BGP), 1 mM Na3V04, 0.5% NP40, and 0.1% Brij-35) containing protease inhibitor cocktail (PIC) (Sigma) at a 1:100 dilution. Cell lysates were cleared by centrifugation in a cooled centrifuge for 5 min at maximal speed. High

Capacity Streptavidin Agarose Resin (Thermo Scientific/Pierce) was washed 3x in PBS, and tumbled with cell lysates at 4C for 3hrs to overnight to pulldown biotinylated proteins. Beads were then washed 3x in PBS and 1x in BLB. Following the final wash, the lysate/bead slurry of approx. 50ul was combined with 50ul of 2x Laemmli Sample buffer containing βME and boiled for 10min. Surface and total protein levels were analyzed via Western Blot (15ul loaded per well). Surface protein expression was normalized to surface levels of Transferrin receptor (TfR).

Western Blot: Cells were lysed in BLB containing PIC, as described above, or lysed in RIPA buffer containing 50mM BGP and PIC for analysis of Arc protein levels. Supernatants were combined with 2x Laemmli buffer, boiled for 10min, separated by SDS-PAGE (5 µg of protein loaded per lane), and transferred to PVDF membrane (Millipore). PVDF membranes were blocked with 2% milk (BioRad) in TBS-T (Tris-buffered saline pH 7.4, containing 0.1% Tween-20) and probed with primary antibodies diluted in 2% BSA or 2% milk in TBS-T, depending on the antibody (see below for description of antibodies and respective dilutions). Anti-mouse, anti-rabbit, or anti-goat IgG-HRP (Millipore) secondary antibodies were diluted in the same buffer as the respective primary antibody. HRP signal was developed with West Pico Substrate or West Femto Substrate (Thermo Scientific). Protein bands were visualized and quantified with using LI-COR C-Digit and Image Studio software. Western blot band intensity in the linear range was measured with Image Studio software.

Antibodies for Western Blot: The following primary antibodies were used. From R&D systems: anti-Nogo (1:5000 in milk, R&D #AF3098). From Cell Signaling Technologies: anti-phospho-p70S6K (Thr389) (1:1000, #9234), p70S6K (1:500, #9202), pAKT (Ser473, #4060) (1:2000), AKT (1:10,000, #4691), pERK (1:2000, #4695), ERK (1:2000 #4376), p4EBP1 (1:1000, #9459), 4EBP1 (1:1000, #9452), TSC1 (Tuberin) (1:2000), TSC2 (Hamartin) (1:2000, #4308), Sumo2/3 (1:1000, #4971). From Promega: BetaIII Tubulin (TUJ1) (1:50,000, #PRG7121). From Millipore: GluA1 (N terminal) (1:2000, MAB2263), GluA1 (Cterminal) (1:2000, #AB1504), GluA2 (1:1000, #MABN71), PSD95 (1:2000, #AB9708), GAD67 (1:2000, #MAB5406), GluN2B (1:1000). From Santa Cruz: Arc (1:200, #sc-17839), Sumo1 (1:1000, sc-5308). From Sigma: Actin (1:5000), Transferrin Receptor (1:2000, #C2063), Ubiquitin (1:200, #U5379).

NogoA Immunoprecipitation: Primary hippocampal or cortical cultures were lysed in BLB as described above. Protein A/G Beads (Calbiochem) were prepared by washing 3x in PBS. Lysates were pre-cleared by tumbling at 4C with washed protein A/G beads for 30min. Beads were spun down at 5,000 rpm for 3min, and pre-cleared lysate supernatant was transferred to a new 1.5ml tube. Anti-Nogo antibody (R&D Systems) was added at 2-4ug/mL per 1mg of lysate, along with protein A/G beads, and tumbled overnight at 4C. Beads were washed 3x with PBS and 1x with BLB. For analysis by western blot, beads were boiled in 2x Laemmli sample buffer containing βME for 10min, spun down at 5,000 rpm, and 20ul of supernatant loaded per lane.

Immunocytochemistry: Cells were fixed with cold 4% PFA for 15min, washed 2x with PBS, and incubated in blocking solution for 1hr at room temp. For labeling of surface proteins, a non-permeabilizing blocking solution of PBS containing 3% horse serum was used. For total protein labeling, a permeabilizing blocking solution of PBS, 3% horse serum, and 0.1% Triton X-100 was used. Cells were incubated overnight at 4C in blocking buffer containing primary antibodies against Nogo (1:1000, R&D Systems) and GluA1-NT (1:500, Millipore). The following day, cells were washed 3x 5min with PBS, then incubated in the appropriate Alexa-Fluor conjugated secondary antibody (1:1000, Life Technologies) in blocking buffer for 1-2 hr at room temp. Coverslips were washed 3x in PBS and 1x in dH2O, then mounted on slides using ProLong Gold DAPI (Life Technologies). Images were acquired using an inverted microscope (IX71; Olympus) attached to a digital camera (DP72; Olympus).

RT-PCR: RNA was isolated from rat primary hippocampal cultures at 16 DIV (LV treatment at 9 DIV) using the RNeasy Mini Kit (Qiagen) with the QiaShredder Kit (Qiagen) and on column DNase I digestion option (Qiagen). 1ug of RNA was used to synthesis first strand cDNA using the Superscript III First Strand Synthesis Systerm (Invitrogen). mRNA levels of target genes were assessed using RT^2 Profiler PCR Arrays from Qiagen according to the manufacturers instructions: Rat mTOR Signaling (PARN-098ZC-12), GABA & Glutamate (PARN-152ZC-12). Reactions were carried out on an Applied Biosystems StepOne Plus RT-PCR Thermocycler, and data collected and analyzed with StepOne Software (v.2.2.3). Cycle thresholds for each sample were normalized to actin levels. The relative quantity of mRNA in

NogoA shRNA treated cultures was compared to control treated cultures. Four independent experiments were performed.

CalPhos Transfection: Rat primary hippocampal cultures were transfected with 1ug of a plasmid containing NogoA shRNA or control shRNA at 17 DIV using a modified CalPhos Transfection kit (Clontech) protocol. After incubation with DNA, cells were briefly incubated in a 10% CO2 incubator and DNA-containing medium was discarded. Electrophysiological analysis was performed at 3-4 days after transfection (20-21 DIV).

Electrophysiology: Whole-cell patch-clamp recordings of mEPSCs were made with an Axopatch 200B amplifier from cultured hippocampal neurons bathed in Hepes-buffered saline [HBS; 119 mM NaCl, 5 mM KCl, 2 mM $CaCl_2$, 2mM $MgCl_2$, 30mM glucose, 10 mM Hepes (pH 7.4)] plus 1μM TTX and 10μM bicuculline. The pipette internal solution contained 100 mM cesium gluconate, 0.2 mM EGTA, 5 mM $MgCl_2$, 40 mM Hepes, 2 mM Mg-ATP, 0.3 mM Li-GTP, and 1 mM QX314 (pH 7.2), and had a resistance of 3–5MΩ. mEPSCs were analyzed off-line using MiniAnalysis (Synaptosoft).

Mass Spec/Proteomics: For proteomic analysis of NogoA post-translation modification, 70ul of supernatant was loaded into a 1.5mm thick 7.5% gel, and separated by SDS-PAGE. The gel was stained with Imperial Protein Stain (Life Technologies, #24615) according to the manufacturers instructions, in a clean Stainease Staining Tray (Life Technologies, #NI2400). The NogoA band excised, digested with trypsin, and analyzed by liquid chromatography tandem mass spectrometry (LC-MS/MS) using an Orbitrap Fusion Tribrid Mass Spectrometer (Thermo Scientific). Samples were run in both collision-induced dissociation (CID) and higher-energy collisional dissociation (HCD) fragmentation methods. Data were analyzed using X!Tandem/TPP software suite and Proteome Discoverer 1.4.

Lambda Phosphatase Experiment: Primary hippocampal neurons were lysed in BLB containing no phosphatase inhibitors. Since BLB normally contains the phosphatase inhibitor β-glycerophosphate, a new solution of BLB was prepared without this inhibitor. Lambda Phosphatase (NEB) treatment was completed according to manufacturers instructions. Briefly, 39ul of protein lysate was combined with 5ul of 10x Buffer for Metallophosphatases, 5ul of 10x $MnCl_2$, and 1ul of lambda phosphatase (400U, from 400,000 U/mL stock). This solution was then incubated at 30˚C for 30 minutes, then combine with 50ul of 2x Laemmli sample buffer containing βME and boiled for 10min. As a control, the an additional 39ul of the same protein lysates treated as describe above, but without the addition of the lambda phosphatase. 15ul of sample was analyzed by western blot.

A.6 Acknowledgments:

Yevgeniya Mironova performed the electrophysiological recordings described in Figure A.3. Dr. Xiaofeng Zhao generated the myc-NogoA construct. We thank the Sabatini lab for the Syn-GFP-IRES-Cre and Syn-GFP constructs, Dr. Christine Bandtlow for the NogoA shRNA constructs, and the University of Michigan Vector Core for producing all of the LVs used in this study. This work was supported by the Cellular and Molecular Biology Training Grant T32GM007315 (K.T.B.), the Ruth Kirschstein Fellowship F31NS081852 (K.T.B.), and R01NS081281 (R.J.G.).

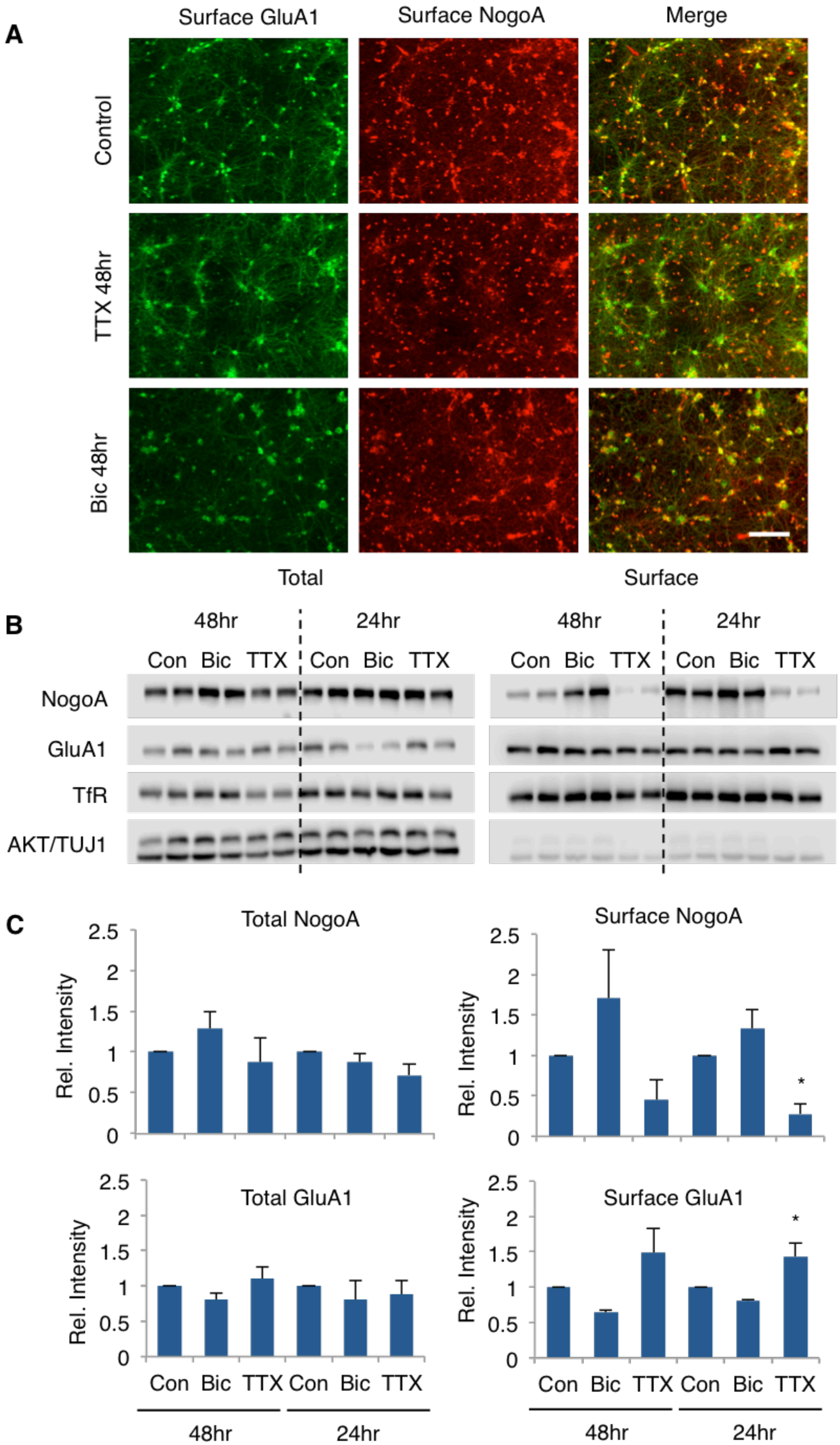

A
Surface GluA1
Surface NogoA
Merge
Control
TTX 48hr
Bic 48hr
B
Total
Surface
48hr
24hr
Con Bic TTX Con Bic TTX
NogoA
GluA1
TfR
AKT/TUJ1
C
Total NogoA
Surface NogoA
Total GluA1
Surface GluA1
Rel. Intensity
2.5
2
1.5
1
0.5
0
*
Con Bic TTX Con Bic TTX
48hr
24hr

Figure A.1: Chronic changes in neuronal activity regulated NogoA surface levels
Rat primary hippocampal neurons (17-19 DIV) were treated with TTX (2μM) or Bicuculline (40μM) for 24 or 48 hours. **(a)** After 48hr of TTX or Bic treatment, neurons were fixed and stained under non-permeabilizing conditions for immunofluorescence labeling of surface GluA1 (green) and surface NogoA (red). TTX treatment caused a noticeable increase and Bic a decrease in GluA1 surface labeling. TTX appeared to decrease surface NogoA on neurites, but not on cell bodies. Scale bar 200μm. (**b**) Western blot analysis of total and surface protein levels of NogoA and GluA1 after TTX or Bic treatment and cell surface biotinylation. Transferrin receptor (TfR) was used as a loading control for surface proteins, while AKT and TUJ1 were used as intracellular controls. **(c)** Quantification of Western blots from averaged duplicates. At total of three independent experiments (n= 3) for each condition were carried out and quantified. Signal was acquired using a LICOR C-Digit scanner. Band intensity in the linear range was determined using Image Studio Software. NogoA and GluA1 total protein levels were normalized to TUJ1. NogoA and GluA1 surface levels were normalized to TfR. Data are presented as mean ± SEM. * $P<0.05$, one-way ANOVA, Dunnett's multiple comparisons test.

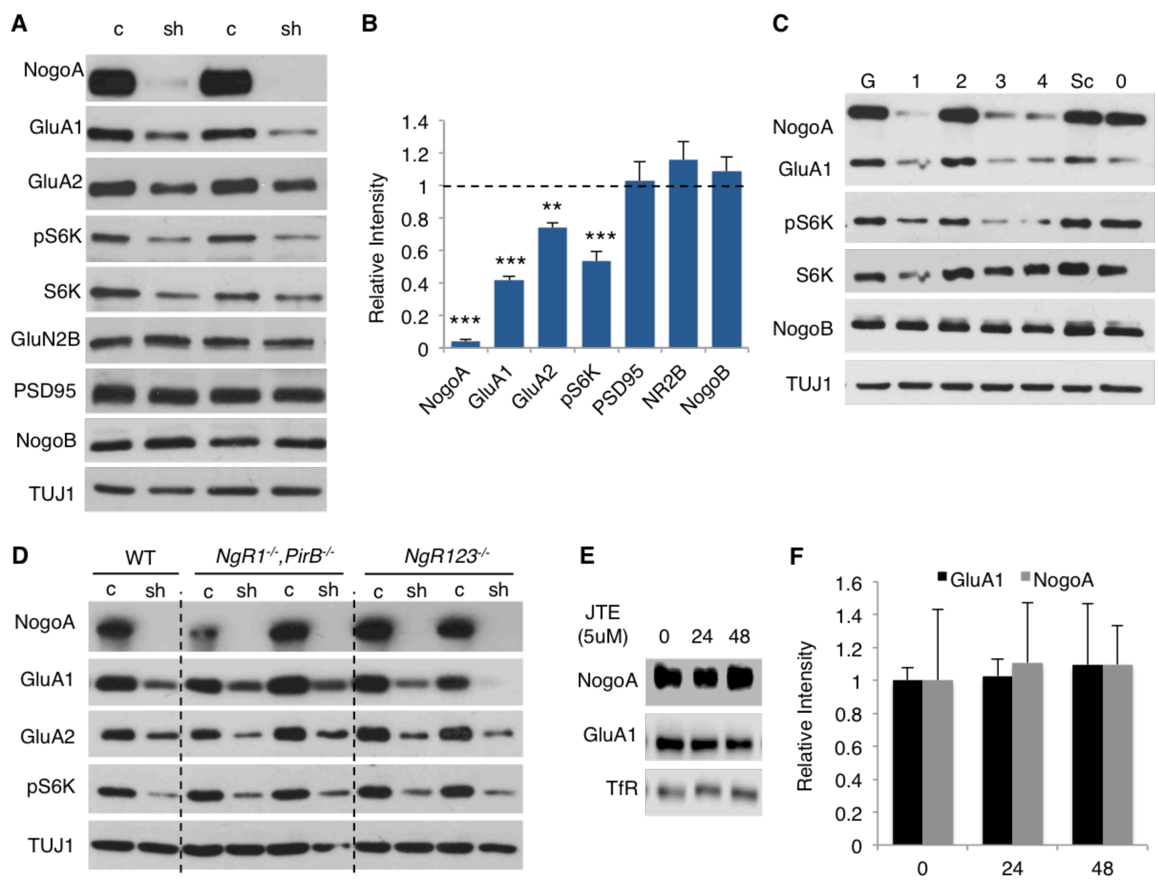

Figure A.2: Loss of NogoA reduces expression of GluA1, GluA2, and S6K
(a) Rat primary hippocampal neurons treated with LV-shNogoA or LV-control at 10 DIV, lysed at 17 DIV, and cell lysates were analyzed by Western blot. Levels of GluA1, GluA2, and pS6K are significantly reduced with NogoA knockdown, while NogoB, GluN2B, and PSD95 levels are not affected. **(b)** Quantification of western blots from averaged triplicates from 3 independent experiments. Data are presented as mean ± SEM, the relative intensity of each protein in LV-shNogoA treated cultures to LV-control treated cultures. *** $p<0.001$, ** $p<0.01$, unpaired student's t-test. **(c)** Comparison of LVs containing different NogoA shRNA constructs or various controls. G=LV-GFP, 1=LV-shNogoA, 2=NogoA shRNA from OpenBiosystems, 3=NogoA shRNA Origene #1, 4=NogoA shRNA Origene #2, Sc=scrambled shRNA, 0=no LV treatment. Constructs 1, 3, and 4 effectively reduced levels of NogoA, and decreased levels of GluA1, pS6K, and S6K. **(d)** Western blot of primary hippocampal cultures from WT *NgR1/PirB*, or *NgR123* mutant mice. Cultures were treated with LV at 10 DIV and analyzed at 17 DIV. Loss of NogoA decreased levels of GluA1, GluA2, and pS6K regardless of genotype. (**e**) Western blot analysis of surface proteins from primary hippocampal cultures treated with JTE-013 (5uM) for 24 or 48hr, followed by cell surface biotinylation. No significant change in GluA1 or NogoA surface levels was observed. Results are presented as mean ± SEM.

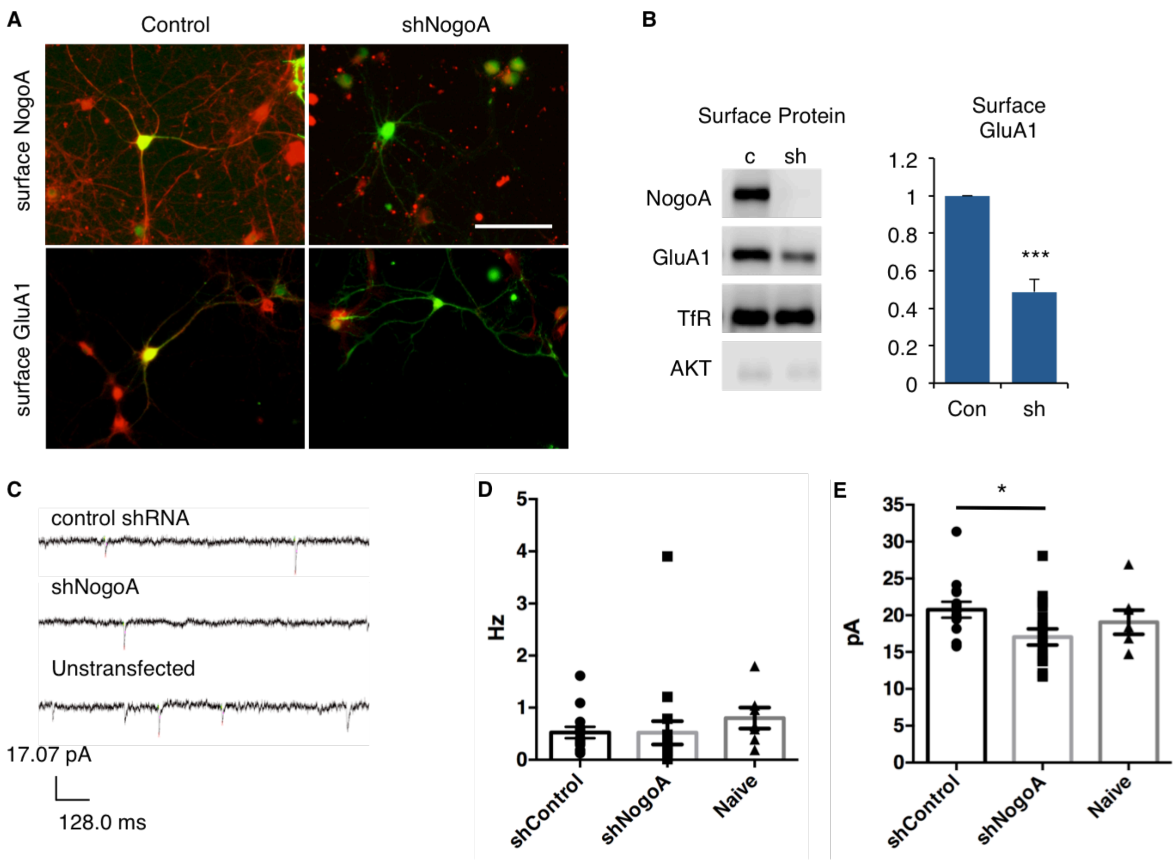

Figure A.3: NogoA regulates GluA1 expression and synaptic transmission in a cell-autonomous manner

(a) Rat primary hippocampal neurons transduced with LV-shNogoA or LV-control and stained under non-permeabalizing conditions to label surface NogoA or surface GluA1. Transduced cells are GFP positive. Scale bar 100µm. **(b)** Western blot analysis of surface protein levels in LV-control and LV-shNogoA cultures following cell surface biotinylation. NogoA knockdown leads to a significant reduction in surface GluA1 levels. ***$p<0.001$, unpaired student's t-test. **(c)** Representative traces of mEPSCs from primary hippocampal neurons at 20-21 DIV following CalPhos transfection of shNogoA or shcontrol DNA plasmids. **(d)** Frequency of mEPSCs is unchanged between shcontrol (n = 14), shNogoA (n = 17), and naïve (n = 7) hippocampal neurons **(e)** Amplitude of mEPSCs in shNogoA neurons (n = 17) is significantly reduced compared to shcontrol neurons (n = 14). *$p<0.05$, unpaired student's t-test.

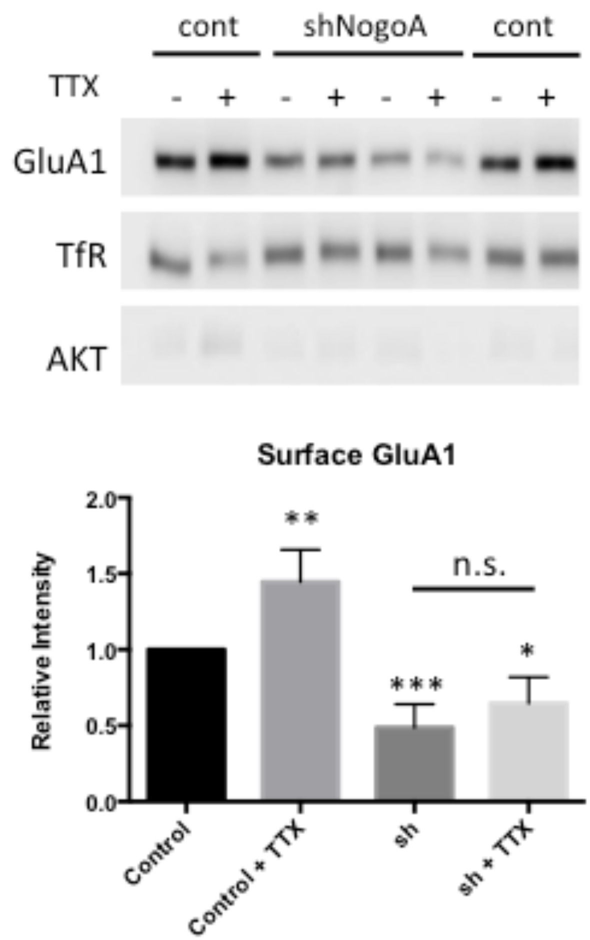

Figure A.4: NogoA knockdown attenuates TTX-mediated scaling up of surface GluA1
Cell surface biotinylation of primary hippocampal neurons transduced with LV-control or LV-shNogoA at 10 DIV and lysed at 17 DIV following 24hr TTX (2µM) treatment. **(a)** Western blot analysis of GluA1 surface levels. **(b)** Quantification of surface GluA1 levels normalized to surface TfR levels. TTX increases surface GluA1 in LV-control, but not in LV-shNogoA neurons. Data are presented as mean ± SEM from averaged triplicates from five independent experiments (n=5). *$p<0.05$, **$p<0.01$, ***$p<0.001$ one-way ANOVA Tukey's post hoc.

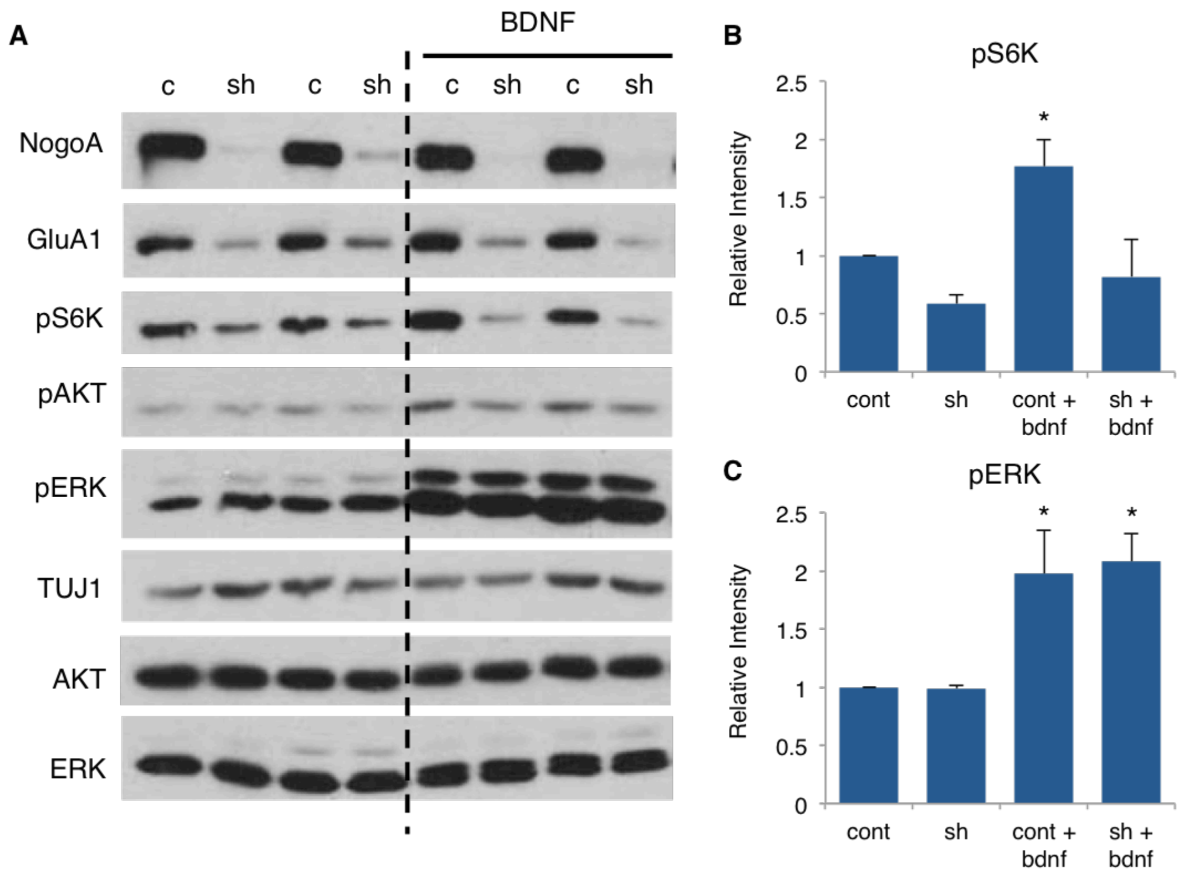

Figure A.5: Loss of NogoA selectively impairs BDNF signaling
(**a**) Rat primary hippocampal neurons transduced with LV-control or LV-shNogoA at 10-11 DIV and lysed 7 days later at 17-18 DIV following treatment with BDNF (100ng/ml) for 30 minutes. (**b**) Quantifaction of pS6K levels normalized to TUJ1. In LV-control, but not in LV-shNogoA transduced cultures, BDNF significantly increases pS6K levels. (**c**) Quantification of pERK levels normalized to TUJ1. BDNF significantly increases pERK levels in both LV-control and LV-shNogoA transduced cultures. Data are presented as mean ± SEM of averaged duplicates from three independent experiments. * $p<0.05$, one-way ANOVA, Fisher's post test.

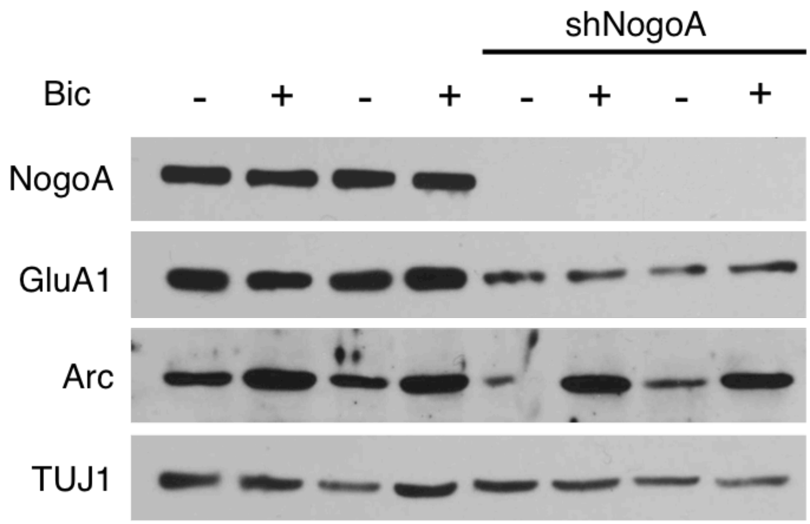

Figure A.6: NogoA knockdown does not impair bicuculline-mediated increase in Arc protein levels

Rat primary hippocampal neurons transduced with LV-control or LV-shNogoA at 10-11 DIV and lysed 7 days later at 17-18 DIV following treatment with bicuculline (bic) (40µM) for 4hrs. Bic treatment increased Arc expression in both LV-control and LV-shRNA cultures. Blots are representative of three independent experiments.

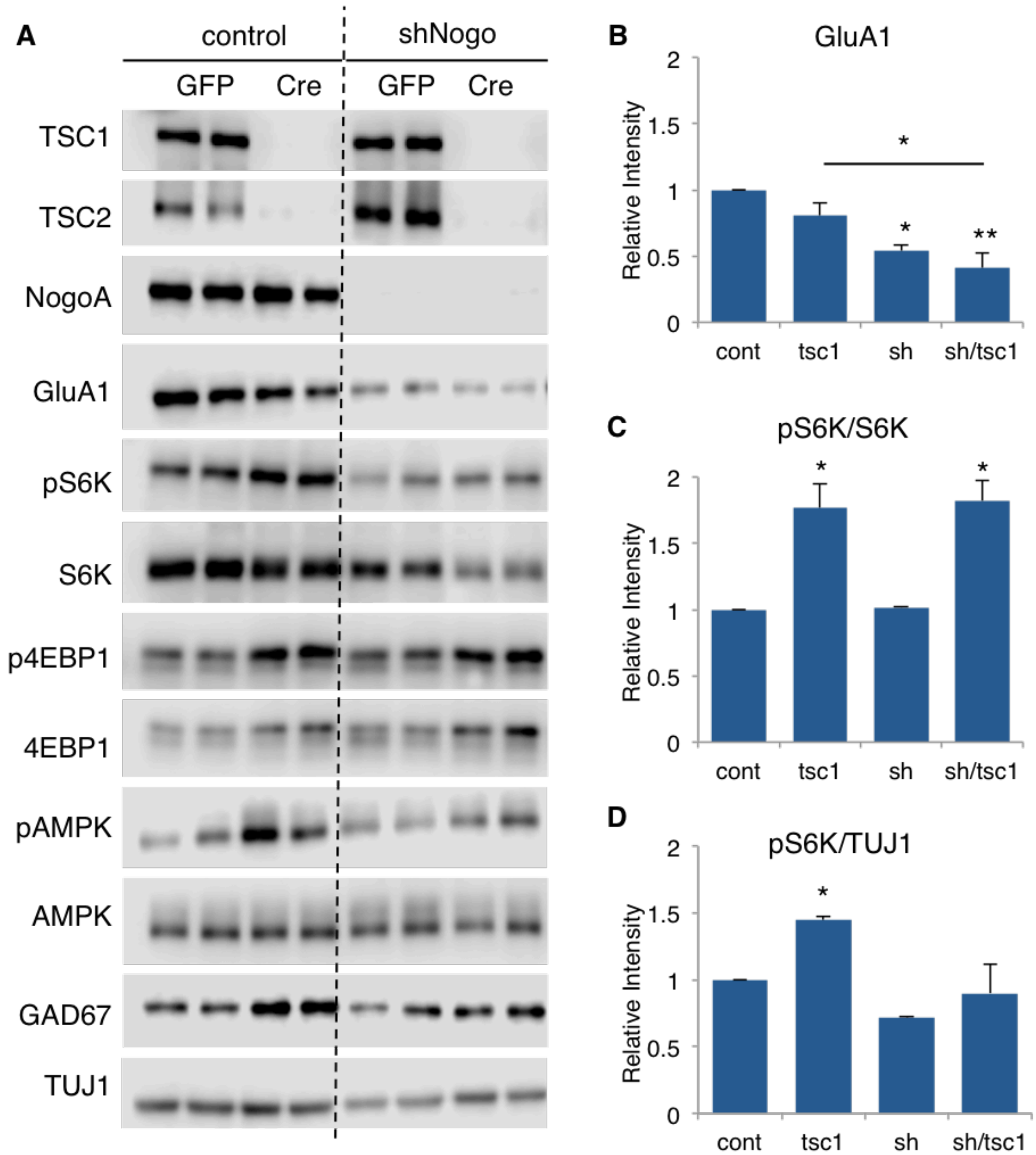

Figure A.7: Enhancing mTORC1 activity does not rescue expression of GluA1 or S6K in LV-shNogoA neurons

(a) Western blot analysis of total protein content in mouse primary hippocampal cultures from *TSC1*$^{f/f}$ mice transduced at 3 DIV with LVsynGFP-Cre to deplete TSC1, or LVsynGFP as a control. Cultures were transduced with LV-shNogoA or LV-control at 10 DIV, and lysed at 17 DIV. (**b**) Quantification of GluA1 protein levels normalized to TUJ1. GluA1 levels are significantly reduced in LV-shNogoA transduced cultures, but not further decreased upon loss of TSC1. (**c**) Quantification of pS6K levels normalized to total S6K levels. Since total S6K decreases in LV-shNogoA cultures, loss of NogoA does not alter the ratio of pS6K to S6K. (**d**) Quantification of pS6K levels normalized to TUJ1. Overall, the total cellular amount of pS6K decreases in LV-shNogoA cultures compared to control, and is not significantly changed upon depletion of TSC1. Results are presented as mean ± SEM from three separate experiments. *$p<0.05$, **$p<0.01$ one-way ANOVA, Fisher's post test.

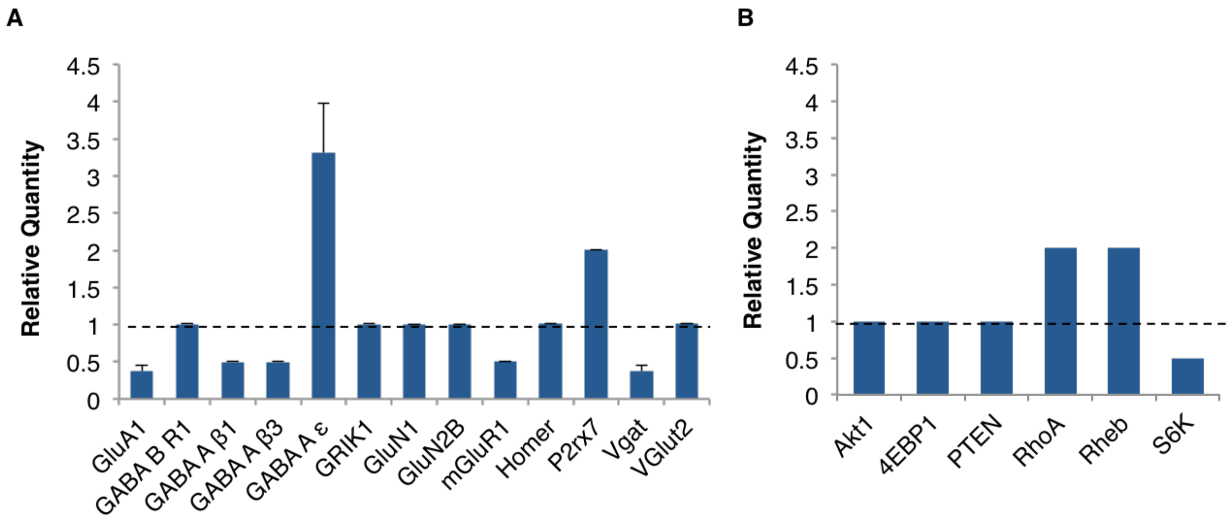

Figure A.8: Loss of NogoA alters gene transcription
Relative quantity of mRNA in LV-shNogoA transduced hippocampal cultures, compared to LV-control transduced cultures. Rat primary hippocampal cultures were transduced with LVs at 9 DIV and RNA was collected at 16 DIV. First strand cDNA was synthesized and analyzed using RT^2 Profiler PCR arrays (Qiagen) for (**a**) GABA/Glutamate related and (**b**) mTOR-related genes. Results are presented mean +/- SEM from four independent experiments for (**a**), and from two independent experiments for (**b**). A complete list of analyzed transcripts and their respective levels are presented in Table A.1 and Table A.2

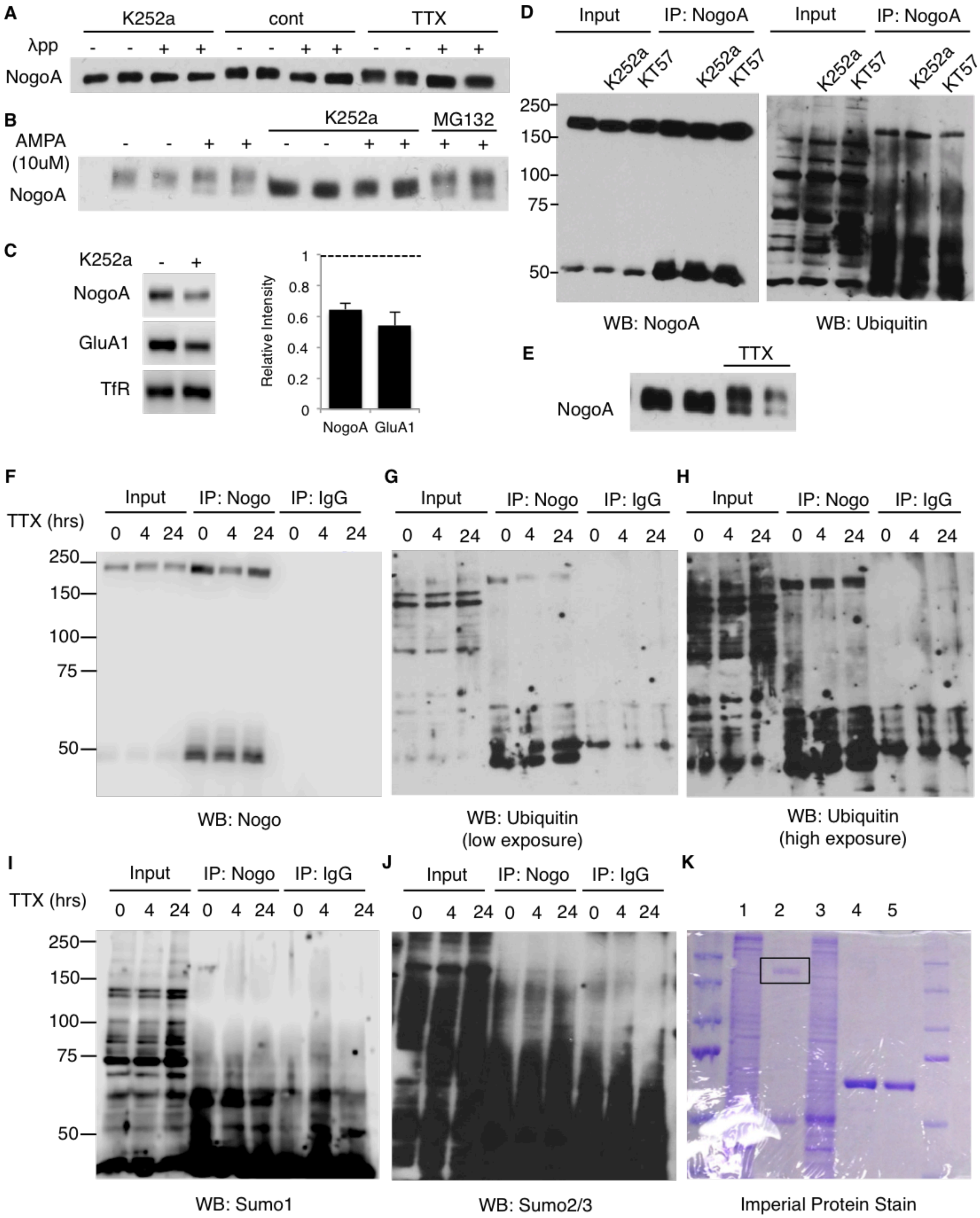

Figure A.9: Post-translational modification of NogoA

(**a**) Western blot analysis of protein lysates from 24 DIV rat hippocampal cultures, lysed in BLB without the presence of phosphatase inhibitors, and blotted for NogoA on a 7.5% gel. Cultures were treated with K252a (200nM) for 2hrs or TTX (2µM) for 24hr prior to lysis, or were untreated (control). Following lysis, an aliquot of each sample was incubated with lambda phosphatase (λpp) for 30min. at 30˚C to remove sites of phosphorylation. Control samples treated with λpp display a slight downward shift in the molecular weight (MW) of NogoA, similar to K252a treated samples without λpp treatment. λpp does not further alter the MW of NogoA in K252a-treated samples. (**b**) 5% gel detailing NogoA MW shifts with greater resolution. Treatment with AMPA (10uM) for 1hr causes the NogoA signal to separate into two distinct bands. K252a (200nM, 2hr) treatment alone decreases the MW of NogoA. K252a also attenuates the MW shift induced by AMPA. Pre-treatment with MG132 (10μM) does not affect the AMPA-mediated band shift. (**c**) Western blot of surface proteins following cell surface biotinylation. Treatment with K252a (200nM, 24hrs) decreases surface levels of NogoA and GluA1 relative to control. Data from two separate experiments of averaged triplicates are presented as mean +/- SEM. (**d**) Western blot analysis of immunoprecipitated (IP) NogoA following treatment with K252a (200nM, 2hr) or PKA inhibitor KT5720 (2μM, 4hr). anti-NogoA antibody pulls down both NogoA (~200 kDa and NogoB ~50 kDa). NogoA is ubiquitinated under control conditions and following treatment with K252a or KT5720. (**e**) 5% gel showing an example of TTX-induced separation of NogoA into two distinct bands, following 24hr TTX (2uM) treatment. (**f-j**) NogoA IP following treatment with TTX (2uM, 4hr or 24hr), and immunoblotted for various post-translation modifications. (**g, h**) NogoA is ubiquitinated under control conditions and following TTX treatment. (**i, j**) NogoA is not sumoylated. (**k**) Example of an Imperial Protein (Coomassie) Stain of a 7.5% gel showing the amount of NogoA protein obtained following IP of 1mg of protein lysate. 1) Lysate, 2) NogoA IP, 3) Lysate, 4) 1μg BSA, 5) 0.5μg BSA. The square indicates the NogoA band.

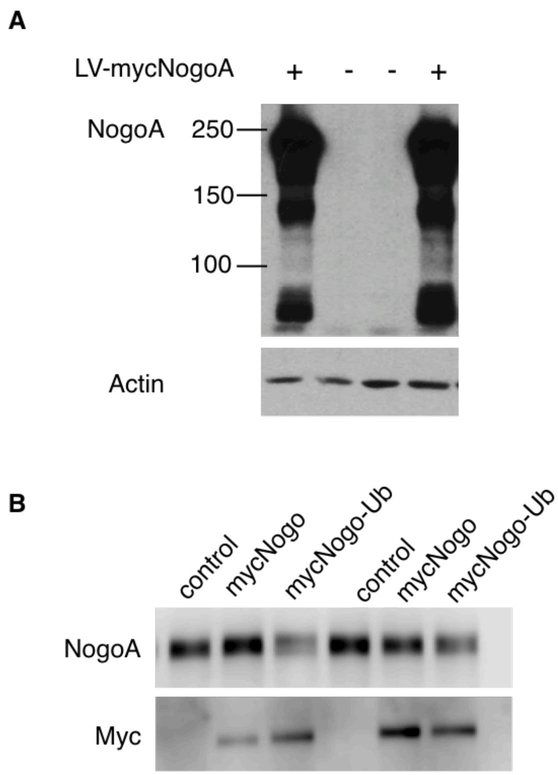

Figure A.10: NogoA overexpression is unsuccessful in neuronal cultures
(**a**) HEK 293T cells transduced with LV-mycNogoA for 72hrs (+) show robust overexpression of NogoA, compared to cells transduced with LV-control (-). (**b**) Rat hippocampal neurons transduced with LV-control LV-mycNogoA (mycNogo), or a mutant form of myc-tagged NogoA in which several C-terminal lysines are mutated to alanine (mycNogo-Ub). While a low level of myc signal is detected by Western blot, overall levels of NogoA do not increase with either LV-mycNogoA or LV-myNogo-Ub.

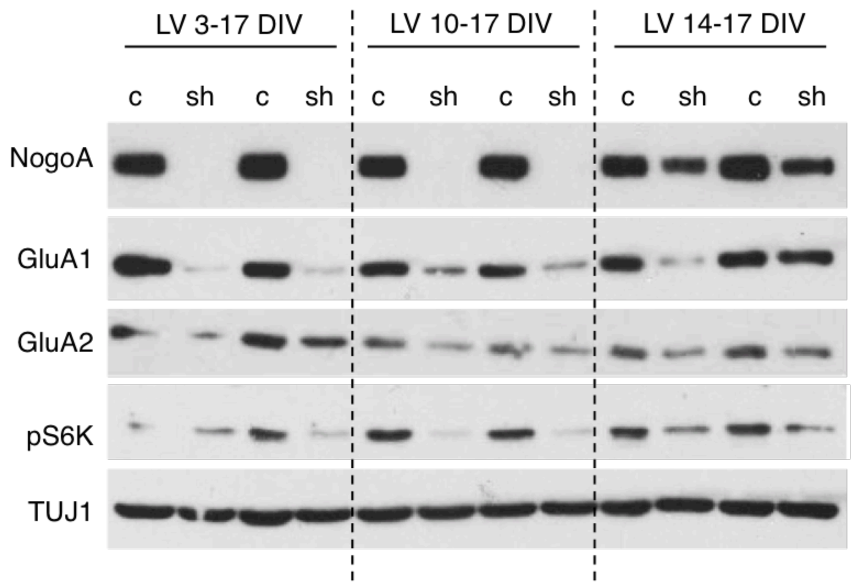

Figure A.11: Time course of LV-mediated NogoA knockdown
Rat primary hippocampal cultures were transduced with LV-control or LV-shNogoA beginning at 3, 10, or 14 DIV. Cultures were lysed at 17 DIV an analyzed via western blot. NogoA knockdown is very robust with LV transduction at 3 DIV or 10 DIV. LV transduction at 14 DIV reveals the gradual nature of LV-mediated gene knockdown, as NogoA levels are only partially reduce. NogoA knockdown leads to a reduction in GluA1, GluA2, and pS6K at all time points.

Target	#1 RQ	#2 RQ	#3 RQ	#4 RQ		Description
Abat	1.0108	0.9916	1.0115	0.4896		4-aminobutyrate aminotransferase
Adcy7	0.4973	1.9837	2.0149	1.9689		Adenylate cyclase 7
Adora1	0.4946	0.9867	1.0127	0.9940		Adenosine A1 receptor
Adora2a	0.4946	1.9937	2.0198	0.9876		Adenosine A2 receptor
Aldh5a1	0.4946	0.4937	0.5025	0.4930		Aldh5 a1
App	0.4946	1.0000	2.0371	1.0011		APP
Avp	#VALUE!	0.8463	1.9399	1.0000		Arginine vasopressin
Bdnf	0.4981	3.9941	2.0234	0.9867		BDNF
Cacna1a	0.4966	0.9927	1.0072	0.9936		Cav2.1
Cacna1b	0.4966	0.4924	1.0002	0.9935		Cav2.2
Cdk5r1	0.4906	1.9977	1.0059	0.9946		Cdk5 r1
Cln3	0.9921	1.9831	2.0168	1.9797		Caeroi-lipofuscinosis, neuronal 3 (battenin)
Dlg4	0.4924	0.9929	1.0027	0.9857		Discs, large homolog 4
Gabbr1	0.4965	0.9895	0.9973	0.9917		GABA B R1
Gabbr2	0.4936	0.9908	1.0058	0.4929		GABA B R2
Gabra1	0.9695	2.0033	0.9929	0.9815		GABA A a1
Gabra2	0.4946	1.0005	1.0120	0.9999		GABA A a2
Gabra4	0.4975	0.9916	0.5045	0.9799		GABA A a4
Gabra5	0.4963	0.9911	1.0067	0.9988		GABA A a5
Gabra6	0.9944	2.0349	1.9853	0.9840		GABA A a6
Gabrb1	0.4968	0.4962	0.5038	0.4962		GABA A b1
Gabrb3	0.2480	0.4963	0.5010	0.4945		GABA A b3
Gabrd	0.4946	0.9984	0.9950	0.9896		GABA A delta
Gabre	1.9579	3.9426	4.0119	1.9860		GABA A epsilon
Gabrg1	0.4864	0.9928	2.0441	0.9850		GABA A g1
Gabrg2	0.5026	2.0077	1.0065	0.9853		GABA A g2
Gabrg3	0.4906	0.9942	1.0026	0.9880		GABA A g3
Gabrq	0.4878	1.9849	1.9841	1.0008		GABAR theta
Gabrr1	0.9914	3.9782	2.0066	0.9827		GABAR rho1
Gabrr2	0.4796	4.0862	1.9810	0.9831		GABAR rho 1
Gad1	0.2481	0.9958	1.0079	0.4935		Glutamate decarboxylase 1
Gls	0.4915	2.0264	1.0083	0.9963		Glutaminase
Glul	0.9938	0.9948	2.0033	0.9920		Glutamate-ammonia ligase
Gnai1	0.9915	1.9994	2.0074	0.9910		G alpha i
Gnaq	0.4959	0.9835	1.0003	0.9954		Gq
Gphn	1.0031	0.9913	1.0027	0.4889		Gephryin
Gria1	0.5020	0.5017	0.5009	0.2473		GluA1
Gria2	0.4956	0.9983	0.4980	0.4905		GluA2
Gria3	0.4988	0.4961	0.4989	1.0046		GluA3
Gria4	0.4944	1.0010	1.0132	0.4887		GluA4
Grik1	0.4876	0.9878	0.9981	1.0100		GluR5 (GRIK1)
Grik2	1.0097	1.0087	0.9996	0.4874		GluR6 (GRIK2)
Grik4	0.4942	0.4968	1.0065	0.4947		GRIK5
Grik5	0.4891	1.0005	0.9926	0.9694		GRIK6
Grin1	0.9986	1.0037	0.9968	0.9959		GluN1 (NR1)
Grin2a	0.5018	1.9847	1.0111	0.9937		GluN2a
Grin2b	0.4948	1.0013	1.0046	0.9933		GluN2b
Grin2c	0.4607	1.0110	1.9800	0.9968		GluN2c
Grm1	0.4942	0.4995	0.5031	0.4955		mGluR1
Grm2	0.4995	0.4926	1.0052	0.4948		mGluR2
Grm3	0.4839	0.9973	1.0036	0.9985		mGluR3
Grm4	0.4949	1.0091	0.4982	0.4943		mGluR4
Grm5	1.0044	0.9959	0.4990	0.4905		mGluR5
Grm6	1.9915	1.9730	2.0141	0.9823		mGluR6
Grm7	0.4856	2.0075	1.0037	0.9922		mGluR7

Grm8	2.0093	0.9934	2.0132	0.9949		mGluR8
Homer1	1.0183	0.9736	1.0108	1.0004		Homer 1
Homer2	0.4952	0.4992	0.4936	1.0025		Homer 2
Il1b	#VALUE!	0.9044	4.2956	#VALUE!		Iterleukin 1 beta
Itpr1	0.4900	0.9954	1.0042	1.0015		Inositol 1,4,5-triphosphate receptor, type 1
Mapk1	0.9984	0.9944	0.9908	0.4864		Mitogen activated protein kinase 1 (ERK2)
Nsf	0.9950	2.0089	0.9998	0.9943		N-ethylmaleimide-sensitive factor
P2rx7	1.0053	2.0168	2.0081	1.9785		P2X purinoceptor 7
Phgdh	0.9942	0.9951	0.9967	0.9920		Phosphoglycerate dehydrogenase
Pla2g6	0.4927	1.0038	1.0032	0.4918		PLA2, group VI
Plcb1	0.4922	1.0018	1.0029	1.0044		PLC beta 1
Prodh	1.0009	0.9814	0.9958	0.4877		proline dehydrogenase
Shank2	1.0013	1.0008	0.4945	0.4874		SH3 and multiple ankyrin repeat domains 2
Slc17a6	0.4884	0.9880	1.0083	0.9948		Vglut2
Slc17a7	0.9995	0.9972	1.0082	0.4970		Vglut1
Slc17a8	0.9966	0.0038	2.0172	0.9896		Vglut3
Slc1a1	0.4944	1.0005	1.0032	0.9892		EEAT3
Slc1a2	0.4907	0.9946	1.0006	0.9967		EEAT2
Slc1a3	0.9884	0.9813	2.0042	2.0094		EEAT1
Slc1a6	0.4972	0.2495	1.0016	1.0002		EEAT4
Slc1a7	0.9741	#VALUE!	#VALUE!	1.9760		EEAT5
Slc32a1	0.4936	0.4989	0.4999	0.2424		Vgat
Slc38a1	0.4910	0.9860	1.0018	0.9923		Solute carrier family 38, member 1
Slc6a1	0.4933	0.9964	1.0084	0.9912		GAT-1
Slc6a11	0.9890	0.4940	0.5047	0.4987		Solute carrier family 6, member 11
Slc6a12	#VALUE!	2.1903	2.0126	0.9853		Solute carrier family 6, member 12
Slc6a13	0.9918	0.4943	1.9983	0.9926		Solute carrier family 6, member 13
Snca	1.0013	0.4870	0.9985	1.0003		alpha-synuclean
Srr	0.4968	1.0006	1.0010	0.9989		serine racemase

Table A.1: qPCR analysis of GABA/glutamate plates
Summary of the relative quantity (RQ) of mRNA transcripts (target) in four separate experiments for LV-shNogoA transduced hippocampal cultures, compared to LV-control transduced cultures. Cultures were transduced with LVs at 9 DIV, RNA collected at 16 DIV, first strand cDNA synthesized and analyzed using the GABA/glutamate RT^2 Profiler PCR Array (Qiagen).

Target	#1 RQ	#2 RQ
Akt1	0.9987	1.0021
Akt1s1	0.9978	0.9982
Akt2	0.9933	1.0030
Akt3	0.9848	1.0159
Cab39	1.0036	1.0099
Cab39l	0.9877	2.0563
Rps6ka4	2.0080	1.0026
Cdc42	0.9932	1.0050
Chuk	1.9911	1.0107
Ddit4	1.9831	0.5035
Ddit4l	0.9857	2.0210
Eif4b	0.9947	1.0063
Eif4e	2.0201	0.9971
Eif4EbP1	0.9932	1.0052
Eif4EBP2	0.9918	2.0359
Fkbp1a	2.0560	1.0004
Fkbp8	0.9928	1.0075
Gsk3b	1.9752	1.9939
Hif1a	1.9924	1.0040
Hras	2.0047	0.4968
Hspa4	0.9968	0.9988
Igf1	0.9892	0.9965
Igfbp3	1.0003	0.5007
Ikbkb	0.9976	2.0053
Ilk	0.9907	0.9954
Ins2	0.9998	1.0121
Insr	1.0009	0.5031
Irs1	0.9991	0.5026
Kras	0.9943	0.9852
Mapk1	2.0160	1.0080
Mapk3	0.9964	1.0008
Mapkap1	2.0245	2.0349
Mlst8	0.9837	1.0066
Mtor	0.9970	0.5062
Myo1c	1.0024	2.0155
Nras	1.9997	1.0023
Pdpk1	1.0087	1.0142
Pik3c3	0.9933	1.0125
Pik3ca	0.9990	1.0045
Pick3cb	0.9979	1.0000
Pik3cd	0.9907	1.0191
Pik3cg	2.1720	#VALUE!

Pik3r1	0.9845	1.0144
Pik3r2	0.4775	0.4934
Pld1	2.0095	2.0262
Pld2	0.9840	0.9986
Ppp2ca	1.0082	1.0026
Ppp2r2b	0.9869	1.0050
Ppp2r4	0.9912	0.9873
Prkaa1	1.9807	1.0108
Prkaa2	0.4935	0.2532
Prkab1	1.9975	1.9920
Prkab2	1.9816	1.0005
Prkag1	2.0017	1.0021
Prkag2	0.9982	1.0144
Prkag3	0.2621	0.5055
Prkca	1.0048	0.4943
Prkcb	0.9991	1.0120
Prkce	0.9969	0.9995
Prkcg	0.4967	1.0051
Pten	1.0006	1.0151
Rheb	1.9725	2.0098
Rhoa	2.0202	2.0235
Rps6	0.9995	1.0098
Rps6ka1	1.9885	1.0092
Rps6ka2	0.9982	1.0125
Rps6ka5	0.9944	0.4947
Rps6kb1	0.5050	0.5048
Rps6kb2	2.0127	1.0007
Rptor	0.9981	1.0046
Rraga	0.9902	1.9982
Rragb	0.9973	1.0079
Rragc	1.0011	1.0020
Rrag3	2.0068	2.0823
Sgk1	0.9961	1.9849
Stk11	0.9920	0.9933
Tp53	0.9979	1.0058
Tsc1	0.9887	2.0341
Tsc2	1.0065	1.0001
Ulk1	1.9905	2.0136
Vegfa	2.0024	1.0053
Vegfb	0.9916	1.0084
Vegfc	0.9809	1.0045
Ywhaq	2.0077	1.0087

Table A.2: qPCR analysis of mTOR plates
Summary of the relative quantity (RQ) of mRNA transcripts (target) in two separate experiments for LV-shNogoA transduced hippocampal cultures, compared to LV-control transduced cultures. Cultures were transduced with LVs at 9 DIV, RNA collected at 16 DIV, first strand cDNA synthesized and analyzed using the mTOR RT^2 Profiler PCR Array (Qiagen).

Description	ΣCoverage	Σ# PSMs	Coverage A3
Reticulon OS=Rattus norvegicus GN=Rtn4 PE=1 SV=1 - [F1LQN3_RAT]	78.93	2055	71.71
Sequence	**# PSMs**	**Modifications**	**phosphoRS Site Probabilities**
AQIITEK	3		
AQIITEKTSPK	10	S9(Phospho)	T(5): 0.1; T(8): 50.0; S(9): 50.0
ASISPSNVSALEPQTEMGSIVK	8		
ASISPSNVSALEPQTEMGSIVK	23	M17(Oxidation)	
ASISPSNVSALEPQTEMGSIVK	23	S4(Phospho)	S(2): 0.6; S(4): 98.9; S(6): 0.6; S(9): 0.0; T(15): 0.0; S(19): 0.0
ASISPSNVSALEPQTEMGSIVK	25	S2(Phospho); M17(Oxidation)	S(2): 78.4; S(4): 10.8; S(6): 10.8; S(9): 0.0; T(15): 0.0; S(19): 0.0
ATNPFVNR	21		
AYITCASFTSATESTTANTFPLLEDHTSENK	8	C5(Carbamidomethyl)	
AYITCASFTSATESTTANTFPLLEDHTSENKTDEK	14	C5(Carbamidomethyl)	
AYLESEVAISEELVQK	103		
CLEDSLEQK	5	C1(Carbamidomethyl)	
DAASNDIPTLTK	18		
DAASNDIPTLTK	1	K12(GlyGly)	
DAASNDIPTLTKK	1		
DEVHVSDEFSENR	44		
DKEDLVCSAALHSPQESPVGK	6	C7(Carbamidomethyl)	
DKEDLVCSAALHSPQESPVGK	3	C7(Carbamidomethyl); S13(Phospho)	S(8): 0.0; S(13): 100.0; S(17): 0.0
DKEDLVCSAALHSPQESPVGKEDR	3	C7(Carbamidomethyl)	
DKEDLVCSAALHSPQESPVGKEDR	3	C7(Carbamidomethyl); S13(Phospho); S17(Phospho)	S(8): 3.4; S(13): 96.6; S(17): 100.0
DKEDLVCSAALHSPQESPVGKEDR	1	C7(Carbamidomethyl); S13(Phospho)	S(8): 0.2; S(13): 99.5; S(17): 0.2
DLAEFSELEYSEMGSSFK	21		
DLAEFSELEYSEMGSSFK	51	M13(Oxidation)	
DLAEFSELEYSEMGSSFKGSPK	10	M13(Oxidation); S20(Phospho)	S(6): 0.0; Y(10): 0.0; S(11): 0.0; S(15): 0.0; S(16): 0.0; S(20): 100.0
DSEGRNEDASFPSTPEPVK	7		
DSEGRNEDASFPSTPEPVK	11	T14(Phospho)	S(2): 0.0; S(10): 0.7; S(13): 49.6; T(14): 49.6
DSEGRNEDASFPSTPEPVK	2	S10(Phospho); S13(Phospho)	S(2): 0.1; S(10): 99.3; S(13): 50.3; T(14): 50.3
DSEGRNEDASFPSTPEPVKDSSR	9		
DSEGRNEDASFPSTPEPVKDSSR	15	T14(Phospho)	S(2): 0.0; S(10): 0.0; S(13): 11.7; T(14): 88.3; S(21): 0.0; S(22): 0.0
DSEGRNEDASFPSTPEPVKDSSR	3	S10(Phospho); S13(Phospho)	S(2): 0.1; S(10): 99.8; S(13): 16.8; T(14): 83.4; S(21): 0.0; S(22): 0.0
EEYADFKPFEQAWEVK	29		
EEYADFKPFEQAWEVKDTYEGSR	4		
EGIKEPESFNAAVQETEAPYISIACDLIK	34	C25(Carbamidomethyl)	
EHGYLGNLSAVSSSEGTIEETLNEASK	51		
EKISLQMEEFNTAIYSNDDLLSSK	7	M7(Oxidation)	
EKISLQMEEFNTAIYSNDDLLSSK	4		

EKISLQMEEFNTAIYSNDDLLSSKEDK	3	M7(Oxidation)	
EPESFNAAVQETEAPYISIACDLIK	9	C21(Carbamidomethyl)	
ESETFSDSSPIEIIDEFPTFVSAK	7		
ESETFSDSSPIEIIDEFPTFVSAK	19	S8(Phospho)	S(2): 0.0; T(4): 0.0; S(6): 8.5; S(8): 82.9; S(9): 8.5; T(19): 0.0; S(22): 0.0
ESETFSDSSPIEIIDEFPTFVSAK	2	S2(Phospho); S6(Phospho)	S(2): 75.4; T(4): 43.9; S(6): 43.9; S(8): 18.3; S(9): 18.3; T(19): 0.2; S(22): 0.1
ESLTEVSETVAQHK	24		
ESLTEVSETVAQHK	11	K14(GlyGly)	
ESLTEVSETVAQHKEER	58		
ESLTEVSETVAQHKEER	3	K14(GlyGly)	
ETKLSTEPSPDFSNYSEIAK	2	S5(Phospho); S9(Phospho)	T(2): 0.1; S(5): 86.7; T(6): 13.2; S(9): 100.0; S(13): 0.0; Y(15): 0.0; S(16): 0.0
ETKLSTEPSPDFSNYSEIAK	3	T6(Phospho)	T(2): 0.3; S(5): 49.8; T(6): 49.8; S(9): 0.1; S(13): 0.0; Y(15): 0.0; S(16): 0.0
ETKLSTEPSPDFSNYSEIAK	1		
EYTDLEVSDK	23		
EYTDLEVSDKSEIANIQSGADSLPCLELPCDLSFK	15	C25(Carbamidomethyl); C30(Carbamidomethyl)	
GESAILVENTK	22		
GESAILVENTK	2	K11(GlyGly)	
GESAILVENTKEEVIVR	113		
GPLPAAPPAAPER	23		
GPLPAAPPAAPERQPSWER	4	S16(Phospho)	S(16): 100.0
GSGSVDETLFALPAASEPVIPSSAEK	12	T8(Phospho)	S(2): 33.3; S(4): 33.3; T(8): 33.3; S(16): 0.0; S(22): 0.0; S(23): 0.0
GSGSVDETLFALPAASEPVIPSSAEK	2		
GSPKGESAILVENTK	1	S2(Phospho)	S(2): 88.9; S(7): 11.1; T(14): 0.0
GVIQAIQK	6		
HQVQIDHYLGLANK	88		
IKESETFSDSSPIEIIDEFPTFVSAK	13		
IKESETFSDSSPIEIIDEFPTFVSAK	20	S11(Phospho)	S(4): 0.0; T(6): 0.0; S(8): 0.2; S(10): 10.8; S(11): 89.0; T(21): 0.0; S(24): 0.0
IKESETFSDSSPIEIIDEFPTFVSAK	28	S8(Phospho); S10(Phospho)	S(4): 70.5; T(6): 81.9; S(8): 27.1; S(10): 16.0; S(11): 4.6; T(21): 0.0; S(24): 0.0
IMDLMEQPGNTVSSGQEDFPSVLLETAASLPSLSPLSTVSFK	12	M2(Oxidation); M5(Oxidation)	
IMDLMEQPGNTVSSGQEDFPSVLLETAASLPSLSPLSTVSFK	30	M2(Oxidation)	
IMDLMEQPGNTVSSGQEDFPSVLLETAASLPSLSPLSTVSFK	28	M2(Oxidation); S34(Phospho)	T(11): 0.0; S(13): 0.0; S(14): 0.0; S(21): 0.0; T(26): 0.0; S(29): 0.0; S(32): 5.7; S(34): 93.7; S(37): 0.4; T(38): 0.1; S(40): 0.1
IMDLMEQPGNTVSSGQEDFPSVLLETAASLPSLSPLSTVSFK	11	M2(Oxidation); M5(Oxidation); S34(Phospho)	T(11): 0.0; S(13): 0.0; S(14): 0.0; S(21): 0.1; T(26): 1.3; S(29): 1.3; S(32): 18.3; S(34): 72.9; S(37): 4.8; T(38): 1.3; S(40): 0.1
IMDLMEQPGNTVSSGQEDFPSVLLETAASLPSLSPLSTVSFK	3		
IMDLMEQPGNTVSSGQEDFPSVLLETAASLPSLSPLSTVSFK	4	S34(Phospho)	T(11): 0.0; S(13): 0.0; S(14): 0.0; S(21): 0.0; T(26): 0.2; S(29): 0.1; S(32): 0.5; S(34): 1.2; S(37): 32.7; T(38): 32.7; S(40): 32.7
ISLQMEEFNTAIYSNDDLLSSK	23	M5(Oxidation)	
ISLQMEEFNTAIYSNDDLLSSK	26		
ISLQMEEFNTAIYSNDDLLSSKEDK	3		
ISLQMEEFNTAIYSNDDLLSSKEDK	2	M5(Oxidation); S20(Phospho)	S(2): 0.0; T(10): 0.0; Y(13): 0.1; S(14): 1.2; S(20): 18.6; S(21): 80.1
KAQIITEK	18		

KAQIITEKTSPK	16	S10(Phospho)	T(6): 0.0; T(9): 7.1; S(10): 92.9
KCLEDSLEQK	7	C2(Carbamidomethyl)	
KLPSDTEK	1		
KLPSDTEKEDR	14		
KPAAGLSAAAVPPAAAAPLLDFSS DSVPPAPR	46		
LEPENPPPYEEAMNVALK	10		
LEPENPPPYEEAMNVALK	32	M13(Oxidation)	
LFLVDDLVDSLK	4		
LPEDDEPPARPPPPPPAGASPLAE PAAPPSTPAAPK	30		
LPEDDEPPARPPPPPPAGASPLAE PAAPPSTPAAPK	10	S20(Phospho)	S(20): 100.0; S(30): 0.0; T(31): 0.0
LPSDTEKEDR	4		
LSASPQELGKPYLESFQPNLHSTK	41	S4(Phospho)	S(2): 50.0; S(4): 50.0; Y(12): 0.0; S(15): 0.0; S(22): 0.0; T(23): 0.0
LSASPQELGKPYLESFQPNLHSTK	40		
LSTEPSPDFSNYSEIAK	20		
LSTEPSPDFSNYSEIAK	12	S6(Phospho)	S(2): 0.0; T(3): 0.0; S(6): 100.0; S(10): 0.0; Y(12): 0.0; S(13): 0.0
LSTEPSPDFSNYSEIAK	1	K17(GlyGly)	
MEDIDQSSLVSSSTDSPPRPPPAF K	2	M1(Oxidation); S7(Phospho)	S(7): 49.9; S(8): 49.9; S(11): 0.1; S(12): 0.0; S(13): 0.0; T(14): 0.1; S(16): 0.0
NEDASFPSTPEPVK	10		
NEDASFPSTPEPVK	13	S8(Phospho)	S(5): 0.0; S(8): 50.0; T(9): 50.0
NEDASFPSTPEPVK	8	S5(Phospho); S8(Phospho)	S(5): 100.0; S(8): 50.0; T(9): 50.0
NEDASFPSTPEPVKDSSR	21		
NEDASFPSTPEPVKDSSR	22	T9(Phospho)	S(5): 0.0; S(8): 90.4; T(9): 9.6; S(16): 0.0; S(17): 0.0
NEDASFPSTPEPVKDSSR	6	S5(Phospho); S8(Phospho)	S(5): 100.0; S(8): 1.7; T(9): 98.3; S(16): 0.0; S(17): 0.0
NIYPKDEVHVSDEFSENR	7		
QPSWERSPAAPAPSLPPAAAVLPS K	2	S3(Phospho)	S(3): 96.8; S(7): 3.2; S(14): 0.0; S(24): 0.0
QPSWERSPAAPAPSLPPAAAVLPS K	1	S3(Phospho); S7(Phospho)	S(3): 100.0; S(7): 100.0; S(14): 0.0; S(24): 0.0
RGSGSVDETLFALPAASEPVIPSS AEK	11	S3(Phospho)	S(3): 79.6; S(5): 10.2; T(9): 10.2; S(17): 0.0; S(23): 0.0; S(24): 0.0
RRGSGSVDETLFALPAASEPVIPS SAEK	35	S6(Phospho)	S(4): 14.6; S(6): 85.4; T(10): 0.0; S(18): 0.0; S(24): 0.0; S(25): 0.0
SDEGHPFR	11		
SEIANIQSGADSLPCLELPCDLSFK	13	C15(Carbamidomethyl); C20(Carbamidomethyl)	
SKDKEDLVCSAALHSPQESPVGK	11	C9(Carbamidomethyl)	
SKDKEDLVCSAALHSPQESPVGK	7	C9(Carbamidomethyl); S15(Phospho)	S(1): 0.0; S(10): 0.0; S(15): 100.0; S(19): 0.0
SKDKEDLVCSAALHSPQESPVGK	3	C9(Carbamidomethyl); S15(Phospho); S19(Phospho)	S(1): 0.0; S(10): 0.0; S(15): 100.0; S(19): 100.0
SLGKDSEGR	1		
SLSAVLSAELSK	21		
SPAAPAPSLPPAAAVLPSK	19		
SPAAPAPSLPPAAAVLPSK	1	S1(Phospho)	S(1): 100.0; S(8): 0.0; S(18): 0.0
SVPEHAELVEDSSPESEPVDLFSD DSIPEVPQTQEEAVMLMK	2	M39(Oxidation); M41(Oxidation)	
SVPEHAELVEDSSPESEPVDLFSD DSIPEVPQTQEEAVMLMK	3	M39(Oxidation)	
TMDIFNEMQMSVVAPVR	28	M2(Oxidation); M8(Oxidation); M10(Oxidation)	

TMDIFNEMQMSVVAPVR	27	M2(Oxidation)	
TMDIFNEMQMSVVAPVR	7		
TMDIFNEMQMSVVAPVR	5	M8(Oxidation); M10(Oxidation)	
TMDIFNEMQMSVVAPVREEYADF KPFEQAWEVK	9	M8(Oxidation); M10(Oxidation)	
TMDIFNEMQMSVVAPVREEYADF KPFEQAWEVK	4	M2(Oxidation); M8(Oxidation); M10(Oxidation)	
TMDIFNEMQMSVVAPVREEYADF KPFEQAWEVK	12	M8(Oxidation)	
TMDIFNEMQMSVVAPVREEYADF KPFEQAWEVK	2		
TSNPFLVAVQDSEADYVTTDTLSK	44		
TSVVDLLYWR	33		
VTEAAVSNMPEGLTPDLVQEACE SELNEATGTK	9	M9(Oxidation); C22(Carbamidomethyl)	
VTEAAVSNMPEGLTPDLVQEACE SELNEATGTK	6	C22(Carbamidomethyl)	
VTEAAVSNMPEGLTPDLVQEACE SELNEATGTK	4	M9(Oxidation); T14(Phospho); C22(Carbamidomethyl)	T(2): 0.0; S(7): 0.0; T(14): 100.0; S(24): 0.0; T(30): 0.0; T(32): 0.0
VVSPEKTMDIFNEMQMSVVAPVR	8	S3(Phospho); M8(Oxidation)	S(3): 11.2; T(7): 88.8; S(17): 0.0
VVSPEKTMDIFNEMQMSVVAPVR	5	S3(Phospho); M8(Oxidation); M14(Oxidation); M16(Oxidation)	S(3): 99.9; T(7): 0.1; S(17): 0.0
VVSPEKTMDIFNEMQMSVVAPVR	6	T7(Phospho); M8(Oxidation); M14(Oxidation)	S(3): 12.0; T(7): 88.0; S(17): 0.0
VVSPEKTMDIFNEMQMSVVAPVR EEYADFKPFEQAWEVK	5	S3(Phospho); M8(Oxidation); M14(Oxidation); M16(Oxidation)	S(3): 95.5; T(7): 4.5; S(17): 0.0; Y(26): 0.0
YQFVTEPEDEEDEEEEEDEEEDD EDLEELEVLER	27		
YSNSALGHVNSTIK	40		
YSNSALGHVNSTIK	1	K14(GlyGly)	

Table A.3: NogoA post-translational modification in control cultures
NogoA was immunoprecipiatated from rat primary hippocampal neurons and subject to LC-MS/MS. This table summaries the peptides identified from both CID and HDC fragmentation methods. The column on the right indicates the probability that each serine, threonine, or tyrosine residue is phosphorylated, for a given phosphopeptide.

Description	ΣCoverage	Σ# PSMs	Coverage A3
Reticulon OS=Rattus norvegicus GN=Rtn4 PE=1 SV=1 - [F1LQN3_RAT]	79.02	1888	68.10
Sequence	**# PSMs**	**Modifications**	**phosphoRS Site Probabilities**
EHGYLGNLSAVSSSEGTIEETLNEASK	64		
RRGSGSVDETLFALPAASEPVIPSSAEK	36	**S4(Phospho)**	S(4): 98.3; S(6): 1.7; T(10): 0.0; S(18): 0.0; S(24): 0.0; S(25): 0.0
KPAAGLSAAAVPPAAAAPLLDFSSDSVPPAPR	29		
ESLTEVSETVAQHKEER	46		
DLAEFSELEYSEMGSSFKGSPK	5	S20(Phospho)	S(6): 0.0; Y(10): 0.0; S(11): 0.0; S(15): 0.0; S(16): 0.0; S(20): 100.0
GESAILVENTKEEVIVR	138		
DLAEFSELEYSEMGSSFKGSPK	12	M13(Oxidation); S20(Phospho)	S(6): 0.0; Y(10): 0.0; S(11): 0.0; S(15): 1.0; S(16): 1.0; S(20): 98.0
LSASPQELGKPYLESFQPNLHSTK	33	S4(Phospho)	S(2): 50.0; S(4): 50.0; Y(12): 0.0; S(15): 0.0; S(22): 0.0; T(23): 0.0
DLAEFSELEYSEMGSSFK	37		
EGIKEPESFNAAVQETEAPYISIACDLIK	21	C25(Carbamidomethyl)	
ISLQMEEFNTAIYSNDDLLSSK	31	M5(Oxidation)	
SPAAPAPSLPPAAAVLPSK	22		
LSASPQELGKPYLESFQPNLHSTK	24		
RGSGSVDETLFALPAASEPVIPSSAEK	22	S3(Phospho)	S(3): 97.0; S(5): 1.5; T(9): 1.5; S(17): 0.0; S(23): 0.0; S(24): 0.0
TSNPFLVAVQDSEADYVTTDTLSK	68		
SEIANIQSGADSLPCLELPCDLSFK	8	C15(Carbamidomethyl); C20(Carbamidomethyl)	
LPEDDEPPARPPPPPPAGASPLAEPAAPPSTPAAPK	20		
NEDASFPSTPEPVKDSSR	20		
HQVQIDHYLGLANK	38		
YSNSALGHVNSTIK	22		
AYITCASFTSATESTTANTFPLLEDHTSENKTDEK	7	C5(Carbamidomethyl)	
ESLTEVSETVAQHK	17		
DAASNDIPTLTK	20		
AYLESEVAISEELVQK	115		
DSEGRNEDASFPSTPEPVKDSSR	5		
NEDASFPSTPEPVK	16		
DEVHVSDEFSENR	25		
GESAILVENTK	19		
KAQIITEKTSPK	30	S10(Phospho)	T(6): 0.0; T(9): 6.6; S(10): 93.4
LSTEPSPDFSNYSEIAK	6		
LEPENPPPYEEAMNVALK	30	M13(Oxidation)	
SLSAVLSAELSK	15		
KLPSDTEKEDR	19		
LEPENPPPYEEAMNVALK	11		
IKESETFSDSSPIEIIDEFPTFVSAK	12		
ASISPSNVSALEPQTEMGSIVK	15		
DLAEFSELEYSEMGSSFK	38	M13(Oxidation)	

KAQIITEK	9		
NEDASFPSTPEPVK	7	S8(Phospho)	S(5): 4.0; S(8): 48.0; T(9): 48.0
DSEGRNEDASFPSTPEPVK	10		
GPLPAAPPAAPER	15		
SKDKEDLVCSAALHSPQESPVGK	7	C9(Carbamidomethyl); S15(Phospho)	S(1): 0.0; S(10): 0.0; S(15): 100.0; S(19): 0.0
DSEGRNEDASFPSTPEPVKDSSR	16	T14(Phospho)	S(2): 0.0; S(10): 0.0; S(13): 12.2; T(14): 87.8; S(21): 0.0; S(22): 0.0
ISLQMEEFNTAIYSNDDLLSSKEDK	7		
TSVVDLLYWR	20		
EEYADFKPFEQAWEVK	21		
ISLQMEEFNTAIYSNDDLLSSK	41		
TMDIFNEMQMSVVAPVR	19	M2(Oxidation); M8(Oxidation); M10(Oxidation)	
TMDIFNEMQMSVVAPVREEYADFKPFEQAWEVK	6	M2(Oxidation); M8(Oxidation); M10(Oxidation)	
ASISPSNVSALEPQTEMGSIVK	35	M17(Oxidation)	
NIYPKDEVHVSDEFSENR	9		
LSTEPSPDFSNYSEIAK	4	S6(Phospho)	S(2): 0.0; T(3): 0.0; S(6): 99.2; S(10): 0.8; Y(12): 0.0; S(13): 0.0
EKISLQMEEFNTAIYSNDDLLSSK	5	M7(Oxidation)	
VTEAAVSNMPEGLTPDLVQEACESELNEATGTK	4	M9(Oxidation); C22(Carbamidomethyl)	
ESLTEVSETVAQHK	4	K14(GlyGly)	
ESETFSDSSPIEIIDEFPTFVSAK	9		
TMDIFNEMQMSVVAPVR	24	M2(Oxidation)	
EYTDLEVSDK	24		
CLEDSLEQK	14	C1(Carbamidomethyl)	
NEDASFPSTPEPVKDSSR	14	S8(Phospho)	S(5): 0.0; S(8): 88.6; T(9): 11.3; S(16): 0.0; S(17): 0.0
ATNPFVNR	21		
KCLEDSLEQK	4	C2(Carbamidomethyl)	
EEYADFKPFEQAWEVKDTYEGSR	3		
TMDIFNEMQMSVVAPVR	12	M8(Oxidation); M10(Oxidation)	
YQFVTEPEDEEDEEEEEDEEEDDEDLEELEVLER	43		
DKEDLVCSAALHSPQESPVGK	8	C7(Carbamidomethyl)	
LFLVDDLVDSLK	6		
ASISPSNVSALEPQTEMGSIVK	11	S4(Phospho)	S(2): 8.6; S(4): 91.3; S(6): 0.1; S(9): 0.0; T(15): 0.0; S(19): 0.0
LPSDTEKEDR	4		
VVSPEKTMDIFNEMQMSVVAPVR	12	S3(Phospho); M8(Oxidation); M14(Oxidation); M16(Oxidation)	S(3): 90.1; T(7): 9.9; S(17): 0.0
TMDIFNEMQMSVVAPVR	4		
EKISLQMEEFNTAIYSNDDLLSSK	2		
LPEDDEPPARPPPPPPAGASPLAEPAAPPSTPAAPK	13	S20(Phospho)	S(20): 100.0; S(30): 0.0; T(31): 0.0
IKESETFSDSSPIEIIDEFPTFVSAK	38	S10(Phospho); S11(Phospho)	S(4): 0.5; T(6): 86.6; S(8): 37.6; S(10): 37.6; S(11): 37.6; T(21): 0.0; S(24): 0.0
SKDKEDLVCSAALHSPQESPVGK	8	C9(Carbamidomethyl)	
ASISPSNVSALEPQTEMGSIVK	45	S4(Phospho); M17(Oxidation)	S(2): 47.4; S(4): 47.4; S(6): 5.3; S(9): 0.0; T(15): 0.0; S(19): 0.0
IKESETFSDSSPIEIIDEFPTFVSA	28	S11(Phospho)	S(4): 0.0; T(6): 0.0; S(8): 0.1; S(10): 9.4; S(11): 90.5;

K			T(21): 0.0; S(24): 0.0
VVSPEKTMDIFNEMQMSVVAPV R	13	T7(Phospho); M8(Oxidation); M14(Oxidation)	S(3): 2.0; T(7): 98.0; S(17): 0.0
VVSPEKTMDIFNEMQMSVVAPV REEYADFKPFEQAWEVK	4	S3(Phospho); M8(Oxidation); M14(Oxidation); M16(Oxidation)	S(3): 93.2; T(7): 6.6; S(17): 0.1; Y(26): 0.1
AYITCASFTSATESTTANTFPLLE DHTSENK	6	C5(Carbamidomethyl)	
EYTDLEVSDKSEIANIQSGADSLP CLELPCDLSFK	4	C25(Carbamidomethyl); C30(Carbamidomethyl)	
VTEAAVSNMPEGLTPDLVQEACE SELNEATGTK	2	C22(Carbamidomethyl)	
ESETFSDSSPIEIIDEFPTFVSAK	24	S8(Phospho)	S(2): 0.0; T(4): 0.0; S(6): 1.1; S(8): 89.1; S(9): 9.7; T(19): 0.0; S(22): 0.0
VTEAAVSNMPEGLTPDLVQEACE SELNEATGTK	5	M9(Oxidation); T14(Phospho); C22(Carbamidomethyl)	T(2): 0.0; S(7): 0.2; T(14): 99.8; S(24): 0.0; T(30): 0.0; T(32): 0.0
GSGSVDETLFALPAASEPVIPSSA EK	11	T8(Phospho)	S(2): 10.4; S(4): 10.4; T(8): 79.1; S(16): 0.0; S(22): 0.0; S(23): 0.0
EPESFNAAVQETEAPYISIACDLI K	11	C21(Carbamidomethyl)	
DKEDLVCSAALHSPQESPVGK	1	C7(Carbamidomethyl); S13(Phospho)	S(8): 0.0; S(13): 100.0; S(17): 0.0
GSGSVDETLFALPAASEPVIPSSA EK	4		
VVSPEKTMDIFNEMQMSVVAPV R	1	S3(Phospho); M8(Oxidation)	S(3): 1.5; T(7): 98.5; S(17): 0.0
IMDLMEQPGNTVSSGQEDFPSVL LETAASLPSLSPLSTVSFK	2	M2(Oxidation); M5(Oxidation)	
SPAAPAPSLPPAAAVLPSK	2	S1(Phospho)	S(1): 100.0; S(8): 0.0; S(18): 0.0
TMDIFNEMQMSVVAPVREEYAD FKPFEQAWEVK	5	M8(Oxidation); M10(Oxidation)	
NEDASFPSTPEPVKDSSR	11	S5(Phospho); S8(Phospho)	S(5): 99.9; S(8): 50.0; T(9): 50.0; S(16): 0.0; S(17): 0.1
IMDLMEQPGNTVSSGQEDFPSVL LETAASLPSLSPLSTVSFK	7	M2(Oxidation); M5(Oxidation); **S37(Phospho)**	T(11): 0.0; S(13): 0.0; S(14): 0.0; S(21): 0.0; T(26): 0.0; S(29): 0.0; S(32): 0.6; S(34): 5.5; S(37): 58.6; T(38): 17.6; S(40): 17.6
DKEDLVCSAALHSPQESPVGKED R	2	C7(Carbamidomethyl); S13(Phospho); S17(Phospho)	S(8): 50.1; S(13): 50.1; S(17): 99.9
DKEDLVCSAALHSPQESPVGKED R	1	C7(Carbamidomethyl)	
SVPEHAELVEDSSPESEPVDLFSD DSIPEVPQTQEEAVMLMK	2	M39(Oxidation); M41(Oxidation)	
QPSWERSPAAPAPSLPPAAAVLP SK	3	S3(Phospho); S7(Phospho)	S(3): 100.0; S(7): 100.0; S(14): 0.0; S(24): 0.0
QPSWERSPAAPAPSLPPAAAVLP SK	2	S3(Phospho)	S(3): 84.4; S(7): 15.6; S(14): 0.0; S(24): 0.0
DSEGRNEDASFPSTPEPVK	5	S10(Phospho); S13(Phospho)	S(2): 0.0; S(10): 66.7; S(13): 66.7; T(14): 66.7
ETKLSTEPSPDFSNYSEIAK	2	S5(Phospho)	T(2): 0.2; S(5): 49.2; T(6): 49.2; S(9): 1.3; S(13): 0.0; Y(15): 0.0; S(16): 0.0
EKISLQMEEFNTAIYSNDDLLSSK EDK	1	M7(Oxidation)	
GPLPAAPPAAPERQPSWER	2	S16(Phospho)	S(16): 100.0
ETKLSTEPSPDFSNYSEIAK	3	S5(Phospho); S9(Phospho)	T(2): 1.1; S(5): 49.5; T(6): 49.5; S(9): 100.0; S(13): 0.0; Y(15): 0.0; S(16): 0.0
TSNPFLVAVQDSEADYVTTDTLS K	2	**S2(Phospho)**	T(1): 23.0; S(2): 76.8; S(12): 0.1; Y(16): 0.1; T(18): 0.1; T(19): 0.0; T(21): 0.0; S(23): 0.0
SDEGHPFR	12		
AQIITEKTSPK	6	S9(Phospho)	T(5): 0.1; T(8): 49.9; S(9): 49.9
SKDKEDLVCSAALHSPQESPVGK	2	C9(Carbamidomethyl);	S(1): 0.0; S(10): 0.0; S(15): 100.0; S(19): 100.0

		S15(Phospho); S19(Phospho)	
ESETFSDSSPIEIIDEFPTFVSAKDDSPK	3	**T19(Phospho)**	S(2): 0.0; T(4): 0.0; S(6): 0.0; S(8): 0.0; S(9): 0.0; T(19): 78.8; S(22): 17.2; S(27): 4.0
IMDLMEQPGNTVSSGQEDFPSVLLETAASLPSLSPLSTVSFK	7	M2(Oxidation); S34(Phospho)	T(11): 0.7; S(13): 2.8; S(14): 2.8; S(21): 13.3; T(26): 2.8; S(29): 0.7; S(32): 13.3; S(34): 31.0; S(37): 13.3; T(38): 13.3; S(40): 6.0
IMDLMEQPGNTVSSGQEDFPSVLLETAASLPSLSPLSTVSFK	1	M5(Oxidation)	
DAASNDIPTLTK	1	K12(GlyGly)	
GVIQAIQK	3		
DSEGRNEDASFPSTPEPVK	4	T14(Phospho)	S(2): 0.0; S(10): 0.0; S(13): 2.7; T(14): 97.3
ESLTEVSETVAQHKEER	2	K14(GlyGly)	
DSEGRNEDASFPSTPEPVKDSSR	4	S10(Phospho); S13(Phospho)	S(2): 2.6; S(10): 97.3; S(13): 13.8; T(14): 86.3; S(21): 0.0; S(22): 0.0
NEDASFPSTPEPVK	4	S5(Phospho); S8(Phospho)	S(5): 99.9; S(8): 50.0; T(9): 50.0
KLPSDTEK	1		
IKESETFSDSSPIEIIDEFPTFVSAKDDSPK	1	**T6(Phospho); S29(Phospho)**	S(4): 3.9; T(6): 3.9; S(8): 12.1; S(10): 40.0; S(11): 40.0; T(21): 2.9; S(24): 8.6; S(29): 88.5
SVPEHAELVEDSSPESEPVDLFSDDSIPEVPQTQEEAVMLMK	1		
DKEDLVCSAALHSPQESPVGK	2	C7(Carbamidomethyl); S13(Phospho); S17(Phospho)	S(8): 0.0; S(13): 100.0; S(17): 100.0
DAASNDIPTLTKK	2		
AQIITEK	3		
GSPKGESAILVENTK	2	S2(Phospho)	S(2): 100.0; S(7): 0.0; T(14): 0.0
ESETFSDSSPIEIIDEFPTFVSAK	1	S6(Phospho); S8(Phospho)	S(2): 12.1; T(4): 27.6; S(6): 69.9; S(8): 81.1; S(9): 8.8; T(19): 0.2; S(22): 0.2
ESETFSDSSPIEIIDEFPTFVSAKDDSPK	1	**S9(Phospho); S22(Phospho)**	S(2): 0.8; T(4): 0.8; S(6): 2.3; S(8): 7.4; S(9): 88.7; T(19): 47.9; S(22): 47.9; S(27): 4.1
YSNSALGHVNSTIK	1	K14(GlyGly)	
MEDIDQSSLVSSSTDSPPRPPPAFK	1	M1(Oxidation); S7(Phospho)	S(7): 27.7; S(8): 27.7; S(11): 7.4; S(12): 7.4; S(13): 27.7; T(14): 2.1; S(16): 0.1
SVPEHAELVEDSSPESEPVDLFSDDSIPEVPQTQEEAVMLMK	2	M39(Oxidation)	
LSTEPSPDFSNYSEIAK	1	K17(GlyGly)	

Table A.4: NogoA post-translation modification in TTX-treated cultures
NogoA was immunoprecipiatated from rat primary hippocampal neurons following 24hr treatment with TTX (2μM) and subject to LC-MS/MS. This table summaries the peptides identified from both CID and HDC fragmentation methods. The column on the right indicates the probability that each serine, threonine, or tyrosine residue is phosphorylated, for a given phosphopeptide.

A.7 References

Akaneya Y, Tsumoto T, Hatanaka H (1996) Brain-derived neurotrophic factor blocks long-term depression in rat visual cortex. J Neurophysiol 76:4198-4201.

Akaneya Y, Tsumoto T, Kinoshita S, Hatanaka H (1997) Brain-derived neurotrophic factor enhances long-term potentiation in rat visual cortex. J Neurosci 17:6707-6716.

Bateup HS, Johnson CA, Denefrio CL, Saulnier JL, Kornacker K, Sabatini BL (2013) Excitatory/inhibitory synaptic imbalance leads to hippocampal hyperexcitability in mouse models of tuberous sclerosis. Neuron 78:510-522.

Beique JC, Na Y, Kuhl D, Worley PF, Huganir RL (2011) Arc-dependent synapse-specific homeostatic plasticity. Proc Natl Acad Sci U S A 108:816-821.

Delekate A, Zagrebelsky M, Kramer S, Schwab ME, Korte M (2011) NogoA restricts synaptic plasticity in the adult hippocampus on a fast time scale. Proc Natl Acad Sci U S A 108:2569-2574.

Diering GH, Gustina AS, Huganir RL (2014) PKA-GluA1 coupling via AKAP5 controls AMPA receptor phosphorylation and cell-surface targeting during bidirectional homeostatic plasticity. Neuron 84:790-805.

Ehlers MD (2003) Activity level controls postsynaptic composition and signaling via the ubiquitin-proteasome system. Nature neuroscience 6:231-242.

Fatemi SH, Folsom TD, Rooney RJ, Thuras PD (2013) Expression of GABAA alpha2-, beta1- and epsilon-receptors are altered significantly in the lateral cerebellum of subjects with schizophrenia, major depression and bipolar disorder. Transl Psychiatry 3:e303.

Henry FE, McCartney AJ, Neely R, Perez AS, Carruthers CJ, Stuenkel EL, Inoki K, Sutton MA (2012) Retrograde changes in presynaptic function driven by dendritic mTORC1. J Neurosci 32:17128-17142.

Huber AB, Schwab ME (2000) Nogo-A, a potent inhibitor of neurite outgrowth and regeneration. Biol Chem 381:407-419.

Inoki K, Li Y, Xu T, Guan KL (2003) Rheb GTPase is a direct target of TSC2 GAP activity and regulates mTOR signaling. Genes Dev 17:1829-1834.

Kempf A, Tews B, Arzt ME, Weinmann O, Obermair FJ, Pernet V, Zagrebelsky M, Delekate A, Iobbi C, Zemmar A, Ristic Z, Gullo M, Spies P, Dodd D, Gygax D, Korte M, Schwab ME (2014) The sphingolipid receptor S1PR2 is a receptor for Nogo-a repressing synaptic plasticity. PLoS Biol 12:e1001763.

Korb E, Wilkinson CL, Delgado RN, Lovero KL, Finkbeiner S (2013) Arc in the nucleus regulates PML-dependent GluA1 transcription and homeostatic plasticity. Nat Neurosci 16:874-883.

Lang SB, Stein V, Bonhoeffer T, Lohmann C (2007) Endogenous brain-derived neurotrophic factor triggers fast calcium transients at synapses in developing dendrites. J Neurosci 27:1097-1105.

Lee H, Raiker SJ, Venkatesh K, Geary R, Robak LA, Zhang Y, Yeh HH, Shrager P, Giger RJ (2008) Synaptic function for the Nogo-66 receptor NgR1: regulation of dendritic spine morphology and activity-dependent synaptic strength. The Journal of neuroscience : the official journal of the Society for Neuroscience 28:2753-2765.

Lyford GL, Yamagata K, Kaufmann WE, Barnes CA, Sanders LK, Copeland NG, Gilbert DJ, Jenkins NA, Lanahan AA, Worley PF (1995) Arc, a growth factor and activity-

regulated gene, encodes a novel cytoskeleton-associated protein that is enriched in neuronal dendrites. Neuron 14:433-445.
Malenka RC, Bear MF (2004) LTP and LTD: an embarrassment of riches. Neuron 44:5-21.
Niederost B, Oertle T, Fritsche J, McKinney RA, Bandtlow CE (2002) Nogo-A and myelin-associated glycoprotein mediate neurite growth inhibition by antagonistic regulation of RhoA and Rac1. The Journal of neuroscience : the official journal of the Society for Neuroscience 22:10368-10376.
O'Brien RJ, Kamboj S, Ehlers MD, Rosen KR, Fischbach GD, Huganir RL (1998) Activity-dependent modulation of synaptic AMPA receptor accumulation. Neuron 21:1067-1078.
Peng X, Kim J, Zhou Z, Fink DJ, Mata M (2011) Neuronal Nogo-A regulates glutamate receptor subunit expression in hippocampal neurons. J Neurochem 119:1183-1193.
Petrasek T, Prokopova I, Bahnik S, Schonig K, Berger S, Vales K, Tews B, Schwab ME, Bartsch D, Stuchlik A (2014a) Nogo-A downregulation impairs place avoidance in the Carousel maze but not spatial memory in the Morris water maze. Neurobiol Learn Mem 107:42-49.
Petrasek T, Prokopova I, Sladek M, Weissova K, Vojtechova I, Bahnik S, Zemanova A, Schonig K, Berger S, Tews B, Bartsch D, Schwab ME, Sumova A, Stuchlik A (2014b) Nogo-A-deficient Transgenic Rats Show Deficits in Higher Cognitive Functions, Decreased Anxiety, and Altered Circadian Activity Patterns. Front Behav Neurosci 8:90.
Raiker SJ, Lee H, Baldwin KT, Duan Y, Shrager P, Giger RJ (2010) Oligodendrocyte-myelin glycoprotein and Nogo negatively regulate activity-dependent synaptic plasticity. J Neurosci 30:12432-12445.
Rutherford LC, Nelson SB, Turrigiano GG (1998) BDNF has opposite effects on the quantal amplitude of pyramidal neuron and interneuron excitatory synapses. Neuron 21:521-530.
Shepherd JD, Rumbaugh G, Wu J, Chowdhury S, Plath N, Kuhl D, Huganir RL, Worley PF (2006) Arc/Arg3.1 mediates homeostatic synaptic scaling of AMPA receptors. Neuron 52:475-484.
Siegelbaum SA, Kandel ER (1991) Learning-related synaptic plasticity: LTP and LTD. Curr Opin Neurobiol 1:113-120.
Takei N, Inamura N, Kawamura M, Namba H, Hara K, Yonezawa K, Nawa H (2004) Brain-derived neurotrophic factor induces mammalian target of rapamycin-dependent local activation of translation machinery and protein synthesis in neuronal dendrites. The Journal of neuroscience : the official journal of the Society for Neuroscience 24:9760-9769.
Tang SJ, Reis G, Kang H, Gingras AC, Sonenberg N, Schuman EM (2002) A rapamycin-sensitive signaling pathway contributes to long-term synaptic plasticity in the hippocampus. Proc Natl Acad Sci U S A 99:467-472.
Tapley P, Lamballe F, Barbacid M (1992) K252a is a selective inhibitor of the tyrosine protein kinase activity of the trk family of oncogenes and neurotrophin receptors. Oncogene 7:371-381.
Tee AR, Fingar DC, Manning BD, Kwiatkowski DJ, Cantley LC, Blenis J (2002) Tuberous sclerosis complex-1 and -2 gene products function together to inhibit mammalian

target of rapamycin (mTOR)-mediated downstream signaling. Proc Natl Acad Sci U S A 99:13571-13576.
Tee AR, Manning BD, Roux PP, Cantley LC, Blenis J (2003) Tuberous sclerosis complex gene products, Tuberin and Hamartin, control mTOR signaling by acting as a GTPase-activating protein complex toward Rheb. Current biology : CB 13:1259-1268.
Turrigiano GG, Leslie KR, Desai NS, Rutherford LC, Nelson SB (1998) Activity-dependent scaling of quantal amplitude in neocortical neurons. Nature 391:892-896.
Willi R, Weinmann O, Winter C, Klein J, Sohr R, Schnell L, Yee BK, Feldon J, Schwab ME (2010) Constitutive genetic deletion of the growth regulator Nogo-A induces schizophrenia-related endophenotypes. The Journal of neuroscience : the official journal of the Society for Neuroscience 30:556-567.